

Modeling of Subsea CO₂ Transportation and Injection Pipe Networks, The Case of Snøhvit

Emmanuel Paul Azebeokhai

January 31, 2024

Summary

Gas injection has been used in the oil and gas industries for years and has helped recover millions of barrels that could not be recovered with the primary drive mechanism. Gas injection distribution networks are not usually built with the field at the early field development phase but are later incorporated into the field after some wells have experienced a drop in pressure to deliver the required rate. However, this new gas injection line must then be modeled to the best optimum position that can achieve the optimum injection before being implemented in the field. Software such as GAP and Prosper are common commercial software implemented in the modeling of efficient pipeline distribution and injection networks and have proven successful. This knowledge of gas injection network modeling can be transferred to the modeling of CO₂ transportation and injection networks.

Captured CO₂ from major emitters such as sizable fossil fuel power plants, cement and steel mills, biomass energy facilities, synthetic fuel plants, and Liquefied Natural Gas (LNG) plants such as the one at Hammerfest, 140 kilometers to Snøhvit field need to be transported and injected subsea using different injection wells. Knowledge from gas injection network modeling can be studied to help appropriately model subsea CO₂ transportation and injection pipe networks.

As part of the study into CO₂ storage, the development of CO₂ injection networks model is an important step in understanding the transporting and injection of CO₂. The main goal of this thesis is to model a synthetic case based on Snøhvit CO₂ storage. Obtain results using GAP and Prosper which are software primarily developed for oil and gas applications. Carryout sensitivity analyses by varying parameters such as injection pressure, temperature, injectivity index, wellhead choke, etc., and predict CO₂ characteristics throughout the pipeline

The modeling of subsea CO₂ transportation and injection pipe networks is a topic covered in very little literature. In light of this, some sections of this thesis were dedicated to reviewing the literature on the sources of CO₂, the history of carbon capture and storage (CCS), CO₂ thermodynamics, Equation of State (EoS), Inflow Performance

Relationship (IPR), Vertical Lift Performance (VLP), history of multiphase flow in pipes, review of Integrated Production Modelling software (IPM) including PVTp, Prosper, and GAP used to create the model.

The result section of this thesis presents the results of the simulation. The phase envelope, hydrate line, temperature gradient, IPR, and VLP plots are all reported and analyzed. Sensitivity analyses including varying parameters such as injection pressure and temperature, injectivity index, wellhead choke, initial reservoir pressure, flowing bottom hole pressure, etc., and CO₂ phase characteristics throughout the 148km long pipeline are analyzed, future research plans and recommendations are also presented. The result of the simulation can be applied in various stages, including design, operational management, and optimization of CO₂ transportation and injection.

Preface

It is with great pleasure that I present my Master's thesis titled "Modeling of Subsea CO₂ Transportation and Injection Networks." My research aligns with the Subsea Production and Processing (SUBPRO)-ZERO goal, which seeks to reduce greenhouse gas emissions by promoting carbon capture and storage (CCS) technologies. This thesis represents my contribution towards this noble goal, and I am grateful for the opportunity it has provided me to contribute to a cause that is important to society and the environment.

I am deeply indebted to my supervisor, Professor Milan Edvard Wolf Stanko, for his guidance and support throughout this project. His vast experience and expertise in the field of petroleum engineering have been invaluable to me, and I am grateful for the time and energy he invested in my development as a researcher. I would also like to express my appreciation to the Norwegian government for providing free education to all international students. This opportunity enabled me to pursue my academic goals at the Norwegian University of Science and Technology and has been a critical factor in my academic success. Lastly, I would like to thank all the students at the Department of Geoscience and Petroleum for their support and encouragement throughout my studies. The intellectual atmosphere and camaraderie of the department were a source of inspiration and motivation for me, and I am grateful to have been a part of such a vibrant academic community. Throughout my thesis work, I had to learn and utilize various features of Integrated Production Modelling software (IPM), including PVTp, Prosper, and GAP. The knowledge and skills I acquired through using these tools will be invaluable as I continue my career in the field of petroleum engineering.

I express my gratitude to Almighty God for every success I have experienced in my life. I extend my appreciation to my late father, Azebeokhai Paul Ivienagbor Imo-ore, my mother, Regina Azebeokhai, my sister and husband, Mr & Mrs. Melody Hannah Aikhoin, my niece, Anita Eghonghon Melody, my brothers, Timothy Azebe and David Iroborghena Azebe, my fiancée, Joan Oritsjolomi Mode, and the entire family. I also want to acknowledge the Churches of Christ. Thank you all for your support and blessings.

List of Abbreviations

AOF	=	Absolute Open Flow [Sm^3/d]
FBHP	=	Flowing Bottom Hole Pressure [Bara]
IPR	=	Inflow Performance Relationship
VLP	=	Vertical Lift Performance
TVD	=	True Vertical Depth [m]
MD	=	Measured Depth [m]
CCS	=	Carbon Capture and Storage
EOR	=	Enhance Oil Recovery
CCUS	=	Carbon Capture Utilization and Storage
PVT	=	Pressure Volume Temperature
P-T	=	Pressure Temperature
CO ₂	=	Carbon Dioxide
PPM	=	Parts Per Million
EoS	=	Equation of State
PR	=	Peng-Robinson
LNG	=	Liquefied Natural Gas
SRK	=	Soave-Redlich-Kwong
PPM	=	Parts Per Million
PDO	=	Plans for Development and Operation
NGL	=	Natural Gas Liquids
IPM	=	Integrated Production Modelling software

Nomenclature

$\alpha(T)$	=	EOS parameter correction term
γ	=	Specific gravity
ω	=	PVT observation data or acentric factor
π	=	Pi
μ_g	=	Gas viscosity [cp]
α	=	EOS parameter
A	=	EOS parameter or area of phase envelope
b	=	EOS parameter [-]
a	=	EOS parameter
B	=	EOS parameter
c	=	Volume shift
$m(\omega)$	=	EOS parameter correction term
p	=	Pressure [bar]
P_c	=	Critical pressure
T	=	Temperature
T_c	=	Critical temperature
T_R	=	Reduce temperature
v	=	Molar volume
P_{wf}	=	Flowing Well pressure [Bar]
P_{wh}	=	Flowing Wellhead pressure [Bar]
P_{compr}	=	Compressor Pressure [Bar]
$\Delta p_{flowline}$	=	Change in Flowline Pressure [Bar]
Δp_{tubing}	=	Change in tubing Pressure [Bar]
p_r	=	Reservoir pressure [Bar]
r_e	=	External radius [m]
r_w	=	Well radius [m]
K	=	Permeability [md]
h	=	Height [m]
J	=	Injectivity [sm ³ /d/bar]
dp	=	Pressure gradient [bar]
dz	=	Elevation gradient
Z	=	Compressibility factor
V	=	Volume
R	=	Universal gas constant
m	=	Mass
\bar{P}_R	=	Average reservoir pressure [bar]
q_{sc}	=	Flow rate [Scf/d]
N_{Re}	=	Reynolds number
$\frac{mv_1^2}{2g_c}$	=	Kinetic Energy

Contents

Summary	iii
Preface	v
List of Abbreviations	vii
Nomenclature	x
Contents	xi
Figures	xv
Tables	xxi
1 Introduction	1
1.1 Field Overview	2
1.2 Objective	3
1.3 Structure of The Report	3
2 Theory	5
2.1 Sources of CO ₂	5
2.2 A History of The Development of CCS Projects	7
2.2.1 CCS Project Categories	9
2.3 Phases of Carbon Capture and Storage	9
2.3.1 CO ₂ Capture	9
2.3.2 CO ₂ Transportation	10
2.3.3 CO ₂ Storage	11
2.4 CO ₂ Thermodynamics	11
2.5 Engineering Considerations and Overview	13
2.5.1 Modeling Fluid Properties for Accurate Prediction of Pressure and Temperature Changes along the Pipeline	16
2.5.2 Nodal Analysis of Injection Wells	17
2.5.3 Inflow Performance Relationship (IPR) Curve	19
2.5.4 Vertical Lift Performance (VLP) Curve	21
2.5.5 Flow in Pipes	22
2.5.6 Basic Equations and Concepts	22
2.5.7 History of Multiphase Flow in Pipes	24
2.5.8 Pressure Drop Through Restriction	26
2.6 The Model-Building Software	28

2.6.1	Prosper Software	29
2.6.2	GAP Software	30
2.6.3	PVTp Software	30
3	Methodology	33
3.1	The Injection System	34
3.2	Case Assembly	35
3.2.1	PVTp Software	36
3.2.2	Prosper Software	38
3.2.3	Options Summary	40
3.2.4	PVT Data	41
3.2.5	IPR Data	43
3.2.6	Equipment Data	47
3.2.7	Analysis Summary	50
3.2.8	Generating VLP Curves	52
3.2.9	GAP Software	56
3.2.10	Imputing Data Into The GAP Model	60
4	Result And Discussion	65
4.1	CO ₂ Phase Envelope	65
4.2	Inflow Performance Relationship IPR Plot	67
4.3	System IPR + VLP	68
4.4	Case Study	69
4.5	Case 1 - Based Case - Homogeneous Formation	70
4.6	Base Case's Analytical Results	71
4.6.1	Variations in Pipeline Pressure (80bar Injection Pressure)	71
4.6.2	Pipeline's pressure variance with different pipe correlations (80 & 100bar Injection Pressure)	73
4.6.3	Friction-induced pressure drop in the 148km pipeline (80 & 100bar Injection Pressure)	74
4.6.4	Variations in Temperature Along the Pipeline (80 & 100bar Injection Pressure at 23 °C & 15 °C)	76
4.6.5	Fluid Phase Transition Along The Pipeline (Injection Pressure 80bar) 78	
4.6.6	Variations in Density Along the Pipeline (80 & 100bar Injection Pressure)	79
4.6.7	Velocity variation along the pipeline (80 & 100bar Injection Pressure at 23 °C & 15 °C)	80
4.6.8	Well Simulation Result (80 & 100bar Injection Pressure at 23 °C & 15 °C)	81
4.6.9	Bottom-Hole Pressure Varied by Pressure and Temperature (80 & 100bar Injection Pressure at 23 °C & 15 °C)	82
4.7	Case Two - Heterogeneous Formation	83
4.7.1	Comparing Injectivity Index in Two Formation (Injectivity 9 & 4.5[t/h/bar] at 80bar & 100bar)	84
4.7.2	Comparing Injectivity Index in Three Formation	85
4.7.3	Pressure Analysis Post Choking of Wells	87

4.8 Case three - Increase in reservoir pressure from 300 to 310bar	88
Conclusion	91
Future Research Recommendations in Subsea CO₂ Transportation and Injection Systems	93
Bibliography	95
A Additional Material	101
A.1	102

Figures

1.1	Advanced Subsea Equipment For CO ₂ Injection At Snøhvit. Image: Statoil, https://www.tu.no/artikler/nytt-co2-prosjekt-pa-snohvit/233578	3
2.1	Shows emissions by source, share, and possible technologies that can address most of the oil and gas industry emissions. [9]	6
2.2	Historical record of global CO ₂ emissions compared with various projections [10]	7
2.3	A Portfolio of Commercial CCS Facilities in Various Power and Industrial Applications Facilities Include Those in Operation, Under Construction and in Advanced Development. Area of Circles Is Proportional to Current CCS Capacities. Source is https://www.globalccsinstitute.com/wp-content/uploads/2021/03/Global-Status-of-CCS-Report-English.pdf	8
2.4	The three main stages of CCS technology [10]	10
2.5	Phase diagram of pure CO ₂ as a function of pressure and temperature, with wellhead and bottom hole situations for Snøhvit, shown as arrows, and reservoir conditions indicated as shaded areas. At Sleipner, the CO ₂ cools down in the reservoir, while it warms up at Snøhvit [34]	12
2.6	Phase diagram for CO ₂ in combinations with other gas [36]	13
2.7	Nodal Analysis Gas Injection Well [42]	19
2.8	Production System Analysis [42]	20
2.9	Possible Pressure Losses In Complete System [42]	22
2.10	Flow System Control Volume [42]	23
2.11	Evolution of multiphase flow modeling, showing a selection of the more widely used models. The timeline (x-axis) is associated with two criteria: Flow Equation Formulation (upper) and Engineering Application (lower). The vertical axis increases with model complexity and is subdivided into five general categories	24
2.12	Shows the variation of liquid holdup with pipe inclination is for the tests conducted by Beggs and Brill [42]	27
2.13	Flowchat For Prosper Model [53].	32

3.1	Snøhvit Field Cross Section: Visual representation showcasing the geological strata, subsurface formations, and reservoir structures within the Snøhvit natural gas field, offering insights into its geological composition and hydrocarbon reservoir dynamics. [32]	33
3.2	Illustrative schematic outlining the CO ₂ separation process specifically designed for Melkøya, providing a visual representation of the intricate steps involved in the separation and capture of CO ₂ [32]	34
3.3	Graphical representation outlining the key operational parameters and geographical layout of the CO ₂ injection pipeline within the Snøhvit project.[32]	35
3.4	Detailed representation of the Snøhvit pipeline configuration, encompassing its structural attributes, specifications, and network topology, within the GAP software. This profile serves as a crucial foundation for conducting accurate and thorough simulations, allowing for an in-depth analysis of fluid dynamics, pressure variations, and transport efficiencies within the pipeline system.	36
3.5	Schematic Illustration of the Snøhvit Simulation Case Study: Depicting the Injection manifold, pipeline, flowline, templates, and the injection wells components for comprehensive analysis and simulation	37
3.6	The PVTp software user interface displays distinct sections including File, Home, Panel Actions, Characterisation, and Calculation interfaces.	37
3.7	Key Steps for Accurate EoS Development Using PVTp Toolkit: Essential Components for Fluid Characterization	38
3.8	Sample Export File (.PRP) from IPM EoS Composition Export Option in PVTp for Prosper	39
3.9	Snøhvit Well Modeling Procedure in Prosper: Sequential Model Setup and Main Screen Organization. The figure shows Prosper's main screen layout order and initiation process	39
3.10	The objective of the setup is to obtain the properties of the "well stream" gas from the separated gas, tank-vented gas, and condensate [53]	40
3.11	shows Initiating Prosper Model: Configuring Well type, adjusting the fluid type and Equation of State setup, calculation method.	41
3.12	Setting Equation of State Options: EoS setup, Peng Robinson as the EoS model. Utilize the Lohrenz, Bray Clark method for fluid viscosity calculations. Set reference temperature and pressure.	42
3.13	This dialog is used to enter/edit/view the fluid composition. Called from the PVT section of PROSPER this dialog allows you to enter the number of components as well as their names. One can then enter the various properties per component. There are additional dialogs which can be accessed from this screen	43
3.14	Shows the Inflow Performance Relationship (IPR) data input menu, this figure describes how Prosper defines the reservoir inflow performance	44
3.15	Allows general reservoir parameters such as pressure, temperature, water cut and GOR to be defined.	45

3.16	Allows an externally generated IPR data set to be imported or directly entered	46
3.17	The IPR curve shows both the variation in bottom hole pressure and bottom hole temperature	47
3.18	show the menu option used to define the well hardware, deviation survey, and formation temperature profile	47
3.19	Allows the user to enter the well deviation survey, measured depth (MD), and the corresponding true vertical depth (TVD). Up to 20 pairs of data points can be entered	48
3.20	Show the Downhole Equipment screen, which enables the down-hole completion data to be entered.	49
3.21	Show the Formation Temperature Gradient screen, the screen enables entry of the flowing temperature profile of the fluid in the well	49
3.22	displays the Analysis Summary section, providing access to both the System Sensitivity Analysis and the VLP section.	50
3.23	Shows the System Calculation input screen which combines the VLP and IPR plots to find the system point at which the well will flow.	51
3.24	Show the Interface for Inputting data and Multiphase Flow Correlation for IPR and VLP Curve Calculation	51
3.25	Shows the VLP screen, which allows the user to generate VLP curves for ranges of different variables. which can then be exported to several different formats.	52
3.26	Show the Interface for Inputting data and Multiphase Flow Correlation for generating Lift Curve	53
3.27	Show the Interface for selecting Sensitivity case variables, and the corresponding variable data	53
3.28	Shows a sample of the VLP Curves, generated for different sensitivity case variables with variable data	54
3.29	Display the screen for Lift Curve Export, where users can choose the export format.	55
3.30	Present a sample of the Exported Lift Curve in TPD file format, intended for import into GAP for simulation.	55
3.31	Shows the user interface consisting of a framework window that contains several child windows, as well as the menu and toolbar from which GAP commands are issued. The child windows include the system windows that contain the system network drawing, and the navigator window that can assist in the viewing of large networks.	56
3.32	Is where the overall system parameters are set up, including the type of system (Production or injection), the prediction mode, and various options on the optimization process.	57
3.33	Shows the section of the Toolbar, It consists of a row of icons that act as accelerators to common menu functions, or allow the addition or manipulation of network icons in the system window.	58
3.34	The screenshot provides an option for the user to choose equipment types.	58

3.35 Is where the overall pipe parameters are set up, including the length, diameter, roughness, and topography. 60

3.36 The figure provides an option for the user to define the type of fluid (water, steam, oil, and gas) and modify the properties by selecting "Edit List". The PVT properties of the source are displayed at the bottom of the screen and by selecting "composition". 61

3.37 GAP Summary Screen, How To Input Prosper File To GAP 62

3.38 The Figure displays a prompt that enables the users to choose between generating IPRs for all Wells or only a selected few 62

3.39 This screen allows the user to specify the data file that contains the VLP tables of the Well 63

3.40 The user can input the injection pressure, then specify the calculation mode, and then solve the system by selecting calculate. 64

4.1 This graph represents the phase diagram of the model's fluid composition, indicating its behavior as a two-phase system. Composing of 98% mole of CO₂ and 2% mole of methane. 65

4.2 The hydrate plot is indicated by the red line in the plot, The injected fluid temperature must be at or above 23°C which is higher than the temperature at which hydrates are formed. To prevent hydrate formation, the temperature of the injected fluid must be above 23°C; otherwise, kinetic inhibitors that act to slow down the formation of hydrate crystals should be added 66

4.3 To illustrate the anticipated rise in temperature as the fluid descends the well. The traverse plot provides a detailed representation of the temperature gradient along the well's depth. 67

4.4 The IPR plot shows the bottom hole pressure variation as a function of rate, this is depicted in the plot by the blue line. The temperature plot, represented by the red line, also displays the change in bottom hole temperature as a function of rate. 68

4.5 Shows how the model predicts the well rate if the wellhead pressure is 100 bar and the WGR and CGR are zero, then the model predicts that the well will flow at approximately 1600 1000Sm³/day and that the corresponding solution node pressure is 326 bar 69

4.6 Illustrate how the model predicts the well rate if the wellhead pressure is 100 bar and the WGR and CGR are zero, then the model predicts that the well will flow at approximately 2739.315 1000Sm³/day and that the corresponding solution node pressure is 323.69 bar 70

4.7 Illustrate how the model predicts the well rate if the wellhead pressure is 100 bar and the WGR and CGR are zero, the model predicts that the well will flow at approximately 3400 1000Sm³/day and the corresponding solution node pressure is 320 bar 71

4.8 Shows a comprehensive representation of the pipeline network, extending from the injection manifold through the flowline, reaching the templates, and subsequently channeling into the six injection wells 72

4.9 The plot shows pressure change along the pipeline, as a function of elevation. Higher elevations cause increased pressure, resulting in pressure loss, and decreases with decreasing elevation. Most pressure loss happens at two main elevation points. 73

4.10 The simulation studied seven different pipeline correlations available in GAP for a 148 km pipeline at two injection pressures (100 bar and 80 bar). The graph shows a consistent pattern among all correlations, indicating their effectiveness in predicting pressure drop despite varied conditions like irregular topography. 74

4.11 The plot depicts friction loss along the 148km pipeline at 100bar and 80bar injection pressure, higher injection pressure leads to increased friction loss, with 100bar showing higher losses than 80bar. Moreso Longer pipes usually exhibit more friction loss compared to shorter ones 75

4.12 shows how temperature changes with different injection temperatures and pressures along a pipeline. At 23°C and 100 bar, the temperature drops to 10°C over 50 km, remaining steady to the end. At 23°C and 80 bar, it stabilizes at 10°C by 30 km. In the second scenario, For 15°C injecting at 80 bar and adjusting to 100 bar, the temperature quickly drops to 10°C. The 80 bar injection pressure causes a faster temperature decrease than 100 bar, regardless of the injection temperature (23°C or 15°C). . . . 77

4.13 The pure CO₂ phase diagram is depicted by the blue line. The three dots on the graph correspond to various points along the pipeline. Based on the graph, it can be inferred that the CO₂ remains in the liquid phase along the whole 148 km pipeline, 78

4.14 The CO₂ density increases with higher injection pressures. At 80 bar injection pressure, the density fluctuates along the pipeline due to elevation changes, varying between 774 kg/m³ and 884 kg/m³. A similar trend is observed at 100 bar injection pressure, where the density also rises and falls in relation to elevation alterations along the pipeline. 79

4.15 shows CO₂ velocity changes along a 148km pipeline at 100 bar and 80 bar injection pressures and temperatures of 23°C and 15°C. Initially, at 100 bar and 23°C, velocity drops from 1.19 m/s to 1.08 m/s over 20km, below the 15°C velocity. At 80 bar, velocities range from 0.873 m/s (15°C) to 0.916 m/s (23°C), ending at 0.81 m/s (23°C) and 0.83 m/s (15°C). lower temperatures exhibit higher velocities compared to higher temperatures . 81

4.16 Compares injection pressures at 80 bar and 100 bar pressures, showcasing temperatures of 15°C and 23°C. At 80 bar and 23°C, the rate is 2422 MSm³/day, while at 15°C, it exceeds this by 58.426 MSm³/day, highlighting the temperature’s impact. Similarly, at 100 bar and 23°C, the rate is 3311 MSm³/day, but at 15°C, it rises to 3357 MSm³/day, reinforcing the temperature’s advantageous effect on injection rates 82

4.17 displays bottom hole pressures at 2798 meters for injection pressures of 100 bar and 80 bar at temperatures of 15 ^o C and 23 ^o C. Differences between 80bar and 100bar injection pressures are evident. However, temperature variations at the same pressure show minimal impact, with a slight difference of 0.56 bar between 15 ^o C and 23 ^o C at 80 bar, the former exhibiting slightly higher pressure.	83
4.18 Comparison of injection rates between Templates 1 and 2 at 100 bar and 80 bar manifold pressures, highlighting varied injectivity impacts on injection rates within different formations.	84
4.19 Implementation of 14 bar and 21 bar Differential Pressure (DP) Chokes on Template 1 wells for equitable injection rates at 80 bar and 100 bar manifold pressures, respectively	85
4.20 Relationship between injectivity index and injection rates of six wells at 80 bar manifold pressure. Higher injectivity wells (Wells 3 and 6) show the highest rates at 3477 MSm ³ /day, followed by Wells 2 and 5 at 2517.645 MSm ³ /day, and Wells 1 and 4 at 1076 MSm ³ /day."	86
4.21 Illustration of choke implementation on Wells 3, 4, 5, and 6, while Wells 1 and 2 remain unchoked. A maximum injection rate limit of 1800 MSm ³ /day was set for Wells 3, 4, 5, and 6, with the choking mechanism automatically adjusting pressure drops to attain the Specified rates	87
4.22 Shows increased pipeline pressure post-choke on high-injectivity wells along the 148km line (red line) compared to pre-choke (blue line)	88
4.23 Comparison of two reservoirs at 300 bar and 310 bar reservoir pressures under varying manifold pressures. At 50 bar, no injection occurred. At 60 bar, Reservoir 1 injected at 1063 Msm ³ /day, while Reservoir 2 had no injection. At 80 bar, Reservoir 1 reached 2480 Msm ³ /day, and Reservoir 2 achieved 2090 Msm ³ /day injection rates.	89
A.1 Hydrodynamic performances of the CO ₂ pipeline in the Base Case (a) pressure change (b) temperature change (c) density change and (d) flow velocity change, along with transport [56]	101
A.2 Pressure drop of the pipeline with a sloping angle [56]	102
A.3 shows a comprehensive representation of the pipeline network, extending from the injection manifold through the flowline, reaching the templates, and subsequently channeling into the six injection wells, in this case all wells have different injectivity, and some wells are choked.	103
A.4 Flowing bottom hole pressure and reservoir pressure history throughout the snøhvit injection well [55]	105

Tables

3.1	Gas Injection Rate Calculation	46
3.2	An expansive overview showing the range of simulations carried out for the three primary cases, offering a comprehensive view on the conducted analyses.	64
4.1	Pipeline Description Table	72
A.1	Composition Table I	103
A.2	Composition Table II	104
A.4	Shows Prosper supported Export formats	104
A.3	Inflow Performance Relationship (IPR) methods available in Prosper . . .	106

Introduction

The transportation and injection of carbon dioxide (CO₂) into subsea reservoirs is an important process for carbon capture and storage (CCS) projects. Carbon capture and storage is a process that aims to mitigate climate change by capturing carbon dioxide (CO₂) emissions from large industrial sources such as power plants, Liquefied Natural Gas (LNG) plants, cement factories, etc, and storing them underground. One of the key components of CCS project is the transportation and injection of CO₂ into subsea reservoirs. This process involves the construction of a network of pipes that transport the captured CO₂ from the capture site e.g (Melkøya LNG Plant) to the subsea reservoir where it is injected and stored e.g the Tubåen sandstone formation at Snøwhit field.

To ensure the success of CCS projects, accurate modeling of the subsea CO₂ transportation and injection pipe networks is critical [1]. This modeling involves a complex set of calculations and simulations that take into account factors such as the physical properties of the CO₂, the geological characteristics of the reservoir, the depth of the reservoir, the pressure and temperature conditions, and the overall system design [2]. The accuracy of the modeling is important for several reasons. First, it ensures that the CO₂ is transported and injected into the reservoir safely and efficiently, minimizing the risk of leaks or other accidents. Second, it helps to optimize the system design and operation, which can reduce costs and increase the overall effectiveness of the CCS project [3]. Finally, accurate modeling can help to ensure that the CO₂ is stored in the reservoirs for long periods, which is essential for the success of CCS as a climate mitigation strategy. Overall, the transportation and injection of CO₂ into subsea reservoirs is a crucial process for CCS projects, and accurate modeling of the subsea CO₂ transportation and injection pipe networks is essential to ensure their success.

Currently, an integrated model (IM) stands as a sophisticated and efficacious solution for a modeling approach that combines various elements, including reservoir and wells, well clusters/templates, and surface facility models into a single, integrated system. The integrated model can simulate the behavior of a CO₂ injection project, including the injection rate, and the transport of CO₂ through pipelines and surface facilities, and can

also incorporate various uncertainties and sensitivities into the model. The model can also account for various factors that affect CO₂ storage capacity and injection efficiency. This allows engineers to better understand and optimize the injection performance of the entire system.[3]

This thesis will use Integrated Production Modelling software (IPM) including PVTp, Prosper, and GAP to create the subsea CO₂ transportation and injection networks model. GAP is a multiphase oil and gas optimizer tool that models the surface gathering network of field production systems when used in conjunction with other software programs such as Prosper. GAP allows for comprehensive field optimization and forecasting. Prosper is a Well modeling software that can simulate well performance and predict flow rates and injection rates. By combining the outputs from Prosper with GAP, engineers can obtain a comprehensive understanding of the entire field production/injection system, including how the reservoir, wells, and surface equipment interact.

1.1 Field Overview

The thesis uses as a study case the Snøhvit field. The Snøhvit development comprises three fields, Snøhvit, Albatross, and Askeladd. These are located in the Barents Sea, about 140 kilometers northwest of Hammerfest in northern Norway. All primarily contain natural gas with small quantities of condensate. The estimated recoverable reserves are 193 billion m³ of natural gas, 113 million barrels of condensate (light oil), and 5.1 million tonnes of natural gas liquids. The gas contains 5-8 mol percent CO₂, which is reduced to less than 50 parts per million (ppm) before the liquefaction process. Geological storage was evaluated already and documented in 1991 and later in 2000, the full CO₂ storage concept was described in the plans for development and operation (PDO) document in 2001. Ocean storage was considered in Kårstad 1999. In 2005 the injection well 7121/4- F-2H was drilled, and a 148 km long pipeline was laid from Melkøya to the F-template. Snøhvit came on stream in August 2007[4]

The field is produced by pressure depletion. The Snøhvit gas field sits under 300m of water, where engineers felt it impractical to build platforms. Snøhvit is the first major development on the Norwegian continental shelf without surface installations. The installations are all subsea. Currently, gas is produced from nine wells, the well stream, with natural gas, CO₂, natural gas liquids (NGL), and condensate, is transported in a 152-kilometre pipeline to the liquid natural gas (LNG) processing facility at Melkøya near Hammerfest where the CO₂ is stripped from the methane, compressed to supercritical state. The CO₂ is pumped again back offshore by a pipeline of about 148km for injection into the aquifer(Stø reservoir) through a single well, see Figure 1.1 for details of the subsea equipment and Figure 3.1 for the Snøhvit field cross-section. The reservoirs lie at a depth of 2,300 meters and have moderate to good quality. The pipeline route is characterized by an uneven seabed the first 20 km from shore and pockmarks and iceberg plough marks at the field see Figure 3.3. The soil varies from hard clay closest to the shore, sand in the midsection, and soft clay at the field. The maximum water depth

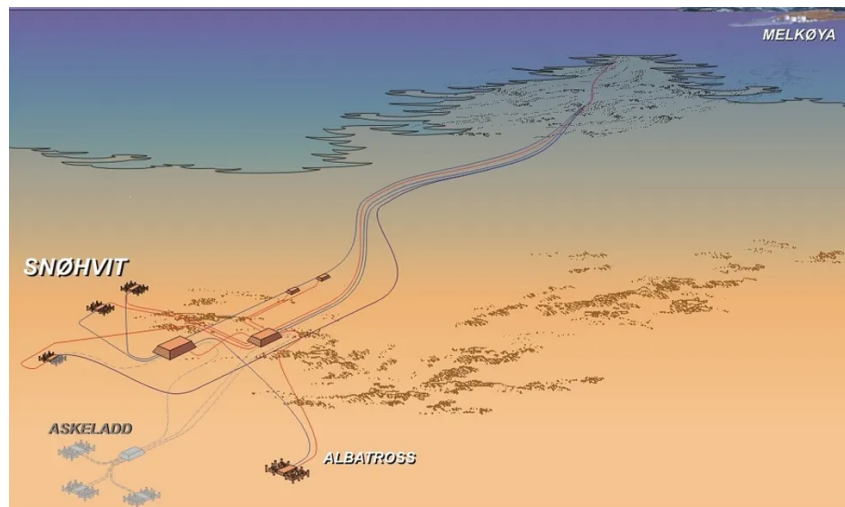


Figure 1.1: Advanced Subsea Equipment For CO₂ Injection At Snøhvit. Image: Statoil, <https://www.tu.no/artikler/nytt-co2-prosjekt-pa-snohvit/233578>

is approximately 345 meters at the field and 445 meters along the pipeline route. The pipeline uses special high-chromium steel alloy to avoid corrosion from CO₂.

1.2 Objective

The main goal is to model a synthetic case based on Snøhvit CO₂ storage and obtain results using GAP and Prosper which are software primarily developed for oil and gas applications. Sensitivity analyses are done by varying parameters such as injection pressure, temperature, injectivity index, wellhead choke, etc., and predict CO₂ characteristics throughout the pipeline.

1.3 Structure of The Report

Chapter 1 provides an introduction to the background and objectives of this thesis. The chapter presents a succinct overview of the Snøhvit field and the software utilized in this study, emphasizing the significance of modeling. The section concludes with a detailed description of the report's organizational structure.

Chapter 2 presents the fundamental theory underpinning this research project. This chapter explores key concepts, including production potential and mathematical optimization, essential for a comprehensive understanding of the research topic.

The strategy to accomplish the goal was covered in Chapter 3. The process for creating PVT tables for use in the simulation, the modeling of the well and every feature of

the well bore model, and the models of the entire field surface network design included the methodology.

The main focus of Chapter 4 was the simulation results, which included temperature changes throughout the 148km pipeline, pressure changes along the pipeline, fluid phase changes along the pipeline, etc, and consideration of various pipe correlations. Every outcome is shown graphically.

Chapter 5: contains the thesis report's conclusion.

Theory

2.1 Sources of CO₂

Before the industrial revolution, the atmospheric CO₂ concentration was around 280 parts per million (ppm). Due to industrialization from the 18th century, this concentration has climbed to a record high of 415 ppm in 2019. Among the greenhouse gases, carbon dioxide (CO₂) is the most important in terms of quantity emitted [5]. Fossil fuels account for about three-quarters of the increase in anthropogenic CO₂ emissions while the remainder is attributed to land-use changes such as deforestation. The recent surge in CO₂ concentration is caused by major sources of CO₂ emissions, such as sizable fossil fuel power plants, cement and steel mills, biomass energy facilities, and synthetic fuel plants. Due to increases in the concentration of CO₂, global averaged land and ocean surface temperatures are currently 1.0°C higher than preindustrial levels, with a predicted range of 0.8°C to 1.2°C see Figure 2.2. The severity of this increase in CO₂ levels has reached a point where it threatens human survival and growth, despite many calls and actions towards reduction in emissions, the only thing that has been achieved is a reduction in the rate of emission [6].

The Intergovernmental Panel on Climate Change (IPCC) on Oct 6, 2018, reported that the world is headed for a painful problem sooner than expected, as emissions keep rising. The scientific findings from the main report are summarized in a 34-page document, approved by all representatives from 195 nations [6]. The report highlights that the planet is already 1°C warmer and we are witnessing extremely chaotic weather patterns. Global temperature is likely to reach 1.5°C in as little as 11 years in 2030 [7]. Despite that under the 2015 Paris Agreement, every country in the world agreed to keep the global temperature well below 2°C, however, the current trend is showing that the global temperature will more likely reach 3°C by 2100 [8]. The IPCC special report shares various pathways to stabilize global warming at 1.5°C. The first one is "*No more fossil fuel, cut their use by 50% in less than 15 years and eliminate them almost entirely in 30 years*"[6]. Considering this fact, the energy industry must step in to make the use of

fossil fuels greener.

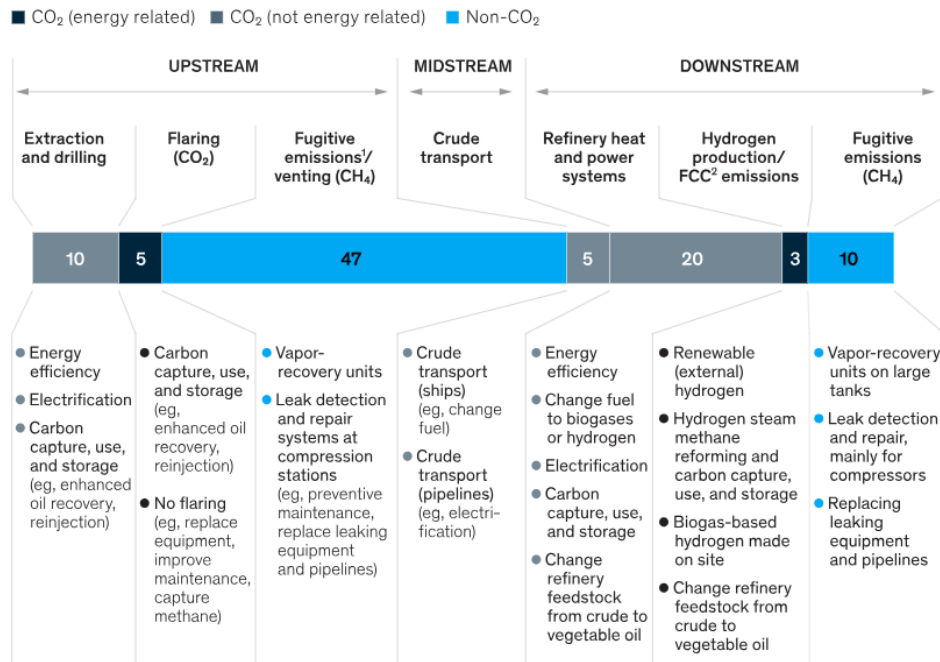


Figure 2.1: Shows emissions by source, share, and possible technologies that can address most of the oil and gas industry emissions. [9]

The oil and gas industry must cut emissions by at least 3.4 gigatons of carbon dioxide equivalent (GtCO₂e) annually by 2050 in order to contribute to climate change mitigation to the required degree. Reaching this target would clearly be easier if the use of oil and gas declined. But even if demand does not fall much, the sector can abate the majority of its emissions and help other industries like cement and power plants to do so through the use of carbon capture and storage (CCS). In this market, the oil industry is well placed to lead because it already uses carbon captured via Carbon Capture Utilisation (or sometimes this is termed 'usage') and Storage CCUS for use in enhanced oil recovery (EOR). The dominant arguments for why CCS is vital for achieving the overall greenhouse gas reduction objectives are multi-dimensional. CCS can provide a mechanism for decarbonizing existing power supply and emissions from industries like cement and steel. The implementation of CCS can also result in economic profitability since it allows for the energy transition to be achieved at a faster pace, and at a cheaper cost than by solely relying on renewable energy sources. These arguments imply that CCS is a vital approach to reducing global emissions [10]

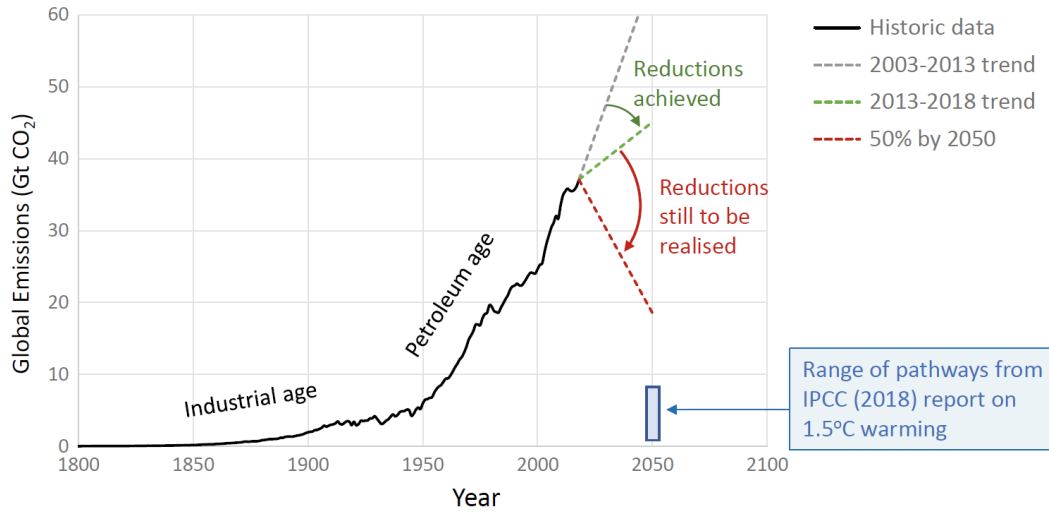


Figure 2.2: Historical record of global CO₂ emissions compared with various projections [10]

2.2 A History of The Development of CCS Projects

CO₂-Enhanced Oil Recovery (EOR) has been carried out in the United States and Canada since the 1960s. The world's first large-scale CO₂-EOR project Scurry Area Canyon Reef Operating Committee (SACROC), was implemented by Chevron in the oilfield in Scurry County, Texas on January 26, 1972 [11]. The CO₂ for this project came from the natural CO₂ fields in Colorado and is pipelined to the oilfield for flooding. More than 175 million tonnes of natural CO₂ in total were injected in the SACROC project during 1972–2009 [12]

Marchetti [13] was the first to suggest the idea of CO₂ capture, transport, and storage in the contemporary sense as a way to lower anthropogenic CO₂ emissions [14]. The first international demonstrations of the large-scale capture, utilization, and storage of anthropogenic CO₂ emissions were the Sleipner Carbon Capture and Storage project, which started CO₂ injection in September 1996, and the Weyburn–Midale CO₂ Monitoring and Storage Project (also known as the Weyburn Project), which started in 2000 as part of the IEA Greenhouse Gas (IEAGHG) Research and Development Programme. [15–17]

The Sleipner Carbon Capture and Storage project, which is a scientific research and large-scale commercial demonstration project implemented by Equinor under the influence of the Norwegian carbon tax policy, captures the CO₂ separated in the natural gas purification process and injects it into deep saline aquifers for storage and emission reduction. The project has stored more than 20 million tonnes of CO₂ in total since 1996. The project has carried out advanced monitoring for 20 consecutive years and has achieved remarkable scientific research results [18].

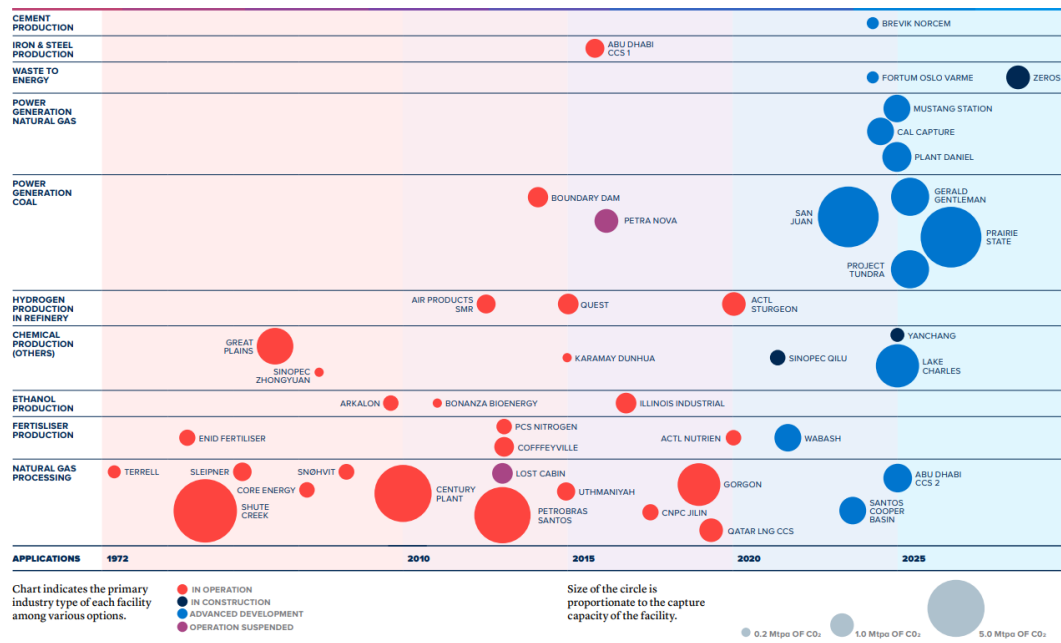


Figure 2.3: A Portfolio of Commercial CCS Facilities in Various Power and Industrial Applications Facilities Include Those in Operation, Under Construction and in Advanced Development. Area of Circles Is Proportional to Current CCS Capacities. Source is <https://www.globalccsinstitute.com/wp-content/uploads/2021/03/Global-Status-of-CCS-Report-English.pdf>.

The Weyburn project is the world's most complete multidisciplinary scientific research project on the geological storage of CO₂. It has been ongoing for 12 years and has safely stored over 35 million tonnes of CO₂ since October 2000. The Weyburn Project is conducted at the largest geoscience test site in the world, which was established in the Weyburn field in Southern Saskatchewan, Canada, with the joint support of Natural Resources Canada, the US Department of Energy, the Saskatchewan government, and other government agencies and enterprises. After completion of the planned scientific research, the project has been converted into a commercial project. The success of the Weyburn Project has established the irreplaceable role of Carbon Capture Storage technology in reducing greenhouse gas emissions. Firstly, it is the world's first project to carry out the large-scale capture and long-distance transportation of low-cost and high-concentration CO₂ from the use of coal (that is, the Dakota Gasification Company) for EOR and storage. It has demonstrated that it is possible to use CCS technology to reduce the CO₂ generated by coal which contributes the highest proportion of carbon emissions in fossil energy use on a large scale.[15, 19, 20]

2.2.1 CCS Project Categories

CCS projects can be categorized in different ways, with that of the Global CCS Institute (GCCSI) being the most well-known [21]. The GCCSI takes projects that capture, transport, and store 400 kt/a CO₂ from industrial emission sources, or projects that capture and store 800 kt/a CO₂ from coal fired power plants, as the threshold for large scale pilot testing, demonstration, or commercialization projects. According to the GCCSI 2020 report, there are currently 65 commercial projects in the world, 26 of which are in operation, while others are at different stages of development. CCS projects can also be classified according to the source of CO₂ that is, CO₂ from natural gas separation (e.g., Sleipner, Snøhvit), carbon capture in the coal chemical plant (e.g., Great Plains Coal Gasification Plant), hydrogen production in oil refining, coal power plants (e.g., SaskPower Boundary Dam and Petra Nova), carbon capture in steelworks (e.g., Al Reyadah), biomass energy capture (e.g., Decatur), and DAC (e.g., Carbfix and Climeworks, Heidelberg Cement's ongoing Norwegian Norcem's Brevik cement plant, and the Canada Lehigh Cement Company) see Figure 2.3 for details. Before going into details about the project, it's important to define the three key terms in CCS which are Carbon Capture and Storage.[12]

2.3 Phases of Carbon Capture and Storage

Carbon Capture and Storage refers to the set of interdisciplinary technical solutions for the removal of CO₂ from industrial processes, and to inject it into the subsurface (e.g Snøhvit) for isolation. The three main phases of Carbon Capture and Storage technology involve Capture, Transport, and Storage see Figure 2.4. These three components will be briefly discussed in the following section.

2.3.1 CO₂ Capture

Processes for extracting carbon dioxide from point sources of gas emissions, such as power stations, gas processing facilities, and other industrial facilities (particularly those that manufacture steel and cement), are referred to as CO₂ capture. Both pre-combustion and post-combustion collection systems are possible for CO₂ capture. The pre-combustion methods are all focused on extracting CO₂ from gas mixes that contain a sizable amount of CO₂. This involves removing CO₂ from natural hydrocarbon gas supplies and from industrial chemical operations that produce CO₂ as a byproduct (fertilizer plants, for example). The removal of CO₂ from the combustion gas streams (flue gas) is the focus of post-combustion technology.[10] The physio-chemical mechanisms that are employed to separate the gases can be utilized to categorize the capture processes:

- Solvent-based where an absorption liquid is used;
- Sorbent-based, where solid particles are used;
- Cryogenic, where different gas condensation temperatures are used;
- Membranes, where solid-state chemical barriers are used.

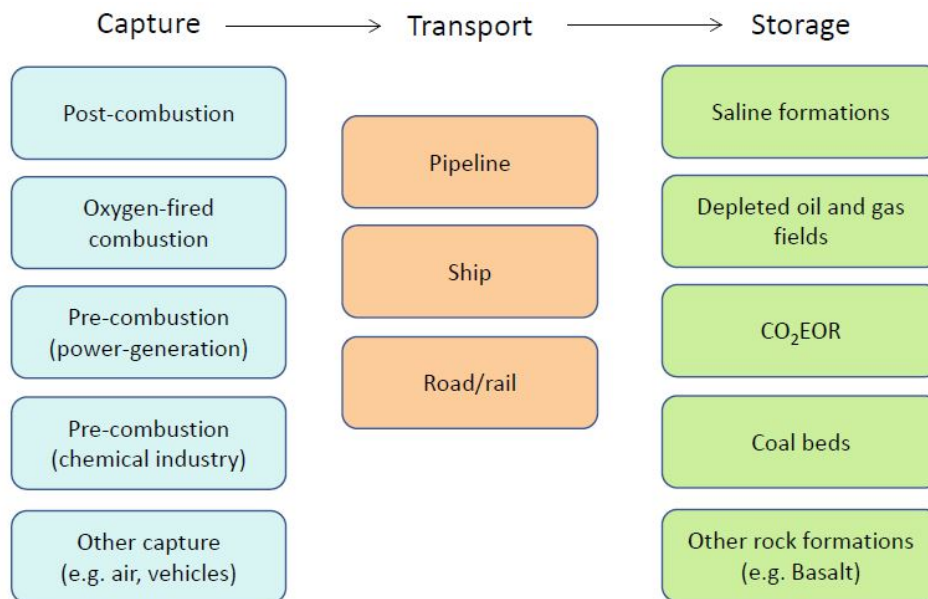


Figure 2.4: The three main stages of CCS technology [10]

The most common commercial CO₂ capture method to date has been solvent-based, with mono-ethanol-amine (MEA) serving as the solvent [10]. What is the composition, pressure, temperature, and flow rate of the captured CO₂-rich gas stream, and what is the regularity by which it will be supplied via the transport system? This question leads to the transportation methods and the amount that can be injected and stored underground at a given time.

Facts About Snøhvit

- During the process of separating CO₂ from natural gas at Melkøya the amine chemical and natural gas are led to a high-pressure/moderate-temperature tank.
- The amine binds to the CO₂ and is drawn off from the bottom of the tank. This is then led to another tank with less pressure and higher temperature. CO₂ will be separated and sent from the tank to the CO₂ injection system.
- The CO₂ is in liquid form when it is piped to the Tubåen sandstone formation for storage,

2.3.2 CO₂ Transportation

CO₂ transport technology involves handling the captured CO₂-rich gas/liquid streams and transporting the CO₂ to the injection wells for storage, using pipelines, ships, or road/rail see Figure 2.4 for details. In comparison to other gas or liquid transport systems, CO₂ transport is more difficult for several reasons. To remove CO₂ from flue gases, a way to get the gas from the source of the emission to a secure disposal site where it may

be stored indefinitely is needed [22]. Removal of CO₂ will result in enormous amounts that need to be disposed of. An average gas-fired power plant with a capacity of 1000 MW will release about three million tons annually, or roughly three million cubic meters of liquid. To put things in perspective, the anticipated annual total CO₂ emissions in Western Europe are almost 1000 times this volume. It is impossible to imagine transporting a liquid volume of 3mill.m³ of CO₂ by rail or road each year. An average LNG-type tanker will need to make about 30 calls a year to transport as much cargo via ship. But these are very expensive vessels, thus the cost of these vessels adds up to a high unit cost of transportation.[23] However, it is considered that pipeline transportation is the most practical option for moving such large amounts of CO₂ [24]. These pipelines can be modeled using GAP to analyze and assess the optimal pipeline distribution network as well as to investigate the CO₂ phase to facilitate effective injection. Be it pipelines, ships, or road/rail, all of these options for transportation are generally expensive, and the price goes up with distance. However, the implementation of large-scale solutions such as very large-diameter pipelines will result in a significant reduction in expenses.

Most research on CCS deals with capture technologies and storage possibilities. Although capture represents the highest cost and storage is critical with respect to security and long-term monitoring, still, there is still a need to identify and structure transportation alternatives, in order to analyse and evaluate future paths comprising CCS. Previous works on transportation of CO₂ have investigated the costs and capacities for pipelines [23, 25], but these investigations have not studied different transportation scenarios in order to evaluate paths for the development of CCS systems. Other work has investigated the technological aspects of CO₂ transportation by pipeline and by specially developed tank vessels at sea [26]. The risk and security issues related to pipeline transmission have also been investigated [24, 27].

2.3.3 CO₂ Storage

The phrase "CO₂ storage" describes the long-term, up to 1000-year-long geological storage of CO₂ in order to prevent it from entering the atmosphere. Salt caves, unmineable coal seams, and deep saline aquifers are a few examples of geological formations for CCS. The biggest estimated CO₂ storage capacity is found in the deep saline aquifers, which may store anywhere from 1738 to 2,551 gigatonnes of CO₂ in just North America [28–30]. In Norway, the development of industrial-scale CCS started with the Sleipner project in 1996, and by the end of 2017, the Sleipner and Snøhvit CCS projects had captured and stored 22 Mt of CO₂ in saline aquifers offshore Norway [31–33]. When considering CO₂ storage, the output from the capture plant is what matters most.

2.4 CO₂ Thermodynamics

CO₂ has thermodynamic properties which means that across the phase transitions gas phase, liquid phase, and dense-phase (super-critical) are all likely to occur in CCS systems. At the Snøhvit site, CO₂ is compressed to over 80 bars at the Melkøya processing facility and is then transported along a 148 km pipeline, as a liquid phase, entering

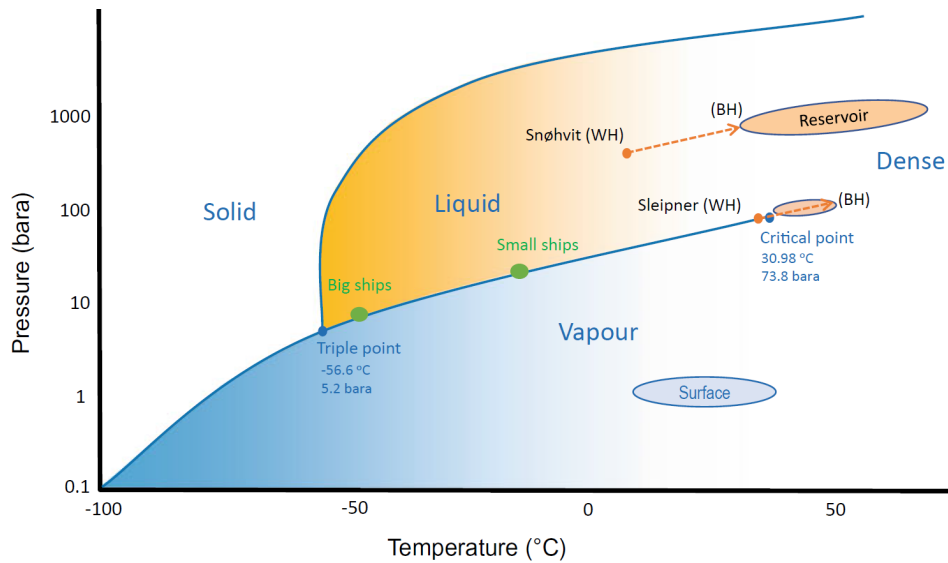


Figure 2.5: Phase diagram of pure CO₂ as a function of pressure and temperature, with wellhead and bottom hole situations for Snøhvit, shown as arrows, and reservoir conditions indicated as shaded areas. At Sleipner, the CO₂ cools down in the reservoir, while it warms up at Snøhvit [34]

the wellhead at around 140 bars, still in the liquid phase see figure 2.5. At bottom-hole conditions the CO₂ then flows into the reservoir, moving into the dense phase as the temperatures rise above the critical point (this phase is also called super-critical CO₂)[10].

At the Sleipner CCS project, the wellhead pressure is much lower, at around 62 bars, because the injection formation is much shallower (1000m deep). With a surface temperature of around 25 °C at the gas processing facility on the Sleipner platform, the CO₂ is initially close to the vapour line at the wellhead, with two-phase flow conditions occurring at this point. With increasing temperature and pressure in the well, the CO₂ soon enters the dense phase and stays in the dense phase in the reservoir. The bottom-hole temperature is estimated (not measured) at about 48 °C, but then the CO₂ cools towards around 35°C as it is within the sandstone reservoir. The behaviour of CO₂ in the multi-layer reservoir at Sleipner is quite complex and strongly dependent on the temperature and pressure flow property. [34]

CO₂ rich streams contain various other gas components (mainly hydrocarbons, nitrogen, oxygen) which complicate CO₂ management see Figure 2.6. In the case of Snøhvit, the composition of the injected fluid exported from Melkøya has been analyzed several times a year. During 2008 and 2009, CO₂ content was about 96- 98%, and the rest was mainly methane and nitrogen. After the 2009 revision stop, the CO₂ has been much cleaner (between 98% and 99.5% purity), Nitrogen and heavier hydrocarbons were removed from the injection stream. The water content is constantly less than 50 ppm [35]. However, for the simplicity of this Model CO₂ composition of 98% CO₂ and 2% Meth-

ane was used (see Figure 4.1 for the phase diagram of the CO₂ composition used for the model).

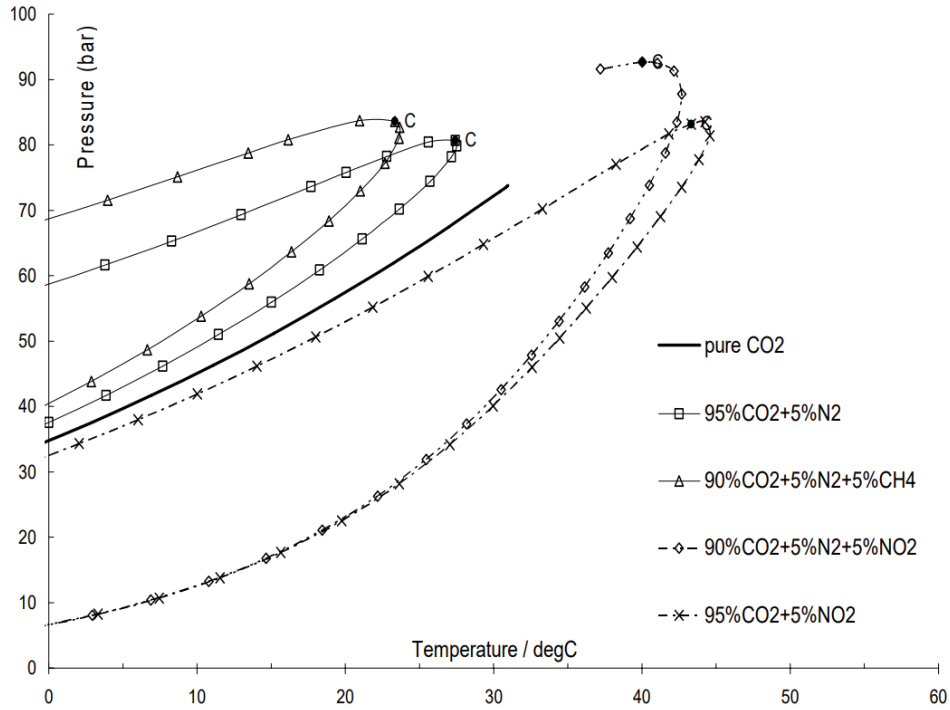


Figure 2.6: Phase diagram for CO₂ in combinations with other gas [36]

CO₂ transport and flow assurance technology are still relatively immature. As earlier mentioned, most research on CCS deals with capture technologies and storage possibilities. However, transport technology and storage technology are rather closely coupled. One of the major essential questions for any CO₂ storage project is how much can be injected. Transportation infrastructure in terms of pipeline distribution network as well as the injection well(s) plays a great role in determining how much can be injected.[10]

2.5 Engineering Considerations and Overview

Once a reasonable expectation of the required storage capacity for a given site has been established say the Snøhvit project, for example, the next thing is to start thinking about modeling, designing, and managing the injection wells and transport infrastructure. Figure 3.2 gives a simple overview of the main engineering aspects of the transport system especially related to pressure management at Snøhvit project.

Understanding the phase behaviour of CO₂ is fundamental to CO₂ storage operations. The whole concept behind CCS is to store CO₂ generated from human activities,

where the CO₂ is in the gas phase at close to atmospheric conditions, and to store it deep underground where it will be in the liquid or dense phase. This phase transition leads to very effective use of the pore space as CO₂ in the subsurface occupies a much smaller volume than at the surface. However, CO₂ in its liquid or dense form is not a substance we are familiar with in everyday life. As a liquid CO₂ is colourless but is less dense than water (a bit like oil on water) but then much less viscous than oil or water such that flows a bit like a gas. Not a substance we are so familiar with at the surface, but nevertheless a naturally-occurring substance in the subsurface (there are many naturally-occurring accumulations of liquid/dense-phase CO₂ on our planet)

When it comes to making detailed engineering assessments of CO₂ transport and storage systems, there is a need for an equation of state (EoS) to make specific assessments or to continuously track the phase behavior. An EoS is a reference function describing the properties of a substance, or mixture, based on thermodynamical theory and experimental data. Equations of State were developed to give a mathematical relationship between pressure, volume, and temperature. They were originally put forward as a method of interpreting the non-ideal nature of many pure substances. With time, this role has been extended successfully to predicting the properties of simple and complex mixtures. [37]

Peng-Robinson and Soave-Redlich-Kwong are two commonly used cubic equations of state because they are relatively simple to implement and are widely used in modeling packages. Peng-Robinson EoS is used for the PVT modeling in this project. The equations used in PVT are derived from the Van der Waals Equation, which represents the total pressure as a summation of an attractive and a repulsive element, details are explained below. The first cubic equation of state (CEOS) was developed by van der Waals in 1873 as part of his Ph.D. dissertation [38]

$$P_{total} = P_{repulsive} - P_{attractive}$$

There are several options for a CO₂ equation of state:

The classic Van der Waals equation describes this relationship as

$$P = \frac{RT}{V - b} - \frac{a}{V^2} \quad (2.1)$$

where b represents the hard-sphere volume of the molecules and a the intermolecular attraction.

The two cubic Equations of State which are available within the PVT package of Prosper and GAP are;

1) the Peng-Robinson (PR)EoS

$$P = \frac{RT}{V - b} - \frac{a(T)}{V(V + b) + b(V - b)} \quad (2.2)$$

2) the Soave-Redlich-Kwong(SRK)EoS:

$$P = \frac{RT}{V-b} - \frac{a(T)}{V(V+b)} \quad (2.3)$$

In addition in IPM, there is a feature within the program that allows the user to customize the general equation to suit a specific need

The attractive term in equation 2.3 is defined as:

$$a(T) = a(T_c)\alpha(T_R, \omega) \quad (2.4)$$

and the $a(T_c)$ function at the critical point is given by the empirical relationship:

$$a = 0.45724 \frac{R^2 T_c^2}{P_c} \quad (2.5)$$

The constant 0.45724 is also called Omega A and is specific to the EoS model (in this case, Peng-Robinson). $\alpha(T_R, \omega)$ is a function of the reduced temperature $\frac{T}{T_c}$ and the acentric factor as shown below:

$$\alpha(T) = \left(1 + m \left(1 - \sqrt{\frac{T}{T_c}} \right) \right)^2 \quad (2.6)$$

m is an empirical quadratic or cubic of the acentric factor:

$$\text{For } \omega < 0.49 m = 0.37464 + 1.54226\omega - 0.2699\omega^2$$

$$\text{For } \omega > 0.49 m = 0.379642 + 1.485030\omega - 0.164423\omega^2 + 0.016666\omega^3$$

In addition, the repulsive factor b within PR is given by

$$b = 0.07780 \left(\frac{RT_c}{P_c} \right) \quad (2.7)$$

The constant 0.0778 is also called Omega B and is specific of the EOS model (in this case, Peng-Robinson).

All cubic Equations of State can be rewritten as a function of the compressibility factor Z e.g. the Peng Robinson equation becomes

$$Z^3 - (1 - B)Z^2 + (A - 3B^2 - 2B)Z - (AB - B^2 - B^3) = 0 \quad (2.8)$$

Where

$$A = \frac{a(T)P}{(RT)^2} \quad (2.9)$$

$$B = \frac{bP}{RT} \quad (2.10)$$

and

$$Z = \frac{Pv}{RT} \quad (2.11)$$

Span and Wagner (1996) proposed a more accurate but also more demanding EoS [39]

In the following section, key parameters crucial for accurately modeling a CO₂ injection system will be discussed.

2.5.1 Modeling Fluid Properties for Accurate Prediction of Pressure and Temperature Changes along the Pipeline

To predict pressure and temperature changes through the reservoir, wellbore, and along the surface flow lines it is necessary to accurately predict the fluid properties as both pressure and temperature change. To generate the CO₂ phase envelope using the Peng-Robinson Equation of State described above, it is essential to provide specific input values to the EoS. These input thermodynamic values were derived from PVTp a specialized petroleum expert software. Table A.1 and A.2 present the key parameters utilized in the Peng-Robinson equation to construct the phase envelope.

2.5.2 Nodal Analysis of Injection Wells

The system analysis approach often called Nodal Analysis has been applied for many years to analyze the performance of systems composed of interacting components. Its application to the well production system was first proposed by Gibert in 1954 [40] and discussed by Nind in 1964 [41]. The production engineer must sometimes design completion configurations or analyze the performance of various types of injection wells. These wells may be used for injecting water or some other fluid for enhanced oil recovery projects or they could be gas injection wells operating in gas storage reservoirs. Nodal analysis may be performed on injection wells by selecting the node at the bottom hole such that the inflow to the node will include the injection pump or compressor and the piping system, while the outflow will consist of the perforation and the reservoir. For example, if gas from the compressor is being injected into the well, the inflow and outflow expressions would be

Inflow

$$P_{compr} - \Delta p_{flowline} - \Delta p_{tubing} = p_{wf} \quad (2.12)$$

Outflow

$$\bar{P}_R - \Delta p_{res} = p_{wf} \quad (2.13)$$

This type of analysis could be used to determine the effects on injection rate of various compressor pressures, flowlines sizes or tubing sizes. For this example, it is assumed that wellhead pressure is constant so that the inflow will include only the pressure drop in the tubing. That is,

$$P_{wh} + \Delta p_{el} - \Delta p_f = p_{wf} \quad (2.14)$$

Equation 2.15 may be used to calculate P_{wf} for various rate

$$P_{wf}^2 = P_{wh}^2 EXP(S) - \frac{C_l \gamma_g q_{sc}^2 \bar{T} \bar{Z} f(MD)(EXP(S) - 1)}{S d^5} \quad (2.15)$$

Where

$$S = C_z \gamma (TVD) / (\bar{T} \bar{Z}) \quad (2.16)$$

$$f = \left(1.14 - 2 \log \left(\frac{\epsilon}{d} + \frac{21.25}{N_{Re}^{0.9}} \right) \right)^{-2} \quad (2.17)$$

$$N_{Re} = 20011 \gamma q_{inj} / \mu_g d \quad (2.18)$$

C_1, C_2 = constants depending on units

T^0R = average flowing temperature,

TVD = True Vertical depth, ft

MD = Measured depth, ft

d = Pipe inside diameter, in.

P_{wf}, P_{wh} = pressure, psia

q_{sc} = flow rate, MMscf/d

$C_1 = 25$

$C_2 = 0.0375$

In this equation \bar{T} and \bar{Z} are the average temperature and Z-factor existing in the well, which makes the solution iterative since $Z=f(p)$

The outflow performance may be calculated using the back pressure equation for gas wells. That is

Outflow

$$\bar{P}_R + \Delta p_{res} = P_{wf} \quad (2.19)$$

Where,

$$q_{inj} = c(P_{wf}^2 - \bar{P}_R^2)^n \quad (2.20)$$

$$P_{wf}^2 = \bar{P}_R^2 + \left(\frac{q}{c} \right)^{\frac{1}{n}} \quad (2.21)$$

The intersections of the various inflow curves with the outflow curve in Figure 2.7 represent the injection rates possible for three tubing sizes. In gas storage operations,

the static reservoir pressure will increase as gas is injected, and this would cause an upward shift in the outflow curve in Figure 2.7. This would result in a decreasing injection rate with time, as the intersection of the inflow and outflow curves would shift to the left.

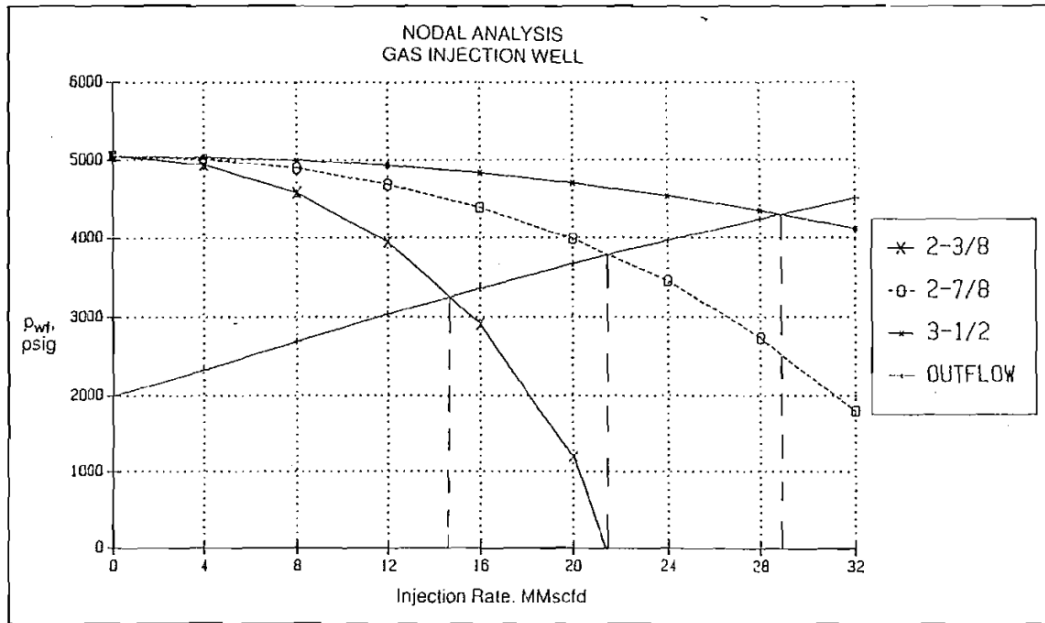


Figure 2.7: Nodal Analysis Gas Injection Well [42]

Analysis of flowing well performance requires an understanding of two concepts: Inflow Performance Relationship (IPR) (see section 2.5.3) and Vertical Lift Performance (VLP) (see section 2.5.4). These concepts are discussed in more detail in the following sections. As the entire system is simulated, each of the components is modeled using various equations or correlations to determine the pressure loss through that component as a function of flow rate. The summation of these individual losses makes up the total pressure loss through the entire system for a given flow rate. This total loss is ultimately realized as the overall difference between average reservoir pressure and wellhead pressure. [42, 43]. The procedure consists of selecting a node and dividing the system into two parts. Usually, the system is divided between reservoir and piping system namely reservoir dominated part and piping system-dominated part [44]

2.5.3 Inflow Performance Relationship (IPR) Curve

The Inflow Performance Relationship (IPR) defines the flow into the well from the reservoir in a production system (see Figure 2.8). This concept is also applied in CO₂ injection. Calculating an IPR results in a relationship between the bottom hole pressure and the flow rate passing into the reservoir. Inflow performance relationship (IPR) curve is one of the two curves that are required to be developed for obtaining deliverability, it shows the relationship between rate q and bottomhole flowing pressure P_{wf} . Fluid flow type,

Production Systems Analysis

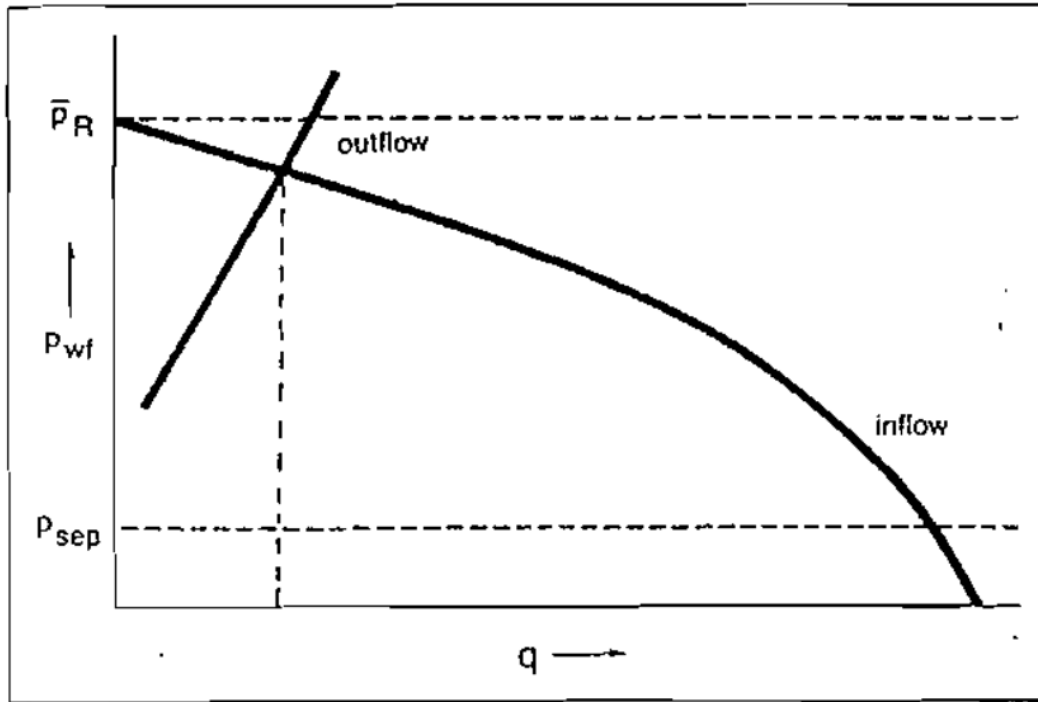


Figure 2.8: Production System Analysis [42]

boundary pressure or reservoir average pressure, and other reservoir and fluid properties play a vital role in developing the IPR curve.[45]

There are over twenty inflow options available for modeling IPR in Prosper software. The choice depends upon the available information and the type of sensitivities to be run. The following lists of correlations are available for Inflow Performance in gas and condensate; Jones, Forcheimer, Back pressure, C and N, External entry, and Petroleum Experts, etc (see more details in Table A.3). The External Entry method was used in this model. This option allows an externally generated IPR data set to be imported or directly entered into the software. The equations used for externally generated Linear IPR are detailed below see equation 2.22

$$Q = J(P_{wf} - P_r) \quad (2.22)$$

$$J = \frac{2\pi Kh}{18.68Z\mu_g \left(\ln \frac{r_e}{r_w} - 0.75 + s \right)} \quad (2.23)$$

Combining equations 2.23 and 2.24

$$Q = \frac{2\pi Kh}{18.68Z\mu_g \left(\ln \frac{r_e}{r_w} - 0.75 + s \right)} (P_{wf} - P_r) \quad (2.24)$$

Where;

Q = Flowrate [Sm^3/day]

J = Injectivity Index [$t/h/bar$] or [$Sm^3/d/bar$]

P_{wf} = Bottom Hole flowing Pressure [bar]

P_r = Reservoir Pressure [bar]

r_e = External Radius [m]

r_w = Well Radius [m]

The Injectivity Index for Tubåen formation is approximated as follows

$$J = \frac{2\pi Kh}{18.68Z\mu_g \left(\ln \frac{r_e}{r_w} - 0.75 + s \right)} \approx 105,000 [Sm^3/d/bar] \quad (2.25)$$

For sensitivities studies the injectivity Index(J) values were approximated to 4.5, 9, 13.5[t/h/bar], and CO₂ density at standard conditions is 1.8682 [kg/m³], the CO₂ density standard condition is required to convert injectivity from [t/h/bar] to [Sm³/d/bar] [4]

2.5.4 Vertical Lift Performance (VLP) Curve

The vertical lifting performance (VLP) curve also shows the relationship between the rate q and bottomhole flowing pressure (p_{wf}). But unlike the IPR curve, it is developed based on the flow of the fluid from the wellbore to the wellhead at a specific wellhead pressure. VLP is also named as tubing performance relationship (TPR) or wellbore flow performance or outflow performance relation. As the fluid flows from the wellbore to the wellhead, pressure drop occurs, the pressure drop is a function of the mechanical configuration of the wellbore, the properties of the fluids, and the production rates. It happens in three forms such as frictional pressure loss, potential pressure loss, and kinetic pressure loss [46]. VLP curves report the flowing bottom-hole pressure (and various other results depending on the well type) for various rates at a given set of flowing conditions, at each reported rate, a gradient calculation is carried out to find the flowing bottom-hole pressure (P_{wf}) and then these pressures are joined together to form a curve (see Figure 2.7).

2.5.5 Flow in Pipes

To determine the performance of any injection or production system, it is necessary to be able to calculate the pressure losses in all components of the system. These pressure losses and where they occur in the system are illustrated in Figure 2.9. The following sections will explain methods to calculate pressure drop in pipes. Many factors must be considered in designing a modern pipeline system or a gas injection well. These include the nature and the volume of gas to be transmitted, the length and the size of the pipeline, the depth of the well, the operating temperature and pressure, the type of terrain to be crossed, the capacity of injection wells, the type of gas, process plant operating conditions, plant location, the elevation change over the route, and so on. Among these, the pressure drop along the pipe and the quantity of natural gas that flows through the pipe are the most important of the first items of information required for design. Flow of natural gas in wells and pipelines is dependent upon Reynolds number, friction factor, pipe roughness, pipe diameter, pipe length, temperature, pressure, pressure drop and gas properties. Accurate predictions are required for optimum design [46].

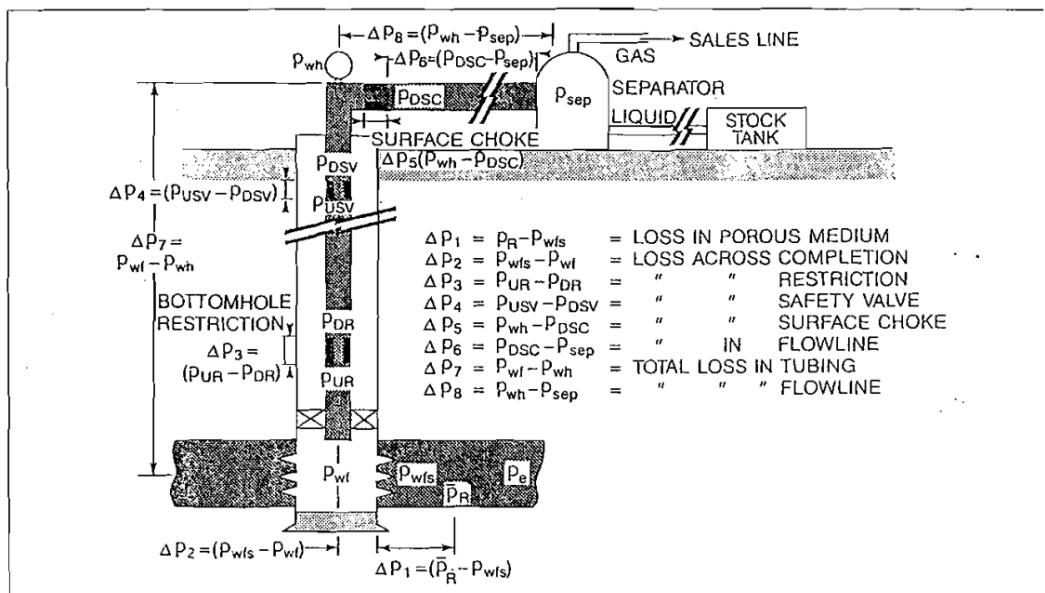


Figure 2.9: Possible Pressure Losses In Complete System [42]

2.5.6 Basic Equations and Concepts

All multiphase flow correlations were developed from the general energy equation which expresses an energy balance between two points in a fluid flow system. It follows the law of conservation of energy, which states that the energy of a fluid entering section 1 of a pipe, plus any additional work done on the fluid between sections 1 and 2, minus any energy losses by the system between sections 1 and 2, is equal to the energy of the

fluid leaving section 2 [47]. Figure 2.10 may be used to illustrate this principle. The energy balance equation is given in the following form:

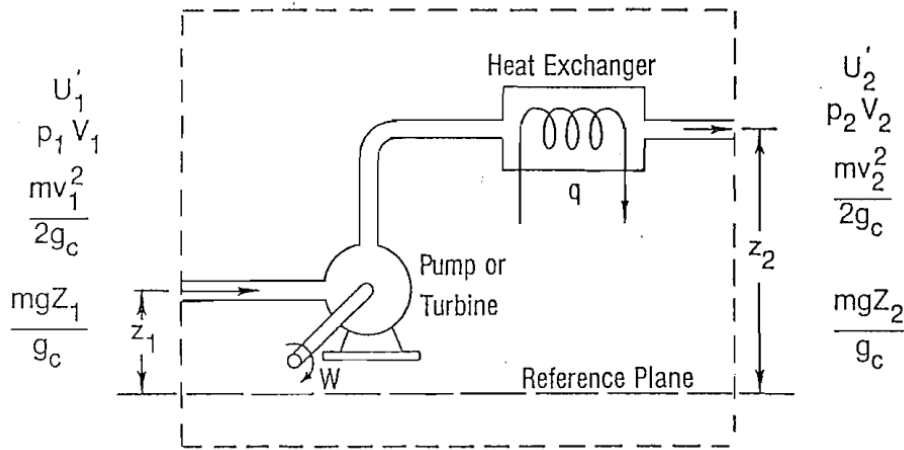


Figure 2.10: Flow System Control Volume [42]

$$U_1 + \frac{mv_1^2}{2g_c} + P_1V_1 + q - W = U_2 + \frac{mv_2^2}{2g_c} + P_2V_2 \quad (2.26)$$

The above equation can be manipulated and written in terms of pressure drop per unit length of pipe as follows, the pressure gradient equation, can be applicable to any fluid at any inclination angle [42]

$$\frac{dp}{dz} = \frac{g}{g_c} \rho \sin \theta + \frac{\rho v}{g_c} \frac{dv}{dz} + \frac{fv^2 \rho}{2g_c d} \quad (2.27)$$

Therefore, the equation can be expressed in terms of the pressure gradient (psi/ft.) as follows:

Total gradient = Elevation gradient + Friction gradient + Acceleration gradient [48]

$$\left(\frac{dp}{dz} \right)_{total} = \left(\frac{dp}{dz} \right)_{elevation} + \left(\frac{dp}{dz} \right)_{friction} + \left(\frac{dp}{dz} \right)_{acceleration} \quad (2.28)$$

Many correlations with varying degrees of sophistication have been presented in the literature [49]

2.5.7 History of Multiphase Flow in Pipes

The multiphase flow correlations have been used for many years to calculate the pressure drop in tubing and flow lines. They started with simple modifications of pressure drop calculations for single-phase flow, moved to two-phase flow correlations that did not take into consideration flow pattern maps or slip velocity, to more sophisticated two-phase models that accounted for slip and flow pattern maps, and then to more sophisticated two and three-phase mechanistic models [50].

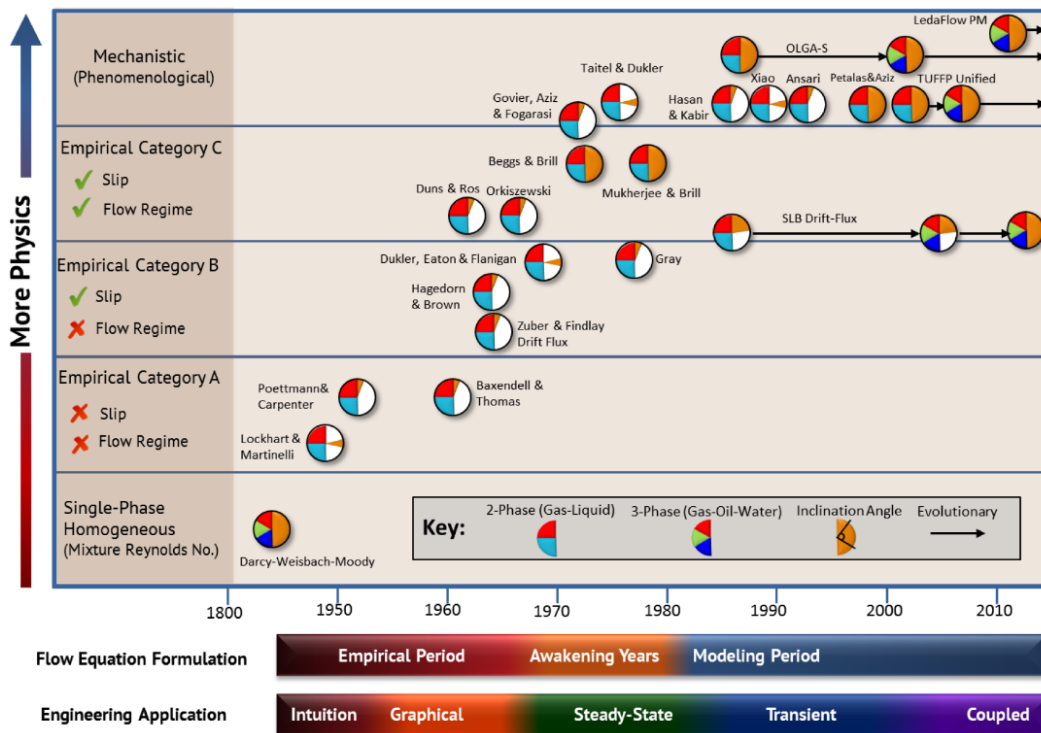


Figure 2.11: Evolution of multiphase flow modeling, showing a selection of the more widely used models. The timeline (x-axis) is associated with two criteria: Flow Equation Formulation (upper) and Engineering Application (lower). The vertical axis increases with model complexity and is subdivided into five general categories

[49]

The idea for each correlation was based on defining some parameters that affect the multiphase flow pressure drop (e.g. mixture properties instead of single phase properties such as density) and correlate those parameters with the pressure drop. Also, and due to the mixture phenomena, new parameters have appeared like slippage and holdup to accurately predict the pressure drop resulting from multiphase flow.

In 1992, Brill and Arirachakaran presented a classification to distinguish multiphase flow models based on the level of physics used to derive them, see the vertical axis in Figure 2.11. These authors also identified three general stages in the evolution of

multiphase flow research, which are shown on the horizontal time scale in Figure 2.11, labeled “Flow Equation Formulation. A second time-based scale has been added to Figure 2.11, labeled “Engineering Application”, which chronicles advancements in the methods applied to multiphase flow engineering solutions.[49]

In this thesis, Petroleum Experts 2 was used as the Vertical Lift Correlation for the well model in Prosper. In a series of correlations, Petroleum Experts incorporated techniques from different correlations to improve the predictability of their correlations. They also incorporated mechanistic model approaches in some of their more recent correlations [50]. Beggs and Brill were used for the pipeline model in GAP. Beggs and Brill is an empirical two-phase flow correlation published in 1972[51]. It distinguishes between four flow regimes. Beggs and Brill is the default VLP correlation in sPipe. Briggs and Brill’s correlation is the best correlation for inclined flow, with many gathering lines and long-distance pipelines passing through areas of hilly terrain at any angle of inclination like the case of the Snohvit pipeline.

According to Beggs and Brill, the equation used to calculate pressure gradient when gas or liquid, or both, flow in a pipe is;

$$\left(\frac{dp}{dz}\right)_{total} = \left(\frac{dp}{dz}\right)_{elevation} + \left(\frac{dp}{dz}\right)_{friction} + \left(\frac{dp}{dz}\right)_{acceleration} \quad (2.29)$$

Frictional Pressure Gradient

By definition, the frictional pressure gradient is given by;

$$\left(\frac{dp}{dz}\right)_{friction} = \frac{f_t P G_m V_m}{2g_c d} \quad (2.30)$$

Acceleration Pressure Gradient

To analyze the kinetic energy or acceleration term, which is negligible for most practical cases, several simplifying assumptions are made

$$V_m = V_s L + V_s g = \frac{G_L}{\rho_L} + \frac{G_g}{\rho_g} \quad (2.31)$$

The above equation can be manipulated and written in terms of pressure drop per unit length of pipe as follows

$$\left(\frac{dp}{dz}\right)_{acceleration} = -\frac{f_t P V_m V_s g}{g_c P} \frac{dp}{dz} \quad (2.32)$$

Gravity Pressure Gradient

$$\left(\frac{dp}{dz}\right)_{elevation} = \frac{g}{g_c} \rho_{tp} \sin\theta \quad (2.33)$$

Calculating the pressure gradient caused by elevation change, requires a procedure to determine the in-situ density of the gas-liquid mixture ρ_{tp} . For this purpose, a liquid holdup factor is defined as

$$H_L = \frac{\text{Volume of liquid in an element}}{\text{Volume of the element}} \quad (2.34)$$

The in-situ density of the fluid mixture may now be represented by

$$\rho_{tp} = \rho_L H_L + \rho_g (1 - H_L) \quad (2.35)$$

Therefore the above equation becomes

$$\left(\frac{dp}{dz}\right)_{elevation} = \frac{g}{g_c} [\rho_L H_L + \rho_g (1 - H_L)] \sin\theta \quad (2.36)$$

By substitution of the above equation into equation 2.29 the total pressure gradient can be expressed as follows;

$$\frac{dp}{dz} = \frac{\frac{g}{g_c} \sin\theta [\rho_L H_L + \rho_g (1 - H_L)] + \frac{f_t p G_m V_m}{2g_c d}}{1 - \frac{[\rho_L H_L + \rho_g (1 - H_L)] V_m V_s g}{g_c p}} \quad (2.37)$$

The above equation reduces to an equation for a single-phase liquid or single-phase gas flow as $H_L \rightarrow 1$ or $H_L \rightarrow 0$, respectively. Also as the angle of the pipe, θ becomes zero, $+90^\circ$ or -90° , Equation 2.37 becomes applicable to horizontal or vertical flow. Equation 2.37 contains two unknowns: H_L which must be determined to calculate the in-situ density, and $f_t p$, which is used to calculate friction losses. Beggs and Brill developed a correlation for predicting H_L and $f_t p$ from fluid and system properties that are known[51]. The variation of liquid holdup with pipe inclination is shown in Figure 2.12 for the tests conducted by Beggs and Brill.

2.5.8 Pressure Drop Through Restriction

Although the principal pressure losses in the well system occur in the reservoir, the tubing, and the flowline, the pressure loss in restrictions can be substantial in some wells. Surface choke is a type of restriction. The flow through a restriction may be either critical (sonic) or subcritical (subsonic). If the flow is critical, a pressure disturbance downstream of the restriction will have no effect on either the flow rate through the restriction or the upstream pressure. Since one of the main purposes of a choke is to

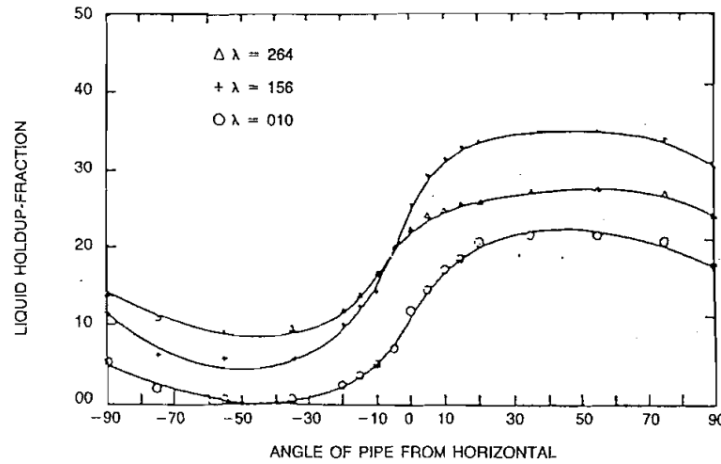


Figure 2.12: Shows the variation of liquid holdup with pipe inclination is for the tests conducted by Beggs and Brill [42]

control flow rate, it will usually be sized so that critical flow will exist. A rule-of-thumb for distinguishing between critical and subcritical flow states that if the ratio of downstream pressure to upstream pressure is less than or equal to 0.5, then the flow will be critical. This is a closer approximation for single-phase gas than for two-phase flow. Some engineers use either 0.6 or 0.7 as the critical pressure ratio in two-phase flow, although research performed at Tulsa University [52] has shown that in some cases, the ratio must be as low as 0.3 before the flow becomes critical [42]

Surface Choke

Equation for estimating the relationship among pressure, flow rate and choke size for both subcritical and critical flow through choke is presented below. For gas flow a general equation for flow through restrictions can be derived by combining the Bernoulli equation with an equation of state. The irreversible losses are accounted for by the use of a discharge coefficient, which depends on the type of restriction. The following restriction applies for gas flow in both the critical and subcritical regimes [42]

For critical flow, the pressure ratio $y = \frac{p_2}{p_1}$ is replaced by the critical pressure ratio y_c

$$q_{sc} = \frac{C_n(p_1)(d)^2}{\sqrt{\gamma_g(T_1)Z_1}} \sqrt{\left(\frac{k}{k-1}\right)(y^{2/k} - y^{(k+1)/k})} \quad (2.38)$$

$$C_n = \frac{C_s(C_d)T_{sc}}{P_{sc}} \quad (2.39)$$

where

- q_{sc} = Volumetric gas flow rate
- C_n = Coefficient based on system of units, discharge coefficient and standard conditions
- d = I.D of bore open to gas flow
- γ_g = gas specific gravity (air=1.0), dimensionless
- k = ratio of specific heats = C_p / C_v dimensionless
- p_1 = upstream pressure, absolute units
- p_2 = downstream pressure, absolute units
- T_1 = upstream temperature, absolute units
- Z_1 = compressibility factor at p_1 and T_1 dimensionless
- C_s = coefficient based on system of units
- C_d = discharge coefficient (empirical), dimensionless
- T_{sc} = standard absolute temperature base, absolute units
- p_{sc} = standard absolute pressure base, absolute units
- y_c = critical pressure ratio, dimensionless

The pressure ratio at which flow becomes critical depends on the k value for the flowing gas and is given by:

$$y_c = \left(\frac{2}{k+1} \right)^{k/(k-1)} \quad (2.40)$$

2.6 The Model-Building Software

To enable the analysis, optimization, and performance prediction of complex CO₂ distribution networks, it is important to develop a model. This model can help reduce costs and risks and improve decision-making. As a result, sophisticated network optimizer software is needed to perform studies to understand the behaviour of fluid as well as design systems and optimize CO₂ injection network. This need can be provided by GAP, Prosper, and PVTp. GAP is specifically designed and built for solving integrated oilfield networks. The Petroleum Expert software has been used in the industry for a while to model gas lift wells. In 2014, Mustafa Al Lawati used Prosper and GAP to model fluid PVT samples, well models, surface production, and gas lift injection networks. The study also includes integrating fluid models, reservoir models, well models, and surface production and gas lift injection network. In the clusters field model solving phase, the production model and gas lift injection model are linked. The gas lift injection network is solved to identify weak injection rate ends and is restructured by rerouting the pipelines. The network optimizer is then run to enhance lifting gas injection depths based on available injection gas rates and pressure. In a specific case study, oil production gain of 15 percent was achieved from rerouting the gas lift network in three clusters wells in field X

by enhancing lifting gas rates and avoiding unnecessary network branching.[1]

2.6.1 Prosper Software

Prosper is a well performance, design, and optimization program which is part of the integrated Production Modelling Toolkit (IPM). This tool is the industry standard well modeling with the major operators worldwide. Prosper is designed to allow the building of reliable and consistent well models, with the ability to address each aspect of wellbore modeling: PVT (fluid characterization), VLP correlations (for calculation of flow-line and tubing pressure loss, and IPR (reservoir inflow).The flow chart in Figure 2.13 gives an outline of the calculation steps required to carry out a simple systems analysis using Prosper.[53]

These are some of the main features available in Prosper

- Prosper is a fundamental element in the Integrated Production Model (IPM) as defined by Petroleum Experts as it creates a robust well model which can be linked to GAP (the production network optimization program for gathering system modeling) and linked to Mbal (the reservoir engineering and modeling tool which allows for making fully integrated total system modeling and production forecasting).
- The PVT section in Prosper can compute fluid properties using standard black oil correlations and these black oil correlations can be modified to better fit measured lab data. Prosper also allows detailed PVT data in the form of tables to be imported for use in the calculations. A third option is to use the Equation of State method. This option allows the user to enter the equation of state model parameters and uses the standard Peng-Robinson or SRK EoS models to generate properties given a multi-stage separator scheme. With this option the users can also import all PVT data in the form of tables, which could have been generated using their own proprietary EoS models.
- The tool can be used to model reservoir inflow performance (IPR) for single-layer, multi-layered, or multilateral wells with complex and highly deviated completions, optimising all aspects of a completion design including perforation details and gravel packing.
- It can be used to accurately predict both pressure and temperature profiles in producing wells, injection wells, across chokes and along risers and flow lines.
- The sensitivity calculations capabilities allow the engineer to model and easily optimise tubing configuration, choke, and surface flow line performance.
- The multiphase flow correlations implemented can be adjusted to match measured field data to generate vertical lift performance curves (VLP) for use in simulators and network models.
- Black Oil PVT tables can be imported directly into Prosper. The black oil tables can be generated by Petroleum Experts' PVTp thermodynamics analysis program or from any third-party application, provided it has the right format (*.PTB file). Equally, compositional models can also be directly imported as *.PRP file.

2.6.2 GAP Software

GAP is a multiphase oil and gas optimizer tool that models the surface gathering network of field production and injection systems. When linked with well models of Prosper and reservoir models of Mbal a full field injection and or production optimization and forecast can be achieved. GAP can model production systems containing oil, gas, and condensate, in addition to gas or water injection systems [53]

Applications

- Full field surface network design
- Multi-phase looped network optimization
- Model full field injection system performance (i.e. water, gas steam)
- Easy to use graphical interface for drawing system network.
- GAP is unique in being able to model, optimize, and run predictions of the entire production system, with Mbal and Prosper etc

2.6.3 PVTp Software

PVTp is Petroleum Experts' advanced Pressure Volume and Temperature analysis software. An understanding of pvt properties is fundamental to all aspects of reservoir, petroleum, and production engineering. PVTp allows tuning of Equation of state (EoS) to match laboratory data. The tuned EoS can be used to simulate a range of reservoir and production processes, which impart equipment sizing and reservoir recovery [53].

PVTp allows analysis and prediction of the compositional behaviour of complex mixtures including gas mixtures, gas retrograde condensates, volatile oils, heavy oils, and black oils with confidence

PVTp has all the features necessary to build and calibrate EoS models from PVT lab report data and to quality check the model by simulating all common lab experiments. The tuned EoS can then be used to simulate a range of reservoir and production processes, which impact processes like equipment sizing and reservoir recovery estimation.

PVTp can be used as a stand-alone analytical tool; or can be used to generate Equation of State (EoS) models, tables of fluid properties, and reduced compositions for applications such as reservoir simulators or nodal analysis packages.

PVTp is part of the Petroleum Experts' IPM (Integrated Production Modelling) Suite and as such allows to export pvt data for **GAP**, **Prosper**, **Mbal**, **Reveal**, and **Resolve**. In addition, OpenServer is fully compatible with PVTp which can be used to automate the most common tasks by running them from a third-party application, like a macro or a Visual Basic application. PVTp allows calibration of EOS models using either of the two industry-standard models:

- Peng-Robinson Equation of State with the option of Volume Shift

- Soave-Redlich-Kwong Equation of State with the option of Volume Shift

Application

- Characterization of fluid
- Phase behavior prediction
- Generation of PVT tables for use in simulation, see Table A.1 and A.2

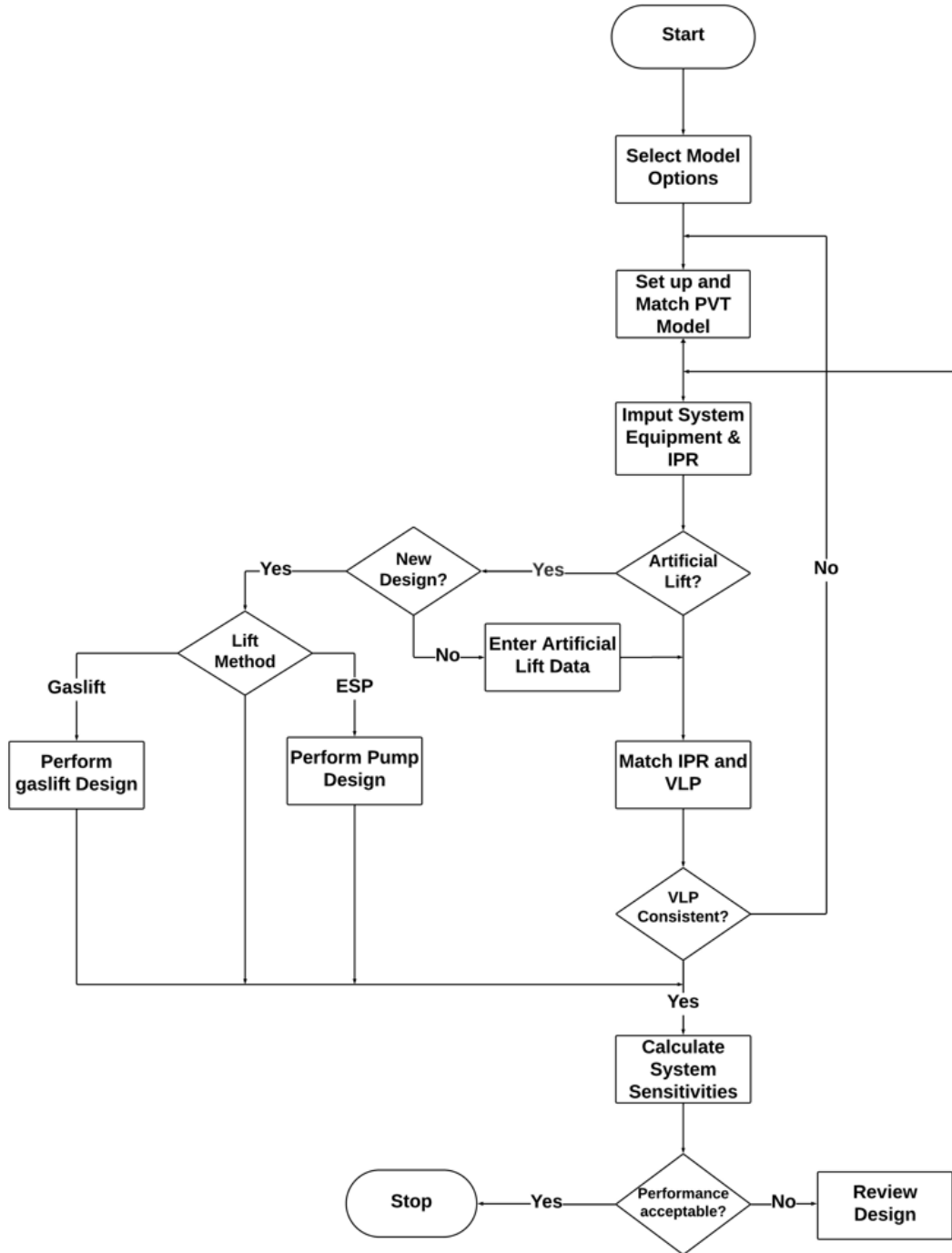


Figure 2.13: Flowchat For Prosper Model [53].

Methodology

For simulation and data acquisition, three software programs PVTp, Prosper, and GAP have been employed. Access to licenses for Petroleum Experts IPM Software 13.0 64bit has been facilitated through The Norwegian University of Science and Technology NTNU. Prosper and GAP are used to construct the well model, pipeline network, and flowline system. Flowline distributes the fluid from the pipeline to the wells. Sensitivity analyses are done by varying parameters such as injection pressure, temperature, injectivity index, wellhead choke, etc. The foundational framework for this model was drawn from the Snøhvit field located in the Barents Sea.

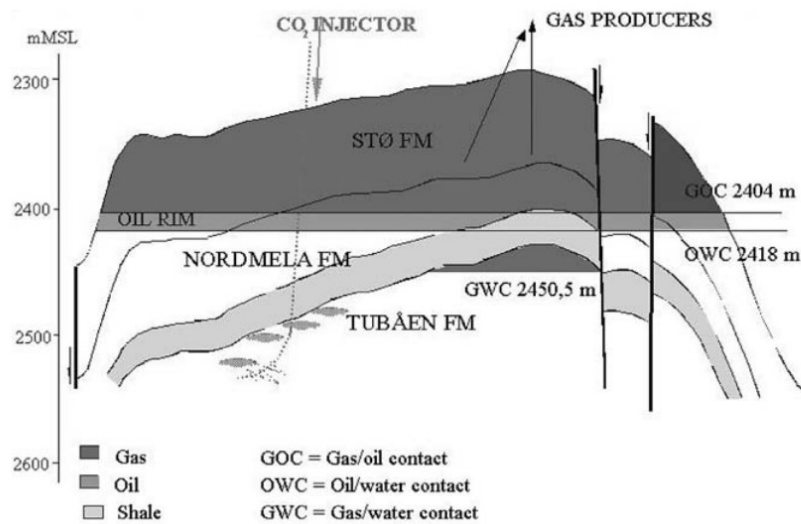


Figure 3.1: Snøhvit Field Cross Section: Visual representation showcasing the geological strata, subsurface formations, and reservoir structures within the Snøhvit natural gas field, offering insights into its geological composition and hydrocarbon reservoir dynamics. [32]

3.1 The Injection System

As earlier mentioned in the introduction, at Snøhvit field, gas is produced from nine wells, the well stream, with natural gas, CO₂, natural gas liquids (NGL), and condensate, is transported in a 152-kilometer pipeline to the liquid natural gas (LNG) processing facility at Melkøya near Hammerfest where the CO₂ is stripped from the methane, compressed to supercritical state. The CO₂ is pumped again back offshore by a pipeline of about 148km for injection into the aquifer (Stø reservoir). At the final stage of the CO₂ separation process at the Melkøya LNG Plant, pumps are installed to increase pressure by a sufficient amount. The design average pressure was about 100 bars see Figure 3.2, and actual pressure has increased from less than 80 bars initially to about 140 bars in June 2010.

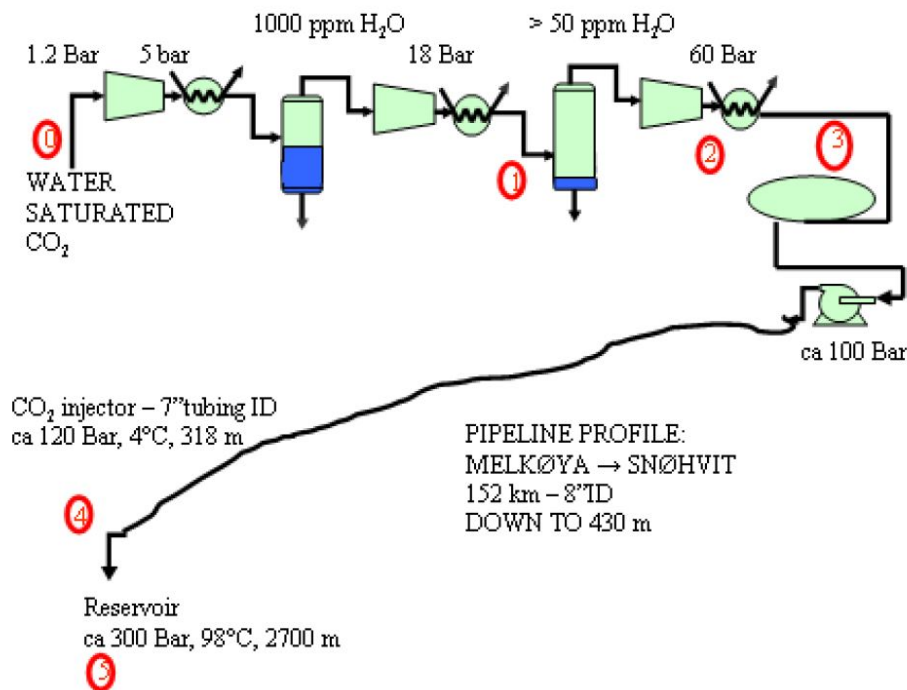


Figure 3.2: Illustrative schematic outlining the CO₂ separation process specifically designed for Melkøya, providing a visual representation of the intricate steps involved in the separation and capture of CO₂ [32]

The CO₂ is injected offshore via a 148 km long 8" inner diameter pipeline to the F-template. CO₂ takes seafloor temperature (around 4°C to 5°C) in the pipeline, and with pressures above 80 bars CO₂ is in liquid phase and density will be around 940 – 1010 kg/m³ see Figure 2.5. Injection started in April 2008. The pipeline has a volume of about 4800 m³. If valves at the wellhead are closed while CO₂ continues to enter the pipe, pressure will increase by about 0,39 bar/ton. Flow velocity is about 2 – 2.5 km/hour when injecting at 60-80 tons/h. This means that it takes 61-76 hours for CO₂

to travel from Melkøya to the Snøhvit field. Pipeline pressure measured on the F template is usually about 10 bar higher than on Melkøya.

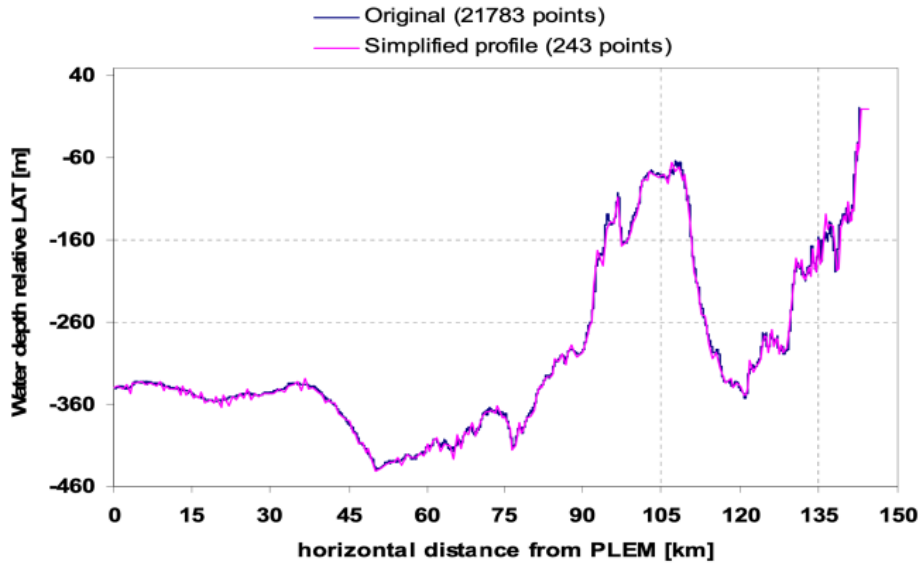


Figure 3.3: Graphical representation outlining the key operational parameters and geographical layout of the CO₂ injection pipeline within the Snøhvit project.[32]

3.2 Case Assembly

Using the existing information in literature for Snøhvit field [4], a simulation scenario was generated using PVTp, Prosper, and GAP softwares. In order to further explore the models, sensitivity cases including changing injection pressure, injectivity index, choking, etc were performed. Specifically, the single injection well as documented in the literature was augmented to encompass two templates, each containing three wells, totaling six wells in all. A diagram illustrating the simulation layout is presented in Figure 3.5. When designing the simulation case for GAP, it was deemed unfeasible and unnecessary to replicate the precise transport pipeline configuration of Snøhvit see Figure 3.3. Given its intricate nature and the multitude of data points involved, a decision was taken to streamline the pipeline configuration. An approximate representation of the profile was sketched out within GAP, and Figure 3.4 displays this simplified pipeline profile.

Most of the simulation parameters were sourced from existing literature on Snøhvit field CO₂ injection, including CO₂ composition (however, only CO₂ and Methane composition were used to simplify the model), pipeline diameter, injection pressure, well depth, tubing diameter, reservoir pressure and temperature, reservoir fracture pressure, and injectivity as documented [4]. However, certain parameters like injection fluid tem-

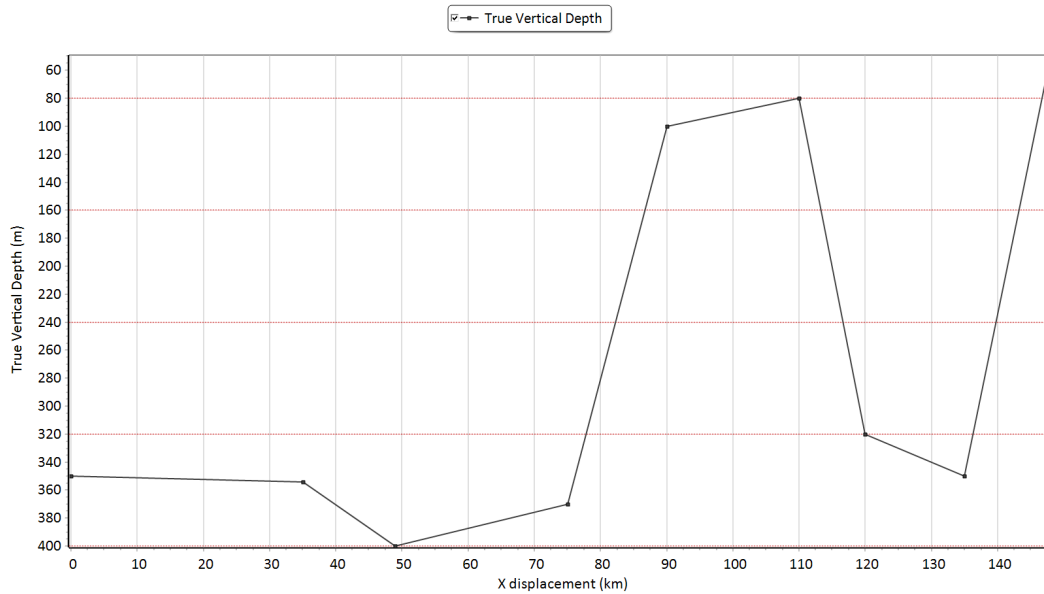


Figure 3.4: Detailed representation of the Snøhvit pipeline configuration, encompassing its structural attributes, specifications, and network topology, within the GAP software. This profile serves as a crucial foundation for conducting accurate and thorough simulations, allowing for an in-depth analysis of fluid dynamics, pressure variations, and transport efficiencies within the pipeline system.

perature and heat transfer coefficient etc were modified to suit the scaling of the number of wells. To simplify the well model, the well configuration was adjusted to a vertical well instead of a 27-degree deviation from the vertical. For simulating CO₂ injection, a straight line Inflow Performance Relationship (IPR) was used. This IPR characterizes the relationship between the production rate and the flowing bottom-hole pressure. Typically used for oil wells, it assumes that the fluid inflow rate is proportional to the difference between reservoir pressure and wellbore pressure. The performance of the injection well can be fine-tuned by adjusting the injectivity index of the well.[45]

The following session will now delve into the specifics of the step-by-step on how the model was built. The First software used was the PVTp for generating the PVT file, followed by Prosper and finally GAP

3.2.1 PVTp Software

When PVTp is opened, the following screen in Figure 3.6 will be shown. To get started, either a new or existing file can be opened by selecting one of the options shown in Figure 3.6, or a recently opened file can be selected from the list shown in the blue box to reopen that file. This session would not delve into the specifics of how the PVT data input was generated. The default PVT file in PVTp was employed because of a lack of

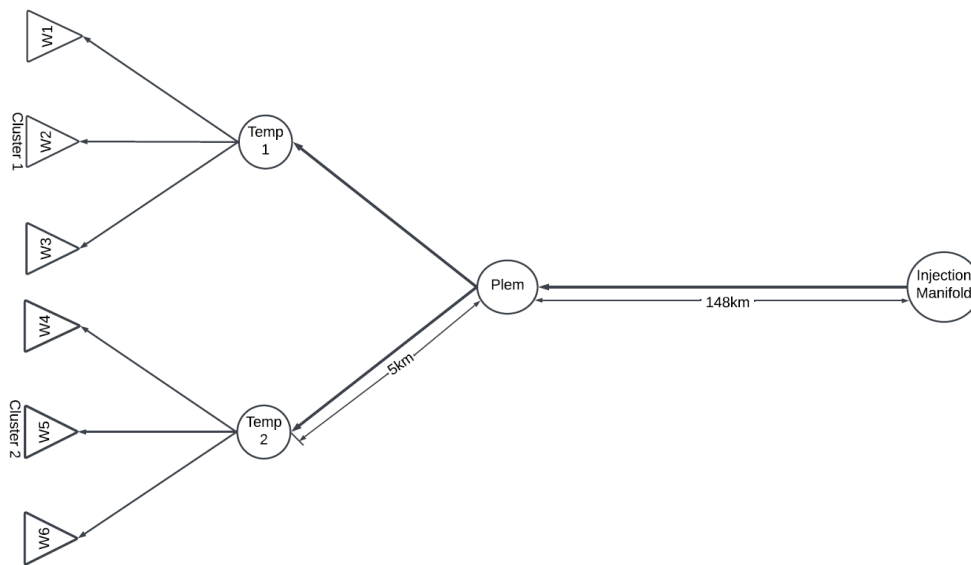


Figure 3.5: Schematic Illustration of the Snøhvit Simulation Case Study: Depicting the Injection manifold, pipeline, flowline, templates, and the injection wells components for comprehensive analysis and simulation

sufficient information for modeling this data in PVTp for the Snøhvit field. Consequently, the default data were utilized, and the composition was adjusted to mirror that of CO₂ at the Snøhvit field.

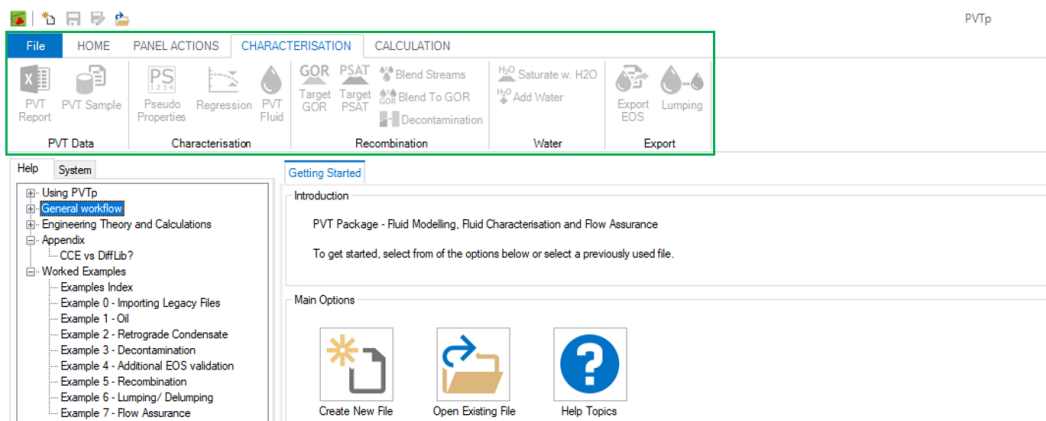


Figure 3.6: The PVTp software user interface displays distinct sections including File, Home, Panel Actions, Characterisation, and Calculation interfaces.

The main PVTp interface is divided up into different sections, as highlighted in the screenshot below in Figure 3.6, there are:

- File
- Home

- Panel Actions
- Characterisation
- Calculation

In order for an EoS to provide an accurate description of a fluid's behavior over the full range of conditions encountered in the field, a characterization against lab data is required. PVTp provides the engineer with the toolkit to develop a characterized EoS description for any fluid. Although there is no single characterization pathway that would work for all fluids, there a number of basic components that are typically used. Some of these steps are essential, while others can be optional depending on the fluid, the most commonly used steps are:

- Reviewing the PVT lab report (PVT Report)
- Defining the sample, composition, etc. (PVT Sample)
- Defining any pseudo components (Pseudo Properties)
- Performing a regression to match lab data (Regression)
- Exporting final characterized EoS (Export)

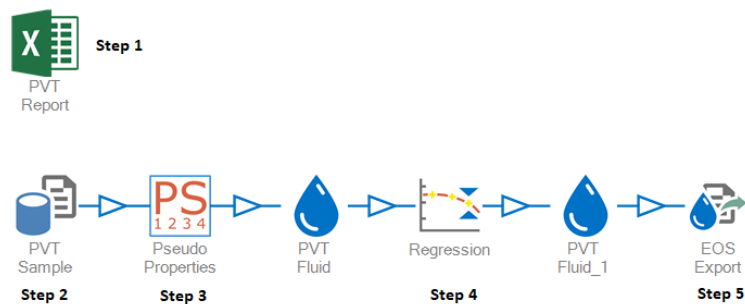


Figure 3.7: Key Steps for Accurate EoS Development Using PVTp Toolkit: Essential Components for Fluid Characterization

Since the default EoS Exported File was used, detailed attention will not be paid to explain the process followed to achieve the above in Figure 3.7, however, the PVTp manual [53] contains more detail on this. Figure 3.8 is an example of the export file in .PRP used in Prosper produced by the IPM EoS Composition Export Option within PVTp

3.2.2 Prosper Software

The Snøhvit well model was done using Prosper, the model setup followed a systematic approach, progressing from the left side to the right side of Prosper's main screen. The main screen is organized in the following order:

- Options Summary
- PVT Data
- IPR Data
- Equipment Data
- Analysis Summary

```

Petroleum Experts - PRP Export File
Export File Signature
Export File Version
*****
***** FILE DETAILS *****
FILE NAME : C:\Users\user\Desktop\Example2_Gas_Samp1.prp
Exported : Tue Mar 31 16:33:19 2021
*****
Equation Type 0 - Peng Robinson 1 - SRK
0
Number of Components Number of Lumped Components - Set to 0 if No Lumping Present
30 0
Mole Critical Critical Accentric Molecular Specific Critical Volume Boiling Parachor Omega Omega Costald Costald
percent Temperature Pressure Factor Weight Gravity Volume Shift degrees F Volume Accentric Component
degrees F psig lb/lb.mole lb/lb.mole 1/kg.mole 1/kg.mole 1/kg.mole 1/kg.mole 1/kg.mole 1/kg.mole
3.79998013 -233.140404 477.212608 0.039000008 28.0100002 1.02600002 89.7999986 -0.151999999 -120.380006 60.4000015 0.457285229 0.0777960739 90.1499015 0.0357998013 "N2"
0.149999012 87.4902013 3058.21991 0.219999993 44.0099983 1.100999993 99.9000016 -0.100999997 -109.209999 78 0.457285229 0.0777960739 99.9299982 0.232727 "CO2"
67.9096024 -116.517998 658.380798 0.020999999 16.0400009 0.414999992 99.2000016 0.135808024 -218.790009 70 0.457285229 0.0777960739 99.3900027 0.0074 "C1"
1.151999004 89.7079965 653.681184 0.088999996 30.1000004 0.846000004 148.2099994 -0.194813399 -127.1899993 115 0.457285229 0.0777960739 145.7499998 0.0983000018 "C2"
1.44910139 204.005997 402.482381 0.113999997 44.0099983 0.84999979 201.000001 -0.188100012 -43.4899988 135 0.457285229 0.0777960739 200.88001 0.113200008 "C3"
1.149999004 707.274494 514.381995 0.182999998 58.0999985 0.600000024 261.000001 -1.63144156 10.8850004 181.5 0.457285229 0.0777960739 256.83001 0.182100005 "IC4"
1.029999007 381.524006 533.281215 0.199000001 58.0999985 0.600000024 254.999994 -0.187346119 11.1900006 140 0.457285229 0.0777960739 254.99001 0.200400001 "IC4"
0.49996026 169.406 468.381511 0.229999998 72.1999989 0.620999992 306.999992 -0.107446243 82.1299971 225 0.457285229 0.0777960739 309.19002 0.2399001 "IC4"
1.00999004 381.524006 474.827719 0.200999987 72.1999989 0.620999992 304.000005 -0.221048134 96.6899994 148 0.457285229 0.0777960739 311.93006 0.321000007 "IC4"
1.149999004 484.100006 421.008311 0.298999995 86.1999989 0.661999975 369.999997 0.015725443 111.71 382.5 0.457285229 0.0777960739 368.199996 0.300700009 "C6"
0.40098029 128.864777 498.623779 0.247932444 97.1318029 0.74744217 421.748144 0.0077804821 194.448005 304.350019 0.457285229 0.0777960739 400.239004 0.28211422 "C11C"
0.12484029 189.174661 451.312743 0.281048887 113.1579002 0.774400715 481.248144 0.0077804821 246.42199 349.461317 0.457285229 0.0777960739 451.31201 0.30811116 "C11C"
4.63264029 650.120999 406.26719 0.334302902 123.583998 0.79294989 560.238144 -0.0004480802 308.21999 375.02705 0.457285229 0.0777960739 550.30874 0.35168935 "C11C"
4.63264029 650.120999 406.26719 0.334302902 123.583998 0.79294989 560.238144 -0.0004480802 308.21999 375.02705 0.457285229 0.0777960739 550.30874 0.35168935 "C11C"
0.00884024 734.790017 356.115219 0.197212134 149.448994 0.81776024 664.810118 0.0408979109 386.142012 438.508641 0.457285229 0.0777960739 581.148514 0.42101415 "C11C10"
0.10024011 769.465441 338.277496 0.424700442 161.448994 0.82810984 711.153451 -0.0408979109 420.240002 460.03904 0.457285229 0.0777960739 635.88792 0.44572792 "C11C11"
0.12991005 809.828491 318.843719 0.46018819 174.690002 0.840462983 773.799233 -0.204921516 461.319 498.025118 0.457285229 0.0777960739 688.90542 0.49013719 "C11C12"
0.05191019 849.792127 298.602746 0.49878992 187.090002 0.851806098 838.448696 -0.194734442 502.540001 522.688977 0.457285229 0.0777960739 741.901516 0.52587345 "C11C13"
0.021978608 890.48999 274.517789 0.539627135 199.347 0.86211019 912.959719 -0.18689963 546.072021 548.494041 0.457285229 0.0777960739 792.042512 0.57848446 "C11C14"
0.020202004 931.50915 260.394165 0.576480821 211.448006 0.866317976 969.151764 0.116020096 577.680029 571.490026 0.457285229 0.0777960739 850.96997 0.60841164 "C11C15"
    
```

Figure 3.8: Sample Export File (.PRP) from IPM EoS Composition Export Option in PVTp for Prosper

- Well Schematic

When Prosper is opened a screen similar to the one in Figure 3.9 will appear. To start Prosper, select the appropriate icon and double-click the program icon. Calculation menus are activated only when the necessary input data has been entered.

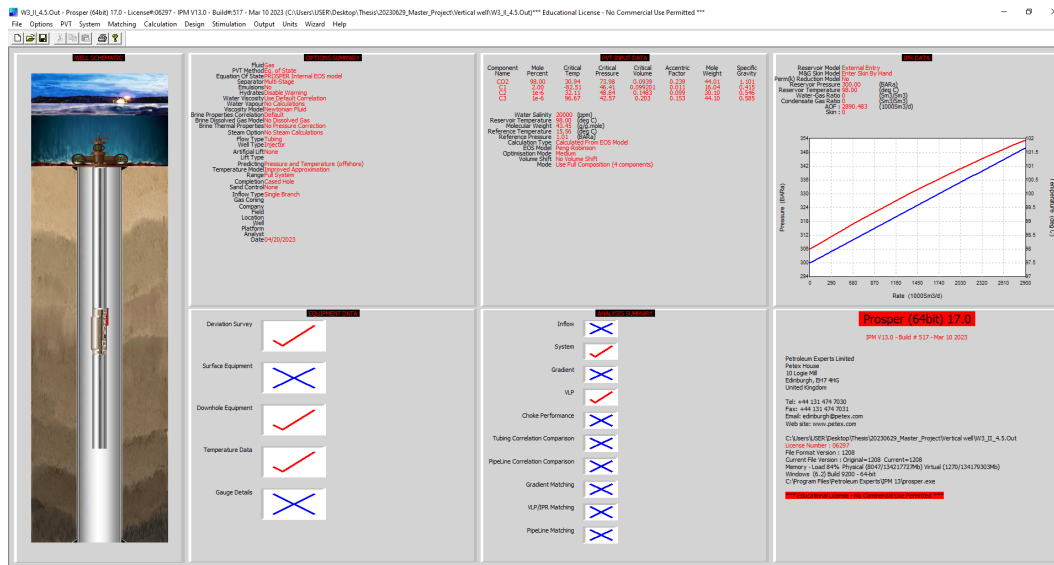


Figure 3.9: Snohvit Well Modeling Procedure in Prosper: Sequential Model Setup and Main Screen Organization. The figure shows Prosper’s main screen layout order and initiation process

The preceding points will be elucidated, along with an explanation of their utilization within this project.

3.2.3 Options Summary

The first step in any Prosper model is to set up the type of well which is to be modeled. The option screen can be accessed by double clicking on the **Options Summary** in Figure 3.9, the screen in Figure 3.11 will then appear, in this case, the data is kept as the default for most of the options with the fluid being changed to Dry and Wet Gas.

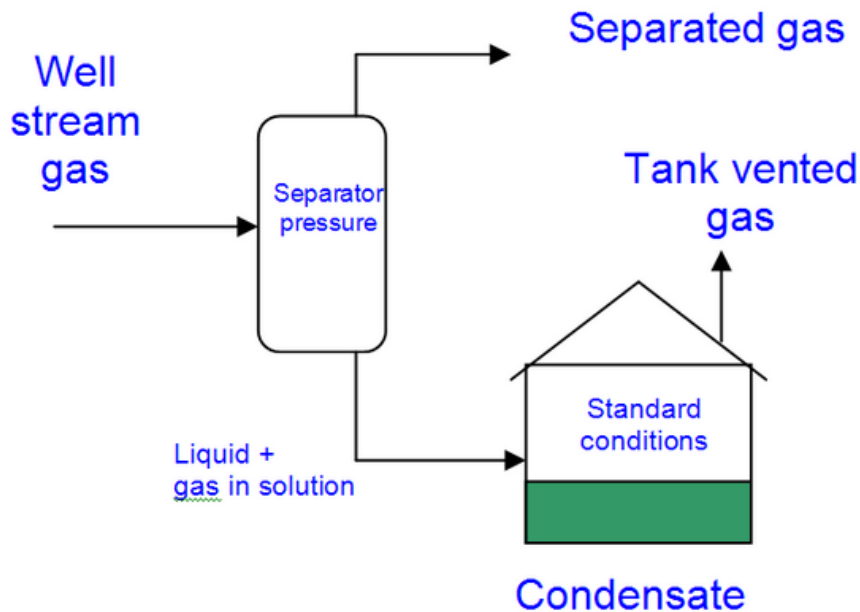


Figure 3.10: The objective of the setup is to obtain the properties of the "well stream" gas from the separated gas, tank-vented gas, and condensate [53]

For Producers and Injectors, the option uses traditional Black Oil models or Compositional (Equation of State), the dry-wet gas model in Prosper assumes that the condensate drops out at the separator and therefore treats the hydrocarbons as a single phase (gas) in the tubing. (Any water present will of course be treated as a separate phase, resulting in a two-phase flow) The objective is to obtain the properties of the "well stream" gas from the separated gas, tank-vented gas, and condensate. As per the diagram in Figure 3.10. The ideal way to do this is to perform a compositional analysis where the composition of the gas separated, condensate, and gas vented are known. Then these fluids are recombined to get the well stream composition and properties [53]. Moreover, the calculation type method was changed to **Improved Approximation**, the Well type was changed to **Injector**, and the method to **Equation of State**. The Improved Approximation makes this model particularly useful when an accurate calculation of temperature is sought and only a few data on the completion are available.

To set up the Equation of State Options, select **EoS Setup** in Figure 3.11, and the below screen in Figure 3.12 will appear. This screen is used to select the EoS model to be used as well as setting the path the fluid will take to the surface and other options.

Figure 3.11: shows Initiating Prosper Model: Configuring Well type, adjusting the fluid type and Equation of State setup, calculation method.

The equation of state that was used during the characterization process was the Peng Robinson and therefore this should be selected at the top of the screen. The viscosity of the fluid was calculated using the Lohrenz, Bray Clark method. This should be selected for both the oil and gas viscosity methods. The reference temperature and pressure are also set.

At the bottom of the screen, the path the fluid takes to the surface can be entered. Since the equation of state model is used, it is important to enter a path to the surface that is representative of the actual field values. In this case, a flash straight-to-stock tank is entered. When this section has been completed, select OK and done to return to the main prosper screen in Figure 3.9

3.2.4 PVT Data

The next stage is to insert the available PVT data into the model. The PVT input screen can be accessed by double-clicking on the **PVT Input Data** tab in Figure 3.9 and the following screen in Figure 3.13 will open. This section allows the engineer to predict pressure and temperature changes along the surface flow lines through the wellbore to the reservoir, it is necessary to accurately predict the fluid properties as both pressure and temperature change. The user must enter data that describes the fluid properties. This dialog is used to enter/edit/view a fluid composition. This main dialog allows user

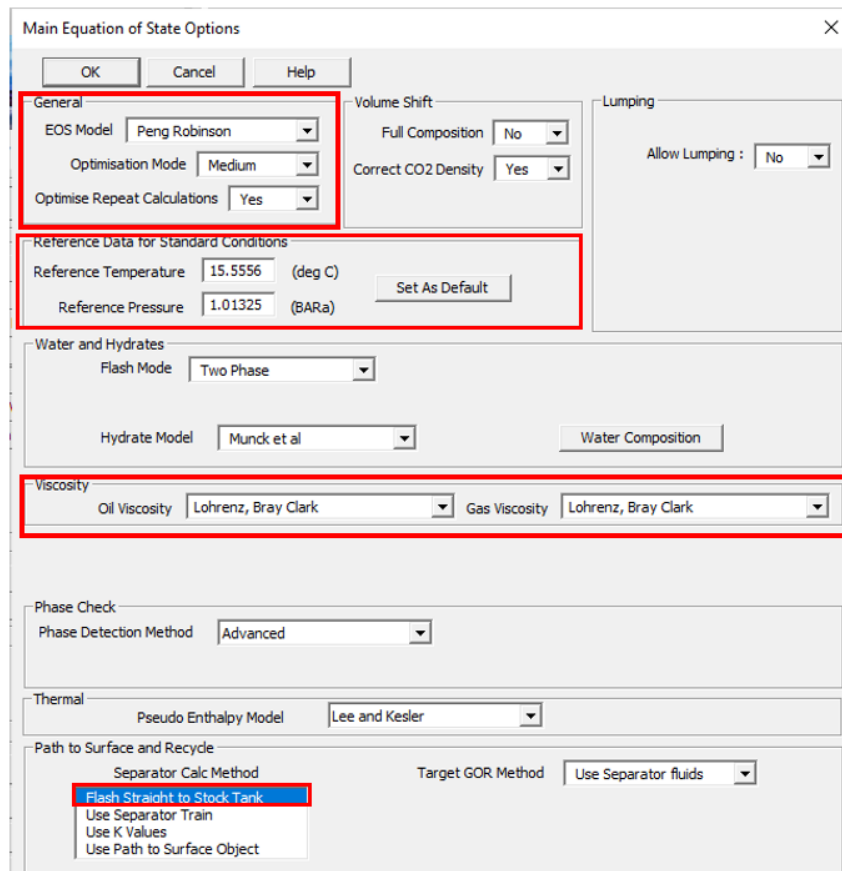


Figure 3.12: Setting Equation of State Options: EoS setup, Peng Robinson as the EoS model. Utilize the Lohrenz, Bray Clark method for fluid viscosity calculations. Set reference temperature and pressure.

to enter the number of components as well as their names. One can then enter the various properties per component.

By clicking on the import PRP in Figure 3.13 a file previously created in PVTp (see Figure 3.8 for sample) which is representative of the injected CO₂ is imputed as seen in Figure 3.13. When the file is imported the CO₂ mole percentage was changed to 98%, and methane 2%. Ethane and propane changed to zero respectively. Reference was earlier made to this in the section 2.4. When the file has been imported, enter the reservoir temperature and water salinity at the bottom of the screen. To view the phase envelope of the fluid select **Phase Env...** To calculate the hydrate formation curve for a fluid click on **calculate hydrate...Wax**.

The critical volume is the main variable used in the LBC Viscosity Model. The parachor is the main variable used in the calculation of Interfacial Tension. Volume Shift can be switched on/off from the main options dialog. OmegaA and OmegaB are normally

constants within the equation of state but they become variables when used as match parameters. Boiling temperature is used as an indicator of the general characteristics of a component. As such it is used as a key in the creation of various correlations. Other keys include specific gravity and molecular weight. For example, all three of these key variables are used in the correlation which calculates the ideal enthalpy of a pseudo component within the EoS [53]

The 'Edit Composition' dialog box is shown with the following data in the component table:

	Name	Mole Percent (percent)	Critical Temp. (deg C)	Critical Pressure (BARa)	Critical Volume (m ³ /kg.mole)	Acentric Factor	Molecular Weight	Specific Gravity (sp. gravity)	Boiling Point (deg C)	Volume Shift	Ome
1	CO2	98	30.94	73.9777	0.0939	0.239	44.01	1.101	-78.45	---	0.4:
2	C1	2	-82.51	46.407	0.099201	0.011	16.04	0.415	-161.55	-0.154	0.4:
3	C2	1e-6	32.11	48.8388	0.1483	0.099	30.1	0.546	-88.55	-0.1002	0.4:
4	C3	1e-6	96.67	42.5668	0.203	0.153	44.1	0.585	-42.05	-0.08501	0.4:
5											
6											
7											
8											
9											
10											
11											
12											
13											
14											
15											
16											
17											
18											

Additional fields in the dialog include: Viscosity Mode OIL: Lohrenz, Bray Clark; Viscosity Mode GAS: Lohrenz, Bray Clark; Pseudo Enthalpy Model; Calculation Type: Calculated From EOS Model; Reservoir Temperature: 98 (deg C); Salinity: 20000 (ppm); Water Composition.

Figure 3.13: This dialog is used to enter/edit/view the fluid composition. Called from the PVT section of PROSPER this dialog allows you to enter the number of components as well as their names. One can then enter the various properties per component. There are additional dialogs which can be accessed from this screen

3.2.5 IPR Data

As earlier explained in section 2.5.3 in the case of injection The Inflow Performance Relationship (IPR) defines the flow into the reservoir from the wellbore. To calculate an IPR results in a relationship between the bottom hole pressure and the flow rate passing into the well the following steps are taken in Prosper. On the Prosper main menu in Figure 3.9 double-click on the IPR data section, and then the main data entry screen will appear see Figure 3.14

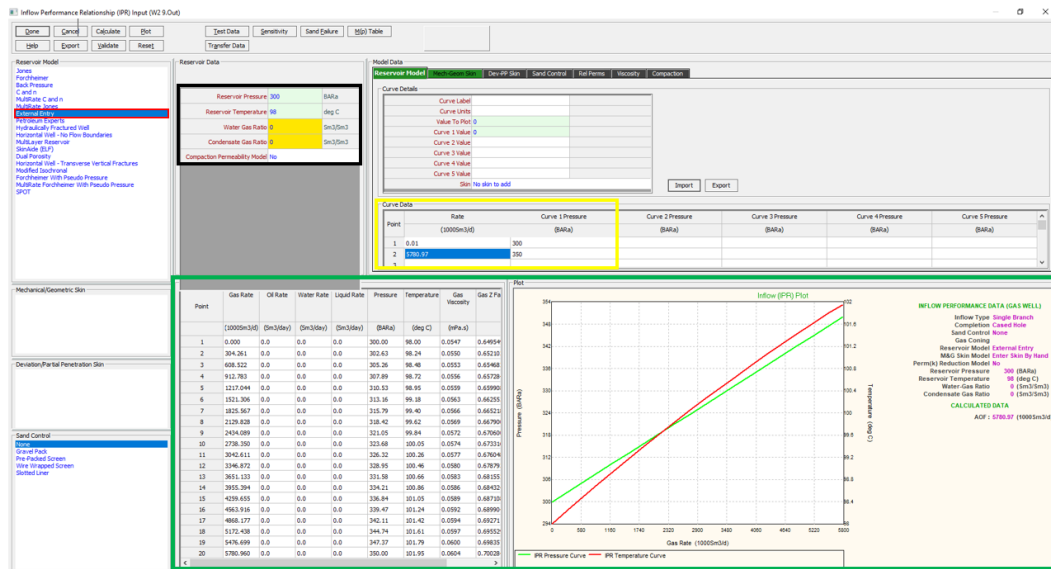


Figure 3.14: Shows the Inflow Performance Relationship (IPR) data input menu, this figure describes how Prosper defines the reservoir inflow performance

The screen consists of four main parts shown below and will be discussed in detail in the following subsection;

- Reservoir Model
- Reservoir Data
- Model Data
- Result

Reservoir Model

As mentioned earlier in section 2.5.3, about twenty inflow options are available in Prosper see Table A.3. In this area, the main parts of the model are defined including the IPR model, which (if any) skin models and sand control devices are being used. The choice depends upon the available information and the type of sensitivities that the user wishes to run. For each fluid, various single-well IPR models are available to be selected. To select the IPR method click on the appropriate field in the reservoir model list box. For this model, the External Entry was used, because this option allows an externally generated IPR data set to be imported or directly entered. However, the simplified Darcy model can be used to generate straight-line IPR if the drainage area, Dietz shape factor, and reservoir thickness parameters are available. The section highlighted in Figure 3.14 called curve data shows the external data calculated from Microsoft Excel entered manually see details in table 3.1.

Reservoir Data

A number of general reservoir parameters such as pressure, temperature, water cut, and GOR are defined in this section see Figure 3.15. As reported in the literature for the Snøhvit field the reservoir pressure and temperature were inputted respectively see Figure 3.15. The relative permeability option can be set to Yes or No in the case of oil. If set to Yes, the user has the option of defining a set of relative permeability curves, which will be used to change the productivity of the system with changing watercut.

Reservoir Data		
Reservoir Pressure	300	BARa
Reservoir Temperature	98	deg C
Water Gas Ratio	0	Sm ³ /Sm ³
Condensate Gas Ratio	0	Sm ³ /Sm ³
Compaction Permeability Model	No	

Figure 3.15: Allows general reservoir parameters such as pressure, temperature, water cut and GOR to be defined.

Model Data / Curve Data

The model data section contains a set of data entry tabbed dialogues that become available depending on the IPR model and other options selected. When the External Entry IPR model is selected, the Curve data option is activated which is highlighted in yellow in Figure 3.14, a snapshot of the highlighted yellow section is shown in Figure 3.16, the 0.01 (1000Sm³/day) rate in line number one was an assumed rate expected to be injected into the formation at a bottom hole flowing pressure of 300 bar. The second line with 5780.97 (1000Sm³/day) is the calculated injection rate at 350 bar flowing bottom hole pressure with injectivity of 9 t/h/bar. Details of the calculations are shown below in Table 3.1 with detailed mathematical equations used to arrive at these figures explained in section 2.5.3.

Description	Unit	Equation	Value
Injectivity (II)	[t/h/bar]	[-]	9
CO2 Density @ Standard Condition	[kg/m ³]	[-]	1.8682
Injectivity (II)	[Sm ³ /d/bar]	(injectivity[t/hr/bar] *1000* 24)/CO2 Density	115619
Initial Reservoir Pressure (Pr)	[bara]	[-]	300
Flowing Bottom Hole Pressure (Pwf)	[bara]	Pr + 50bar	350
Gas Rate	[sm ³ /d]	(Injectivity [Sm ³ /d/bar]* (Pwf - Pr))/1000	5780.97

Table 3.1: Gas Injection Rate Calculation

Curve Data		
Point	Rate (1000Sm ³ /d)	Curve 1 Pressure (BARa)
1	0.01	300
2	5780.97	350

Figure 3.16: Allows an externally generated IPR data set to be imported or directly entered

Result

When the Reservoir Model data, Reservoir Data, and the Model Data/Curve Data have been inputted, click calculate in Figure 3.14 to calculate the IPR and click on plot, to view the curve IPR curve. The results of the IPR calculation are shown in the Results section. The results include

- A breakdown of the results in table form
- A graph of FBHP and FBHT with temperature

More detailed plotting can be obtained from the results menu see Figure 3.17. The IPR curve shows both the variation in bottom hole pressure and bottom hole temperature as the rate changes. See section 4.2 for more on the IPR plot. To close the plot, select the red cross in the top right-hand corner. Then, select Done to return to the main Prosper screen in Figure 3.9. The main screen will now display an IPR curve to show the completed calculation.

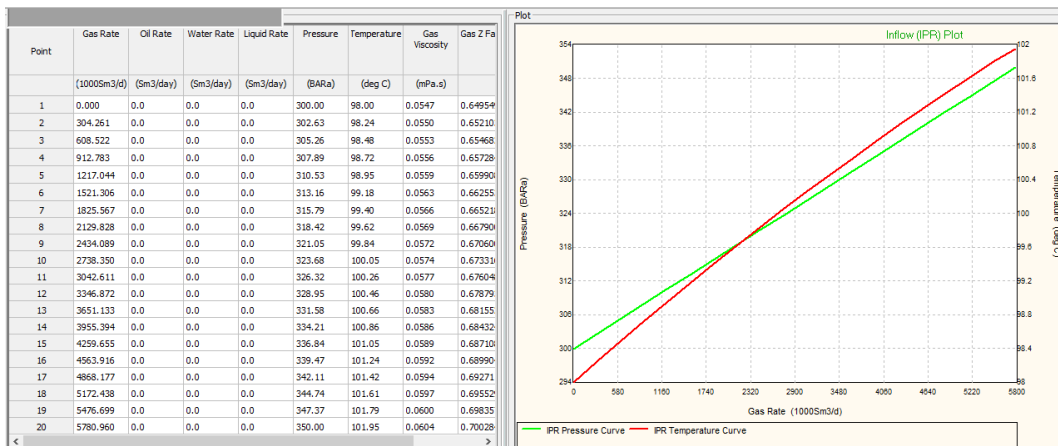


Figure 3.17: The IPR curve shows both the variation in bottom hole pressure and bottom hole temperature

3.2.6 Equipment Data

This section describes the menu option used to define the wells hardware, deviation survey and formation temperature profile. The program requests only the data required by the options that have been selected. In order to calculate the VLP curves for the well, Prosper must have a description of the well and the path through which the fluid flows from the bottom of the well to the wellhead.

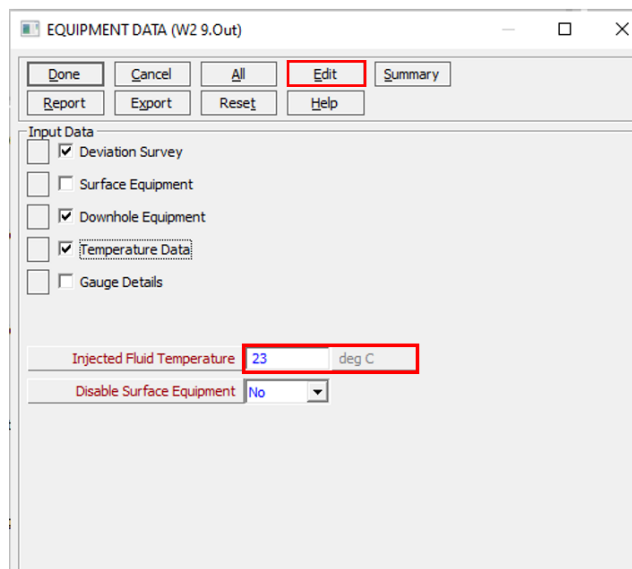


Figure 3.18: show the menu option used to define the well hardware, deviation survey, and formation temperature profile

This is done in the 'Equipment Data' section, which can be accessed by first double-clicking on the Equipment Data section in Figure 3.9. This will bring up the Equipment

Data screen in Figure 3.18. In order to fill in data for all of the appropriate sections, the user can either select All from the top ribbon which will bring up ticks next to each section, or manually tick the box of interest as shown in Figure 3.18 for Deviation Survey, Downhole Equipment, and Temperature Data. If only one section is to be edited, the required section can be accessed by selecting the square to the left of the ticked box corresponding to that section. The Injected Fluid Temperature is set at 23 degrees Celsius. The Surface Equipment is disabled, GAP will be used to model the surface equipment. The Edit button can now be selected to bring up each input section one at a time. The first is the **Deviation Survey**.

Deviation Survey

In the screen in Figure 3.19, the well deviation survey can be added, in this case, two points 0 to 2798m, the well is vertical, Measured Depth(MD) and True Vertical Depth (TVD) are equal hence the angle is zero. From the well deviation survey, a number of depth points can be selected. Enter pairs of data points for measured depth (MD) and the corresponding true vertical depth (TVD). This section is also used to model both deviated and horizontal well. Once depths have been entered, plot the well profile by selecting Plot. To move to the next input screen, select Done

Point	Measured Depth (m)	True Vertical Depth (m)	Cumulative Displacement (m)	Angle (degrees)
1	0	0	0	0
2	2798	2798	0	0

Figure 3.19: Allows the user to enter the well deviation survey, measured depth (MD), and the corresponding true vertical depth (TVD). Up to 20 pairs of data points can be entered

Downhole Equipment

The downhole equipment section defines the path through which the fluid will flow as it is injected into the well bore. Details of the equipment to be installed can be found in Figure 3.20 below. Details of the well-measured depth, and tubing internal diameter are as reported in the Statoil (now Equinor) publication, Snøhvit CO₂ Tubåen Fm Storage Capacity and Injection Strategy Study [4].

The final depth from the down-hole equipment will be used as the solution node depth which splits the well into the VLP and IPR. This depth is also therefore the depth at which the static reservoir pressure is defined in the IPR section. It is normally defined as the top of the perforations and thus this equipment description stops at the top of the perforations. When the data has been inputted, the next input screen can be accessed by selecting **Done**.

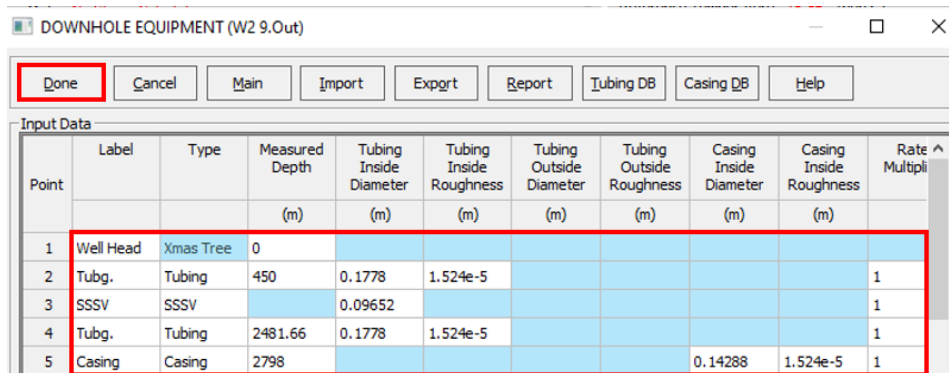


Figure 3.20: Show the Downhole Equipment screen, which enables the down-hole completion data to be entered.

Temperature Data

This screen enables entry of the flowing temperature profile of the fluid in the well. A minimum of two depth and temperature points is required.

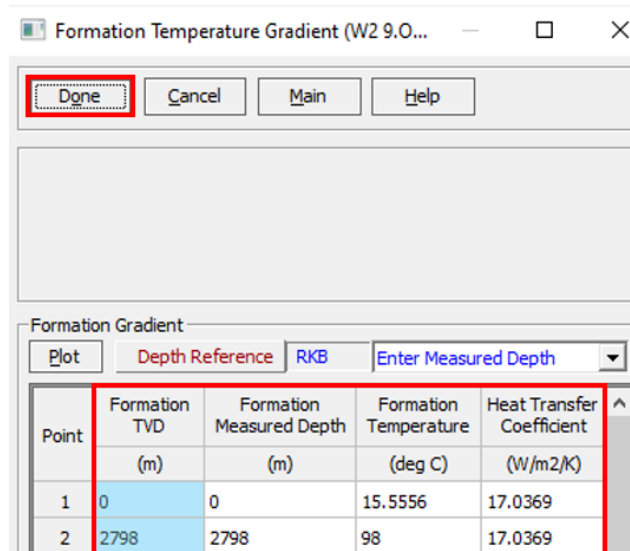


Figure 3.21: Show the Formation Temperature Gradient screen, the screen enables entry of the flowing temperature profile of the fluid in the well

Formation measured depth is manually entered and the Formation's True Vertical depth (TVD) is automatically calculated. The formation temperature is the temperature from the top of the formation to the bottom of the well. Selecting **Done** will exit the geothermal gradient screen and enter the main prosper screen.

3.2.7 Analysis Summary

Now that the well data has been inputted into Prosper, the next step is to calculate the rate at which the well can flow at a given set of conditions. In this section, while the Analysis Summary offers various options, the specific focus narrows down to two: the **System Sensitivity Analysis** and **VLP**. These two components are the sole requirements for the analysis at hand as shown in the highlighted part in Figure 3.22

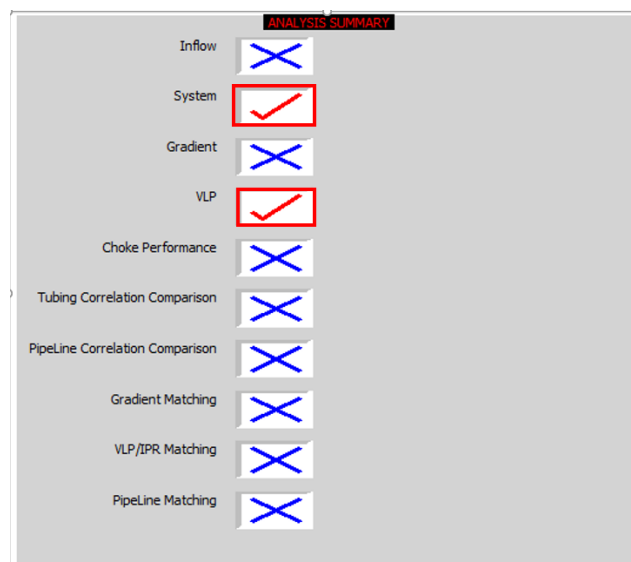


Figure 3.22: displays the Analysis Summary section, providing access to both the System Sensitivity Analysis and the VLP section.

System Sensitivity Analysis

The System Sensitivity Analysis combines VLP and IPR plots to find the system point at which the well will flow see Figure 3.23. The principles of 'nodal analysis' dictate that any single point (in this case the bottom hole) must observe mass balance and can only have one pressure associated with it. This means that the rate at which the VLP and IPR curves across is the rate at which the well will inject fluid under these conditions.

To access the system sensitivity analysis screen, double-click on the system box under the Analysis Summary in Figure 3.22 to enter the System calculation screen shown in Figure 3.23

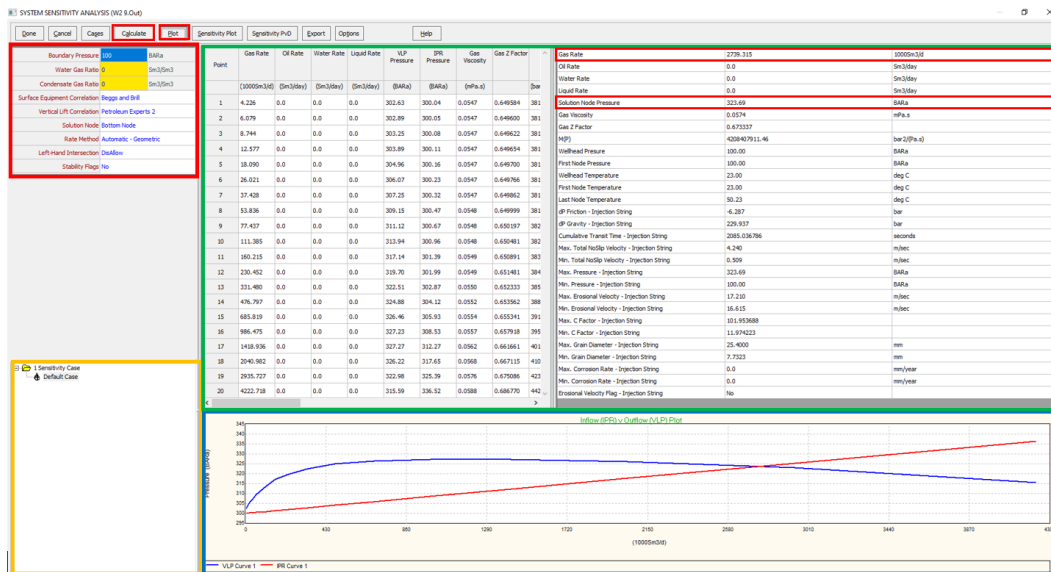


Figure 3.23: Shows the System Calculation input screen which combines the VLP and IPR plots to find the system point at which the well will flow.

The screen is split into 4 main elements;

- **Data Input (Top Left):** contains the input data that will be used for the calculation highlighted in red. The boundary pressure was assumed to be 100bar, and as discussed in section 2.5.7 Beggs and Brill is used for the surface equipment correlation, while for the vertical lift correlation, Petroleum Expert 2 was used see detail in Figure 3.24.

Solution Node: Everything upstream of the node is treated as the 'IPR' and everything downstream of the node will be part of the 'VLP'. The **bottom node** was selected, this means that the solution node pressure will correspond to the FBHP

Boundary Pressure	100	BARa
Water Gas Ratio	0	Sm ³ /Sm ³
Condensate Gas Ratio	0	Sm ³ /Sm ³
Surface Equipment Correlation	Beggs and Brill	
Vertical Lift Correlation	Petroleum Experts 2	
Solution Node	Bottom Node	
Rate Method	Automatic - Geometric	
Left-Hand Intersection	DisAllow	
Stability Flags	No	

Figure 3.24: Shows the Interface for Inputting data and Multiphase Flow Correlation for IPR and VLP Curve Calculation

- **Sensitivity Cases** (Bottom Left, highlighted in orange): contain any information on the sensitivity study cases being considered. No sensitivity case was considered in this section
- **Results** (Top Right): contain information on the system calculation and the solution point which is obtained, this section is highlighted in green.
- **System Plot** (Bottom Right): The results screen shows the system plot at the bottom of the screen it contains the system plot (consisting of the VLP and IPR curves) this section is highlighted in blue.

To perform a System Calculation and generate the system Plots, select **Calculate** in the title bar in Figure 3.23 and the plots can be viewed by selecting **Plot**. Select **Done** to return to the main Analysis Summary screen in Figure 3.22

3.2.8 Generating VLP Curves

An important Prosper application is generating Tubing Lift Curves for use in reservoir and total system simulators. The Calculation VLP (Tubing Curves) option will allow the user to generate Vertical Lift Performance (VLP) curves for ranges of different variables which can then be exported to a number of different formats and used in conjunction with GAP and other software.

To access the VLP (Tubing Curve) Calculations screen, double-click on the VLP box under the Analysis Summary screen in Figure 3.22 to enter the VLP (Tubing Curve) screen shown in Figure 3.25

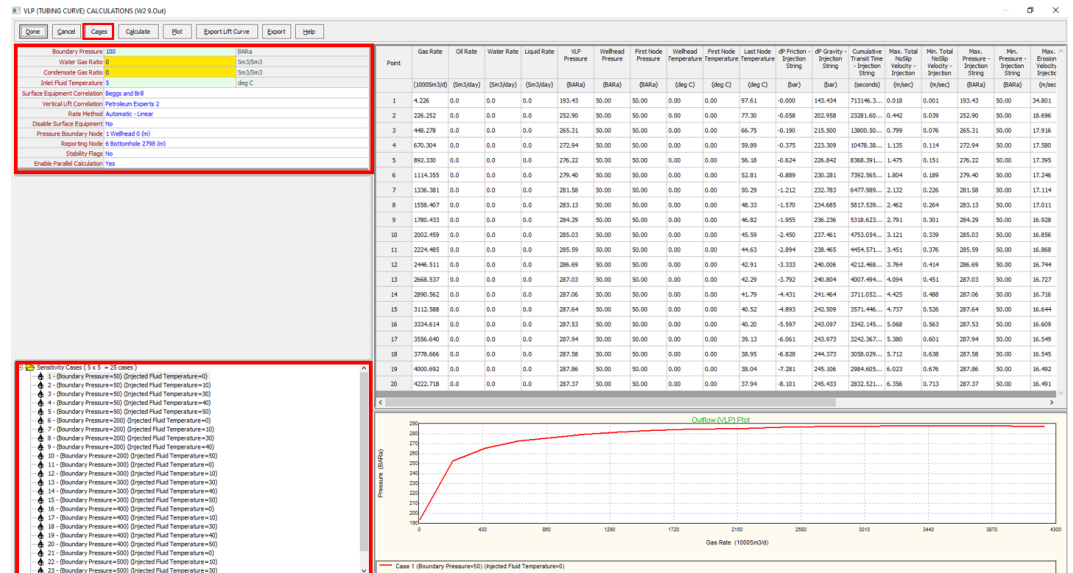


Figure 3.25: Shows the VLP screen, which allows the user to generate VLP curves for ranges of different variables. which can then be exported to several different formats.

Before any calculations can be carried out the conditions to be calculated as well as the correlation to be used must be defined. This is done in the top left corner of the VLP screen in Figure 3.25, detail of the screen is shown in Figure 3.26.

Boundary Pressure	100	BARa
Water Gas Ratio	0	Sm ³ /Sm ³
Condensate Gas Ratio	0	Sm ³ /Sm ³
Inlet Fluid Temperature	5	deg C
Surface Equipment Correlation	Beggs and Brill	
Vertical Lift Correlation	Petroleum Experts 2	
Rate Method	Automatic - Linear	
Disable Surface Equipment	No	
Pressure Boundary Node	1 Wellhead 0 (m)	
Reporting Node	6 Bottomhole 2798 (m)	
Stability Flags	No	
Enable Parallel Calculation	Yes	

Figure 3.26: Show the Interface for Inputting data and Multiphase Flow Correlation for generating Lift Curve

The value entered for the **boundary pressure** was assumed to be 100 bar, the surface equipment correlation and the vertical lift correlation are consistent with the correlation used for calculating the system IPR and VLP curve above. The inlet fluid temperature was initially set to 5⁰C and increased during the sensitivity study.

SELECT VARIABLES (W2 9.Out)	
1	Boundary Pressure
2	Injected Fluid Temperature
3	
4	
5	
6	
7	
8	
9	
10	

Variable Data	
Injected Fluid Temperature	
deg C	
1	0
2	10
3	30
4	40
5	50
6	
7	
8	
9	

Figure 3.27: Show the Interface for selecting Sensitivity case variables, and the corresponding variable data

When generating VLP curve tables for use in GAP, a series of variables are required to be calculated, this can be done using the **sensitivity cases** screen. To enter data for a sensitivity study select **Cases** on the top toolbar in Figure 3.25. This will bring up the sensitivity screen in Figure 3.27. Sensitivity case variables can then be selected, and the corresponding variable data entered manually. Boundary Pressure and Injected Fluid Temperature for different ranges are the two variables used for the sensitivity calculation in this case. Select **Done** to return to the main calculation screen in Figure 3.25 where the calculations can be performed. When the sensitivity study cases have been

set, then the list of **cases** will be shown in the bottom left-hand corner of the screen as shown in Figure 3.25. Selecting one of the cases will display the results and plot on the right-hand side of the screen after the calculation is completed.

After inputting the general data, and the necessary sensitivity cases as done above, the lift curves can then be generated by selecting **Calculate** in the toolbar in Figure 3.25. Once the calculation has been run, the top right-hand side of the screen will show the results of the VLP calculation. The result can be plotted by clicking on the Plot tab on the toolbar in Figure 3.25. See Figure 3.28 for the plot.

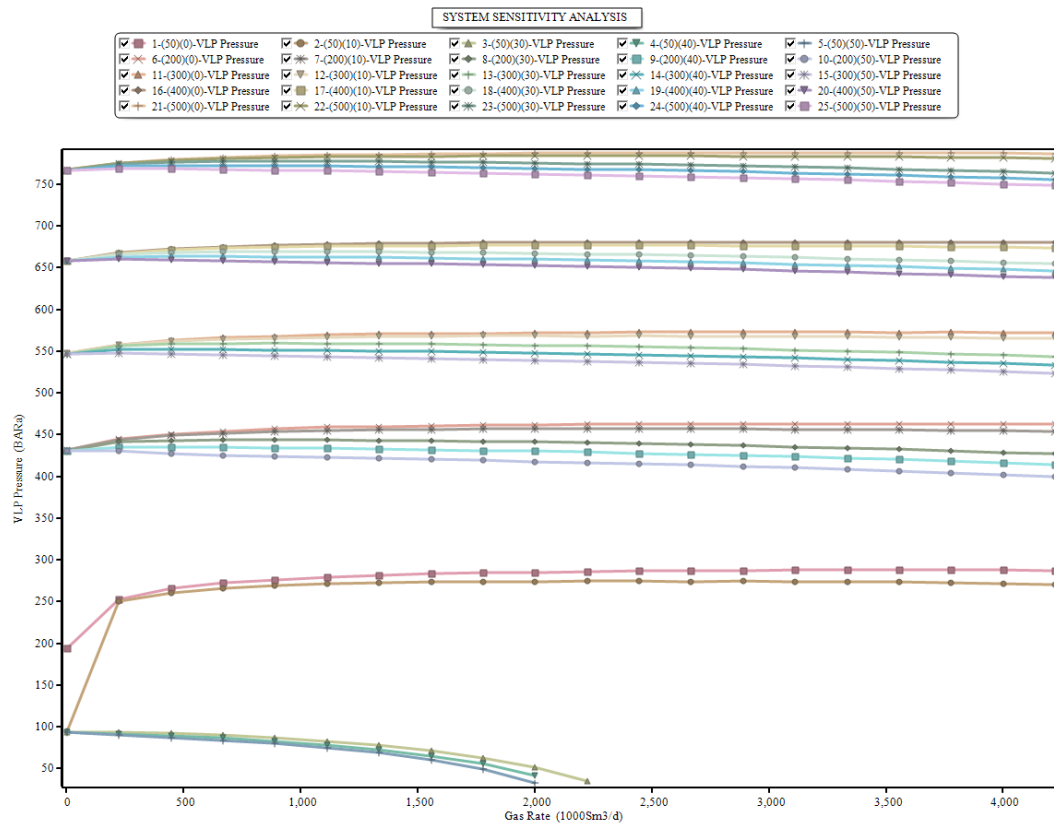


Figure 3.28: Shows a sample of the VLP Curves, generated for different sensitivity case variables with variable data

Once the VLP curves have been generated, the next step is to export them in a format that can be imported into a simulator like GAP or other programs. This can be done by clicking on the **Export Lift Curves** button as highlighted in the toolbar in Figure 3.29.

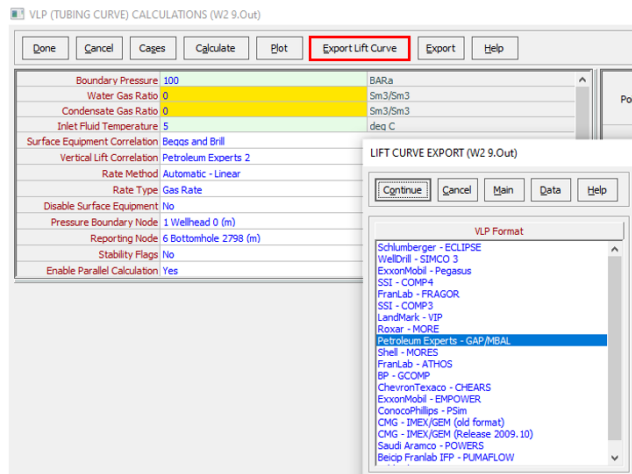


Figure 3.29: Display the screen for Lift Curve Export, where users can choose the export format.

This will bring up the export screen on which the format to be exported can be selected, see Figure 3.29 Lift Curve Export. Once the format has been selected, in this case, since the lift curve will be used in GAP the export format Petroleum Experts - GAP/MBAL was selected. Click Continue to save the file on the desktop. Figure 3.30 shows a sample of the export file.

```

File Preferences Help
# Rate and Variable Types
# Rate Variable = 4002 - Gas Rate
# Variable 2 = 324 - Injected Fluid Temperature
# Variable 1 = 27 - Boundary Pressure
4002,324,27
# Rate Values
0.15, 8.03053, 15.9111, 23.7916, 31.6721, 39.5526, 47.4332, 55.3137, 63.1942, 71.0747, 78.9553, 86.8358, 94.7163, 102.597, 110.477, 118.358, 126.238, 134.119, 141.999, 149.8
# Variable 2 (Injected Fluid Temperature) values
32, 50, 86, 104, 122
# Variable 1 (Boundary Pressure) values
710.493, 2886.06, 4336.44, 5786.81, 7237.19
# 4 Variable TPD Results
2790.83, 207.698, 0.215232, 0.0598084, 114.175, 0.0001, 0, 0, 713146
3653.31, 171.142, 9.46325, 1.45118, 61.3396, 0.172934, 0, 0, 23281.6
3833.31, 152.145, 17.8999, 2.62052, 58.7806, 0.640661, 0, 0, 13800.5
3943.92, 139.81, 26.0933, 3.72408, 57.6774, 1, 0, 0, 10478.4
3991.58, 133.132, 34.3189, 4.8392, 57.0794, 1, 0, 0, 8368.39
4037.64, 127.062, 42.4118, 5.91811, 56.5821, 1, 0, 0, 7392.57
4069.25, 122.515, 50.4989, 6.99626, 56.1499, 1, 0, 0, 6477.99
4091.7, 119.002, 58.5922, 8.07665, 55.8102, 1, 0, 0, 5817.54
4108.63, 116.27, 66.6859, 9.15748, 55.5373, 1, 0, 0, 5318.62
4119.27, 114.07, 74.7829, 10.2394, 55.3016, 1, 0, 0, 4753.05
4127.41, 112.328, 82.8855, 11.323, 55.3405, 1, 0, 0, 4454.57
4143.43, 109.246, 90.7763, 12.349, 54.9328, 1, 0, 0, 4212.47
4148.37, 108.123, 98.8739, 13.4314, 54.8795, 1, 0, 0, 4007.49
4148.71, 107.216, 106.987, 14.5182, 54.8418, 1, 0, 0, 3711.05
4157.19, 104.935, 114.865, 15.5412, 54.6072, 1, 0, 0, 3571.45
4155.55, 104.364, 122.981, 16.6288, 54.4926, 1, 0, 0, 3342.15
4161.52, 102.441, 130.849, 17.6495, 54.2937, 1, 0, 0, 3242.37
4156.24, 102.105, 138.977, 18.7404, 54.2829, 1, 0, 0, 3058.03
4160.3, 100.466, 146.841, 19.7603, 54.1069, 1, 0, 0, 2984.61
4153.19, 100.297, 154.978, 20.8536, 54.1045, 1, 0, 0, 2832.52
    
```

Figure 3.30: Present a sample of the Exported Lift Curve in TPD file format, intended for import into GAP for simulation.

At present, Prosper also supports the following export formats presented in Table A.4.

The upcoming section will delve into the implementation of GAP within the scope of this project. The steps involved in importing the **Lift Curve Exported file** into GAP

for simulation will also be explained.

3.2.9 GAP Software

GAP allows the engineer to accurately model well and pipeline and surface facilities (manifolds, compressors, etc). The pipeline network can be characterized by a very complex topology (with hundreds or thousands of elements and pipe loops). This allows the engineer to perform studies on full-field surface network design and more.

The main screen of GAP has the following structure as shown in Figure 3.31. Clicking **File** and then **New** will start a new system network from scratch. To get started, either a new or existing file can be opened by selecting the **File** option on the Menu bar and then clicking on New to start a new system network from scratch. This option clears the current system memory and begins with an empty main screen to allow a new network to be designed from scratch.

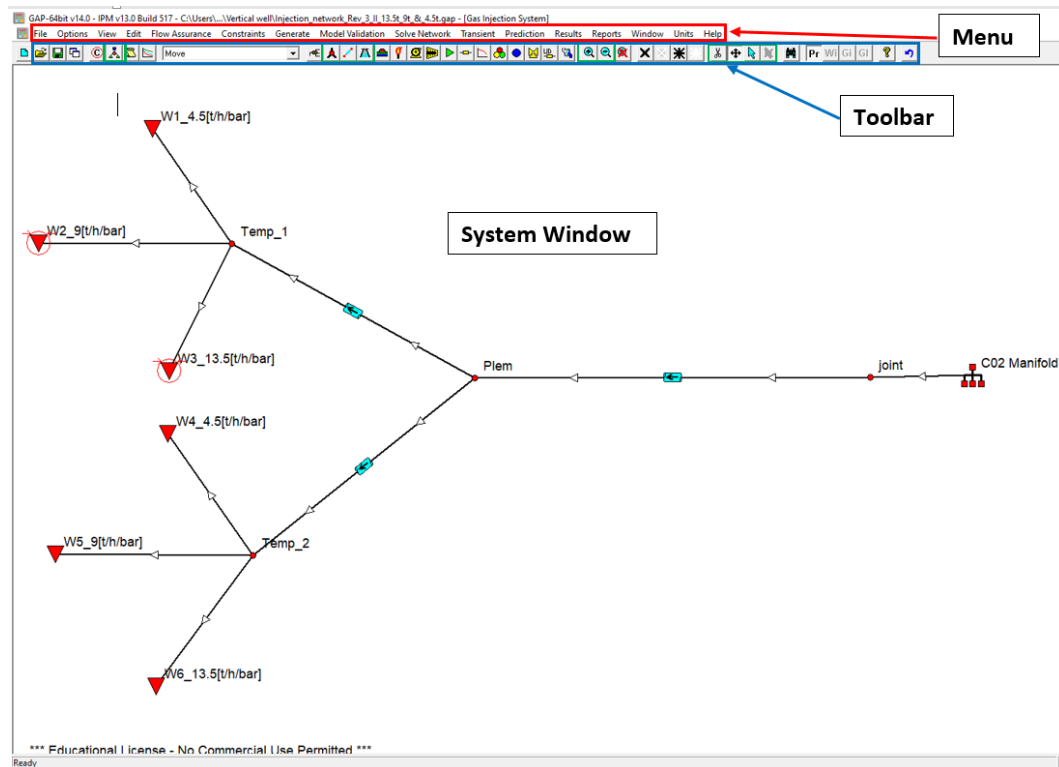


Figure 3.31: Shows the user interface consisting of a framework window that contains several child windows, as well as the menu and toolbar from which GAP commands are issued. The child windows include the system windows that contain the system network drawing, and the navigator window that can assist in the viewing of large networks.

The first step is to define the global system option. To begin setting up the system options, select **options** in the menu bar in Figure 3.31, then click on **Method**, the fol-

Following screen in Figure 3.32 will appear, make the following selections. When modeling pipelines carrying CO₂ for injection purposes, the PVT method must be an Equation of State using "Fully Compositional". On the PVT Model, it is important to select fully compositional, before selecting **Gas injection** under the system type. Selecting the PVT model as fully compositional enables the user to be able to import a **PVTp file** into GAP see Figure 3.8. After making the above selections the following selection from Prediction to Brine Properties correlation can be made respectively. Click 'OK' to exit this screen. This completes the system set-up and reinitializes the program.

To define the unit system, click on Units in the menu bar and select the Norwegian Unit.

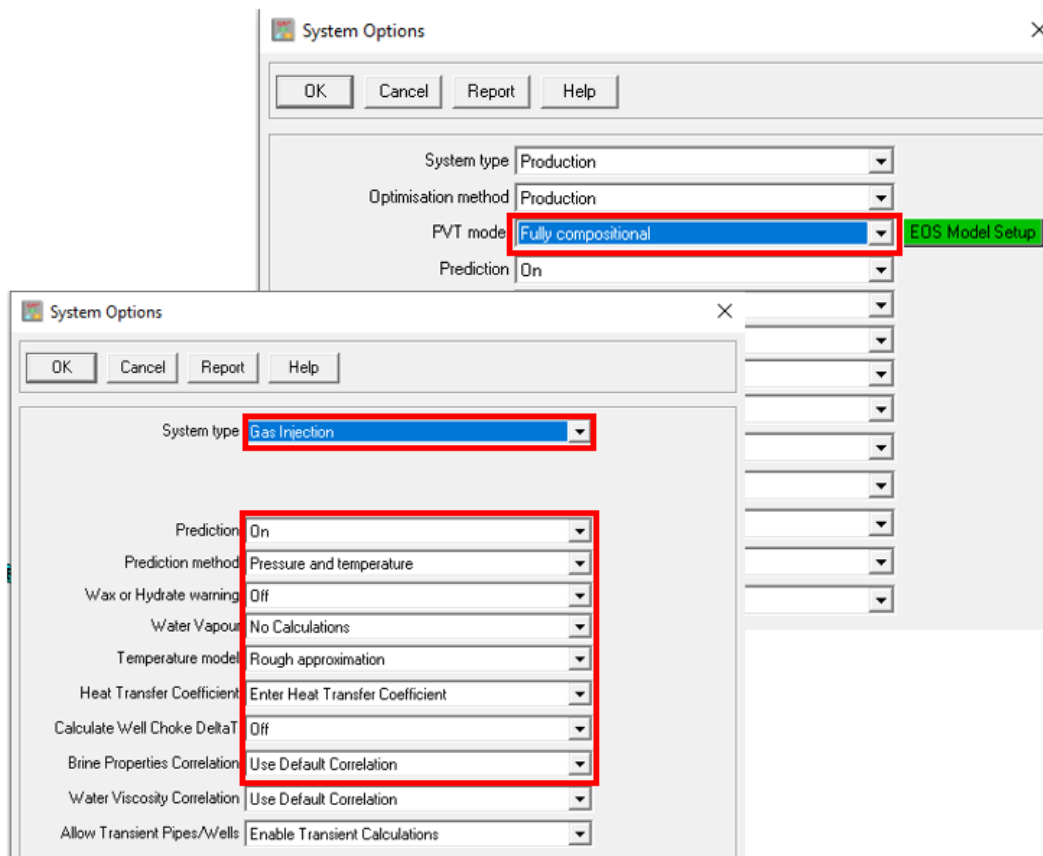


Figure 3.32: Is where the overall system parameters are set up, including the type of system (Production or injection), the prediction mode, and various options on the optimization process.

The functions of the various buttons mentioned in Figure 3.33 will be discussed from left to right as these are the main functions used in this model

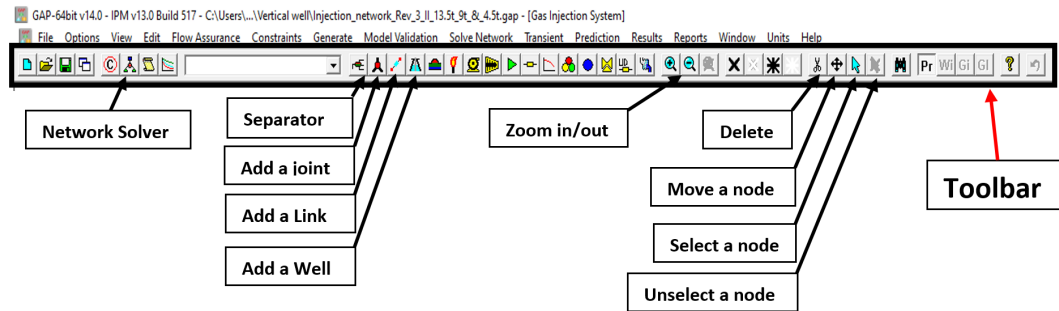


Figure 3.33: Shows the section of the Toolbar, It consists of a row of icons that act as accelerators to common menu functions, or allow the addition or manipulation of network icons in the system window.

Network Solver

This function is used to run the final calculations after the modeling is completed.

Separator

This button is used to add a separator, manifold, and LNG Plant. The Injection Manifold is defined using the same element as the Separator which can be accessed by the Separator button. Selecting this icon and then clicking on the main GAP screen will activate the window in Figure 3.34. Select the 'Gas Injection Manifold' and an element with a manifold sign will appear on the main screen.

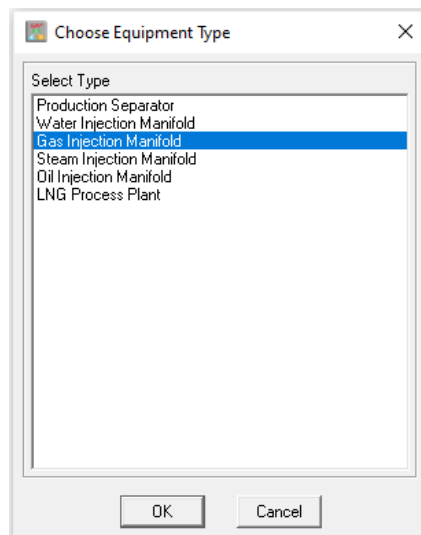


Figure 3.34: The screenshot provides an option for the user to choose equipment types.

The Joints

Click on the Joint icon from the toolbar in Figure 3.33 and add the 4 joints by clicking on the main GAP System Window area as shown in Figure 3.31. The joint elements are labeled as Temp-1, Temp-2, Plem, and Joint respectively.

The links /pipes

Links are connection tools that connect the various nodes/joints in the network system. It is important to note that a link between a well and a joint has no dimension, a link between two joints has dimension. To Link components together, select the link icon from the main toolbar in Figure 3.33. Click on the first component to be connected, keep the left mouse button pressed, and move the cursor from the first component to the second component. A link/pipe will form when the mouse button is released over the second component. see details in Figure 3.31

The Wells

The Well Icon is used to add wells to the model. To add Wells, select the Well icon in Figure 3.33 and add a well from the main toolbar by clicking in the main GAP System Window area in Figure 3.31. Six Wells are added to the model names W1, W2, W3, W4, W5, and W6. The well names can always be modified.

Zoom

Zoom in/out buttons are for zoom in and zoom out

Delete

Elements can be deleted by selecting the scissors icon from the toolbar menu in Figure 3.33 and clicking on any element in Figure 3.31 to be removed.

Move

To move an element of the network to a new location on the screen, select the move button from the main toolbar in Figure 3.33, hover the mouse arrow over the element to be moved, and press the left mouse button and the shift key. Keep the left mouse button pressed and move the element to the new location. Releasing the left mouse button will then position the element in the new location.

Select

After the icon in Figure 3.33 is pressed, a node may be selected by clicking on the item in the system window. A cyan circle around the item indicates the item is highlighted.

Unselect

This icon unselects all items.

3.2.10 Imputing Data Into The GAP Model

In order to describe the procedure for defining pipelines, access the pipe summary screen by double-clicking on the blue icon in the middle of each pipe in Figure 3.31 the following screen in Figure 3.36 will show. Click on the 'Description' tab to enter the geometry of the pipeline. Up to 500 pipeline segments can be entered. Pipe data must be entered from the downstream node to the upstream node as shown in Figure 3.35. Other components of the model can be accessed and modified on the right-hand side of the Figure.

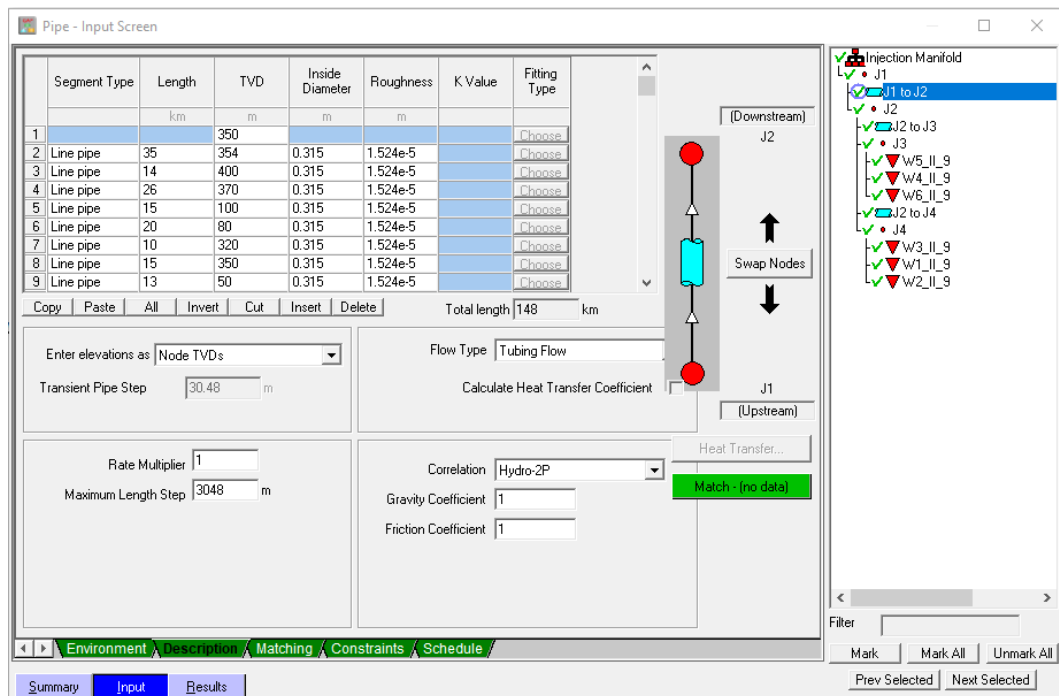


Figure 3.35: Is where the overall pipe parameters are set up, including the length, diameter, roughness, and topography.

To input the fluid parameters on the Injection manifold, double-click on the CO₂ manifold in Figure 3.31, and the image in Figure 3.35 will show. Click on **Input** and then **Fluid** to enter the injected fluid temperature.

Next is to define the CO₂ properties by clicking on **composition**. (This composition is active because the fully compositional option was selected in Figure 3.32). After clicking on the composition button the following screen in Figure 3.13 will show, this same screen as in Prosper, by clicking on import PRP, the PVTp file can be imported following the same procedures as in Prosper.

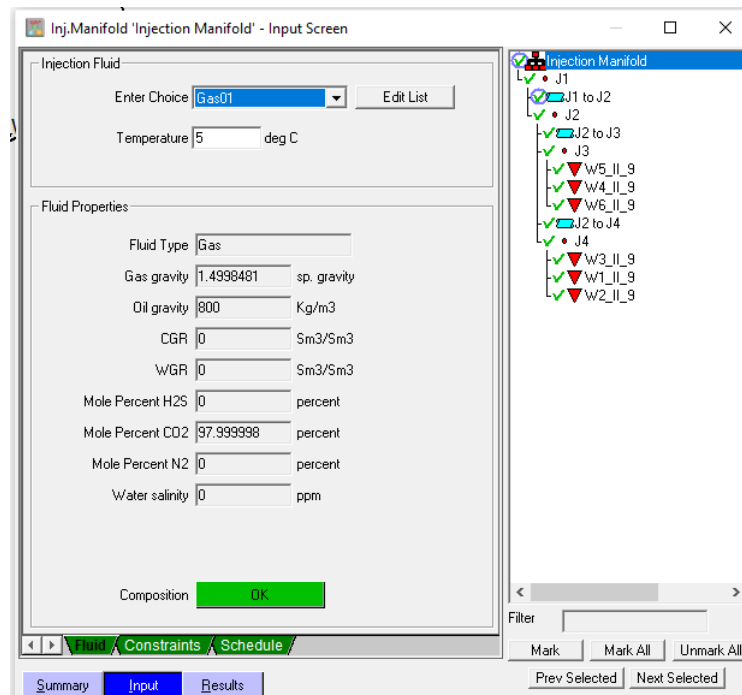


Figure 3.36: The figure provides an option for the user to define the type of fluid (water, steam, oil, and gas) and modify the properties by selecting "Edit List". The PVT properties of the source are displayed at the bottom of the screen and by selecting "composition".

Generating IPR In GAP

The IPR data can be transferred from Prosper using the "Generate" function of GAP in Figure 3.31, then select generate IPR with Prosper from the drop-down. First, to be able to generate IPRs or VLPs, GAP needs to know the path of the Prosper file associated with each specific GAP well model. Therefore a Prosper file needs to be associated with each well in GAP. The following description assumes that a Prosper model which includes an IPR has already been built for each well (*see section 3.2.5 for details*). It is first necessary to tell GAP the location of the Prosper files that describe each well. The method of doing this is summarised below:

- Open the Well summary screen by double-clicking on any Well icon in Figure 3.31. A Well summary screen is shown in Figure 3.37
- Click on the "summary" button in the bottom left-hand corner of the window in Figure 3.37 highlighted in red.
- Click on the "Browse" button to open a file selection dialogue box. From this dialogue box select the appropriate Prosper file for the Well.
- Repeat this process for each of the Wells that require IPR generation. Note that this is an operation that is performed just once when the model is built.

Now that the appropriate Prosper files have been specified for each Well click "gen-

erate" in the menu bar in Figure 3.31, then select "generate Well IPR with Prosper" from the drop-down. There will be a prompt that allows the user to specify whether all of the Wells should have their IPRs generated or only a selected number of Wells see Figure 3.38

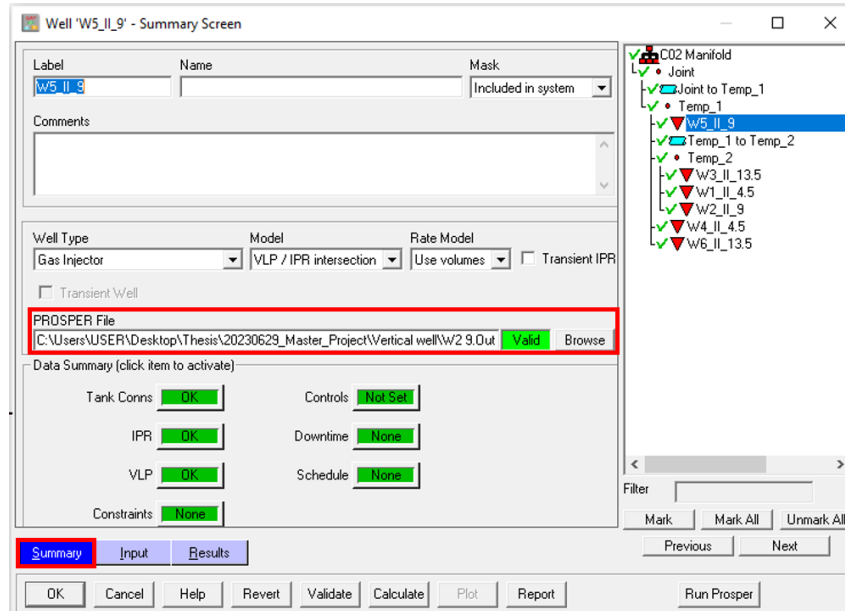


Figure 3.37: GAP Summary Screen, How To Input Prosper File To GAP

GAP uses the IPR model defined in the Well IPR section regardless of the type of IPR model used in Prosper. This means that oil IPRs are always modeled with a PI and Vogel correction, while gas or condensate IPRs are always modeled with either Forcheimer, Forcheimer (with pseudo pressure), or C and n.

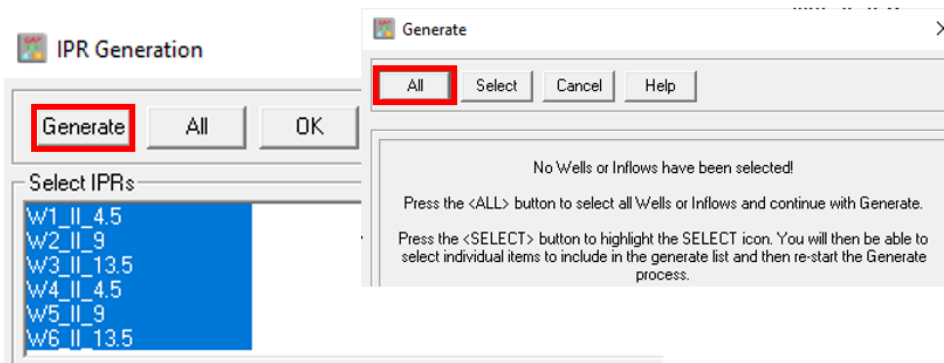


Figure 3.38: The Figure displays a prompt that enables the users to choose between generating IPRs for all Wells or only a selected few

Generating VLP In GAP

To import the VLP curves in GAP, the files must be already generated from Prosper, an example of this file is shown in Figure 3.30. These are saved as *.tpd files. To load these files, double-click on any Well in Figure 3.31 and the screen in Figure 3.39 will be shown then navigate to "Input", and click on the VLP tab. Click on the 'Import' button and then load the "Well.tpd file". The VLP section should then become green which completes the input for the well description. Repeat this process and load the file for each corresponding well.

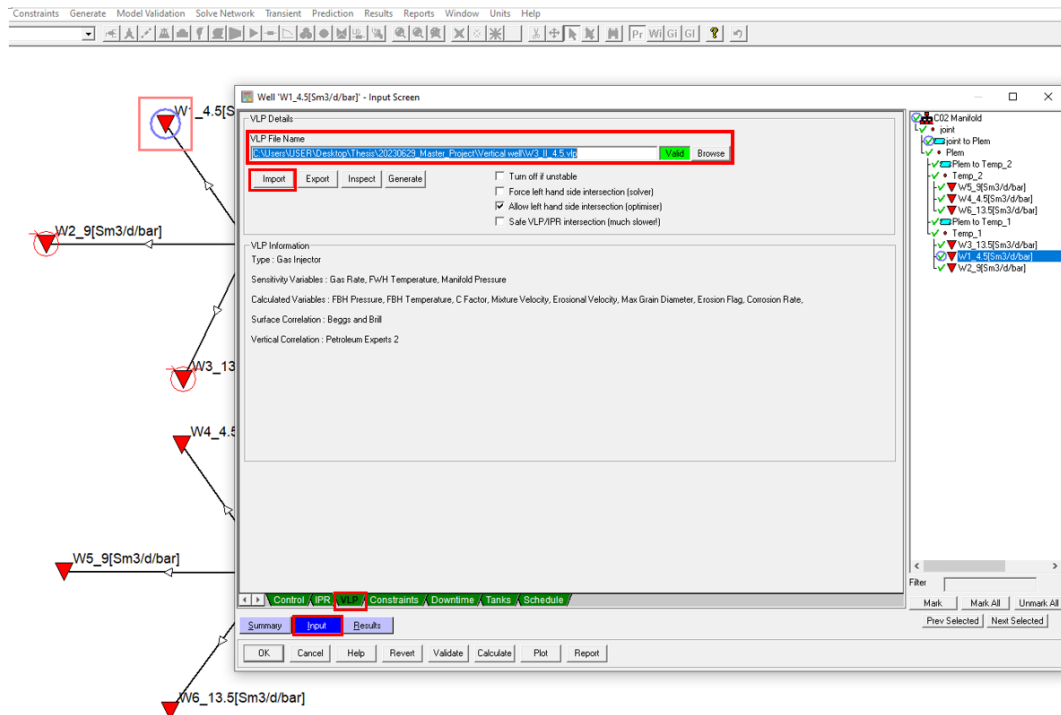


Figure 3.39: This screen allows the user to specify the data file that contains the VLP tables of the Well

Network Solver

At this point, the model is ready to be run. From the toolbar in Figure 3.33 click on the "Solve Network" icon, the first screen in Figure 3.40 will show, enter an injection pressure say 80 bar, and click next, the second screen in Figure 3.40 will appear. (set the mode to "No Optimization" and when the choke is included then select "Optimize with all Constraints"). Run the calculation by selecting "Calculate" to solve the network. To determine the rate of injection per Well, double-click on the Well to access the summary screen and then select 'Results'.

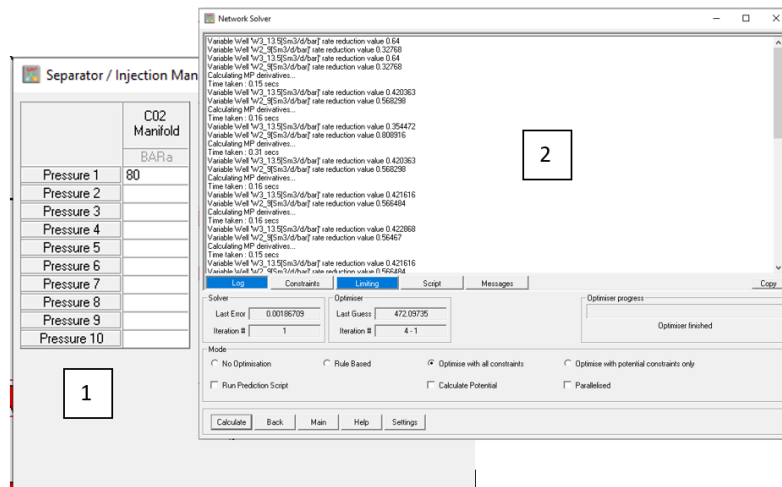


Figure 3.40: The user can input the injection pressure, then specify the calculation mode, and then solve the system by selecting calculate.

All results will be analyzed in the next chapter

S/N	Cases To Be Simulated
1.0	Case One - Based Case - Homogeneous Formation
1.1	Variations in Pipeline Pressure (<i>80bar Injection Pressure</i>)
1.2	Pipeline's pressure variance with different pipe correlations (<i>80 & 100bar Injection Pressure</i>)
1.3	Friction-induced pressure drop in the 148km pipeline (<i>80 & 100bar Injection Pressure</i>)
1.4	Variations in Temperature Along the Pipeline (<i>80 & 100bar Injection Pressure at 23°C & 15°C</i>)
1.5	Fluid Phase Transition along a Pipe (<i>Injection Pressure 80bar</i>)
1.6	Variations in Density Along the Pipeline (<i>80 & 100bar Injection Pressure</i>)
1.7	Velocity variation along the pipeline (<i>80 & 100bar Injection Pressure at 23°C & 15°C</i>)
1.8	Well Simulation result (<i>80 & 100bar Injection Pressure at 23°C & 15°C</i>)
1.9	Bottom-Hole Pressure Varied by Pressure and Temperature (<i>80 & 100bar Injection Pressure at 23°C & 15°C</i>)
2.0	Case Two - Heterogeneous Formation
2.1	Comparing Injectivity Index in Two Formation (<i>Injectivity 9 & 4.5t/h/bar at 80bar & 100bar</i>)
2.2	Comparing Injectivity Index in Three Formation
2.3	Pressure Analysis Post Choking of Wells
3.0	Case Three - Homogeneous Formation - Increase in reservoir pressure 300 to 310bar

Table 3.2: An expansive overview showing the range of simulations carried out for the three primary cases, offering a comprehensive view on the conducted analyses.

Result And Discussion

This chapter presents the results of the Prosper model and the final GAP simulation of the full CO₂ injection system. The CO₂ phase envelope, hydrate line, temperature gradient, IPR, and IPR + VLP plots were all reported and analyzed. However, the emphasis of the chapter is more on the analysis of pressure, density, velocity, and temperature change along the 148km pipeline as injection pressure, and temperature from the manifold changes with time. Table 4.1 presents the parameters used to model the subsea pipeline network and the injection wells for all cases studied. The results from Prosper are presented in Sections 4.1 to 4.3, while section 4.6 focuses on GAP. Figure 4.8 shows the subsea pipeline network profile for all cases.

4.1 CO₂ Phase Envelope

Figure 4.1 shows the plot of the phase diagram of the fluid used for this model as a two-

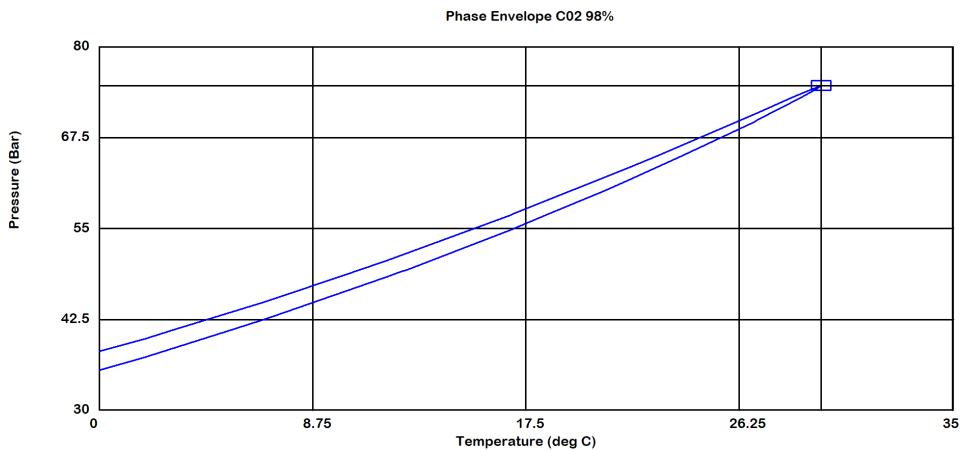


Figure 4.1: This graph represents the phase diagram of the model’s fluid composition, indicating its behavior as a two-phase system. Composing of 98% mole of CO₂ and 2% mole of methane.

phase fluid, the composition of the fluid is discussed in section 3.2.4. Fluid with 100% CO₂ composition will have a phase diagram as the one presented in Figure 2.5. For this model, the hydrate line is shown in Figure 4.2

In the absence of free water, the CO₂ stream may still contain sufficient dissolved water to form hydrates. Therefore, even when the CO₂ is dehydrated, it is important to operate outside the hydrate–liquid CO₂ (H-LCO₂) region[54] Since hydrate formation can be an expensive process problem, much work has to be carried out by engineers to reduce or prevent hydrate formation. The most common methods involve any or all of the following;

- Keeping the temperature higher than the hydrate formation temperature.
- Adding bulk inhibitors such as methanol or sodium chloride will shift the hydration curve downwards to lower temperatures.
- Adding "kinetic" inhibitors which act to slow down the formation of hydrate crystals

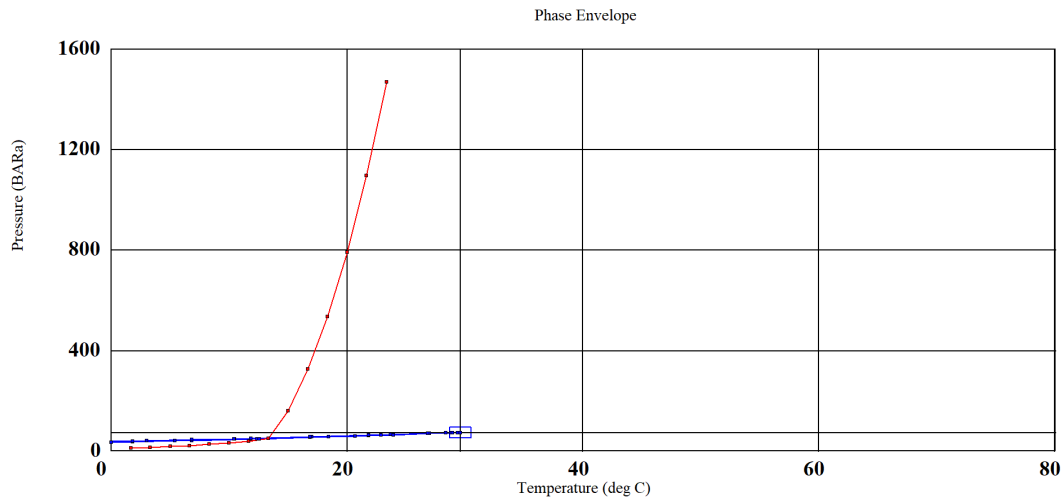


Figure 4.2: The hydrate plot is indicated by the red line in the plot, The injected fluid temperature must be at or above 23°C which is higher than the temperature at which hydrates are formed. To prevent hydrate formation, the temperature of the injected fluid must be above 23°C; otherwise, kinetic inhibitors that act to slow down the formation of hydrate crystals should be added

The first option for this model is to maintain the injected fluid temperature at or above 23°C, which is higher than the temperature at which hydrates are formed, as demonstrated by the hydrate plot in Figure 4.2. The hydrate plot is indicated by the red line. To prevent hydrate formation, the temperature of the injected fluid was maintained at 23°C; nevertheless, 15°C was also used for sensitivity studies, however, kinetic inhibitors are advised to be added at this temperature. As the fluid descends the well, it is anticipated that the temperature will rise; specifics can be found in the temperature gradient traverse plot in Figure 4.3.

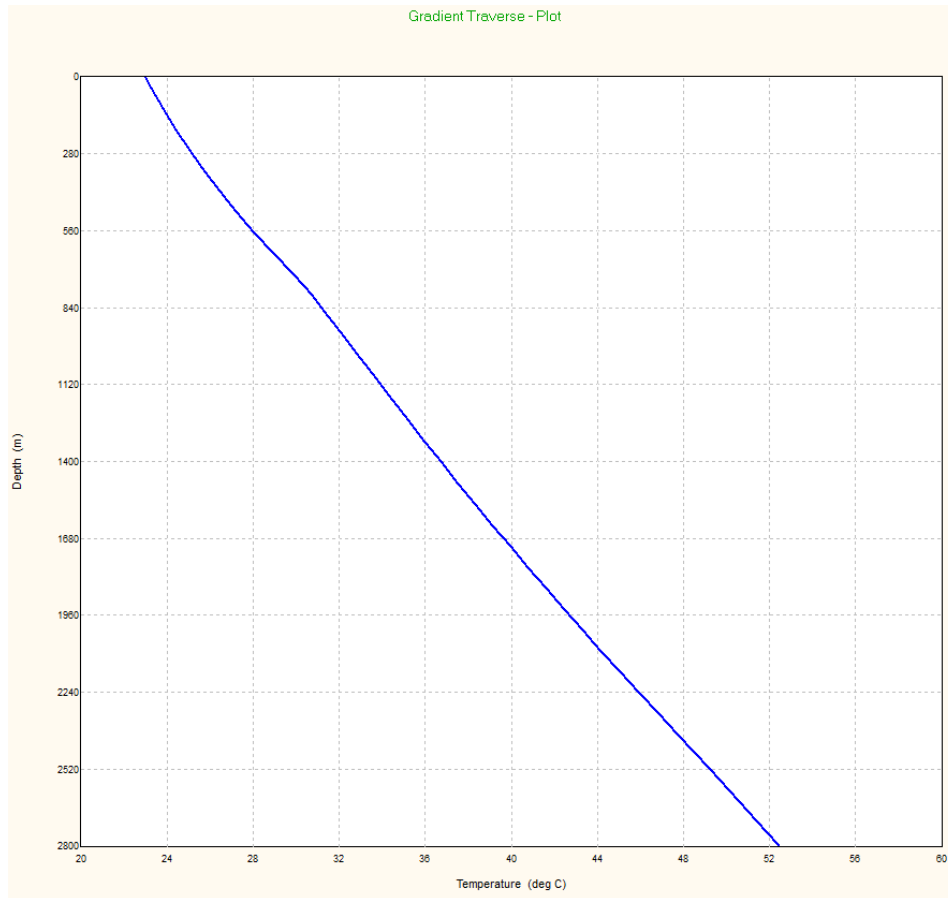


Figure 4.3: To illustrate the anticipated rise in temperature as the fluid descends the well. The traverse plot provides a detailed representation of the temperature gradient along the well's depth.

4.2 Inflow Performance Relationship IPR Plot

Prosper's IPR section specifies the well's inflow, which means that when modeling an injector, it's the relationship between the fluid flow rate that may be injected into the reservoir and the bottom hole pressure. According to Figure 4.4, The bottom hole pressure variation as a function of rate is depicted in the plot by the blue line of the straight line IPR. The temperature plot, represented by the red line in the plot, also displays the change in bottom hole temperature as a function of rate. To determine the maximum range of rates to be employed, the Absolute Open Flow (AOF) of the well is used in numerous computations. As a result, the IPR should be recalculated whenever the well's parameters change. This study involved three case studies, IPR was recalculated for all three cases, however, they all followed the same approach. It is evident from the plot that the Absolute Open Flow (AOF) is 5780.97 MMSm³/day. Unlike a production well, which has a 0 bar bottom hole pressure restriction, the AOF principle is no longer physically applicable to an injector since there is no upper limit to the lowest hole pressure.

The provided curve might not accurately depict the injectivity at lower rates due to the large range of values that were used. When the system computation is carried out, this will be shown in greater detail in section 4.3. When a more thorough examination of gas injection wells is necessary, it is advised to employ a reservoir simulator that can take into account the intricate relationships between temperature fluctuations, water chemistry, and rock mechanics.

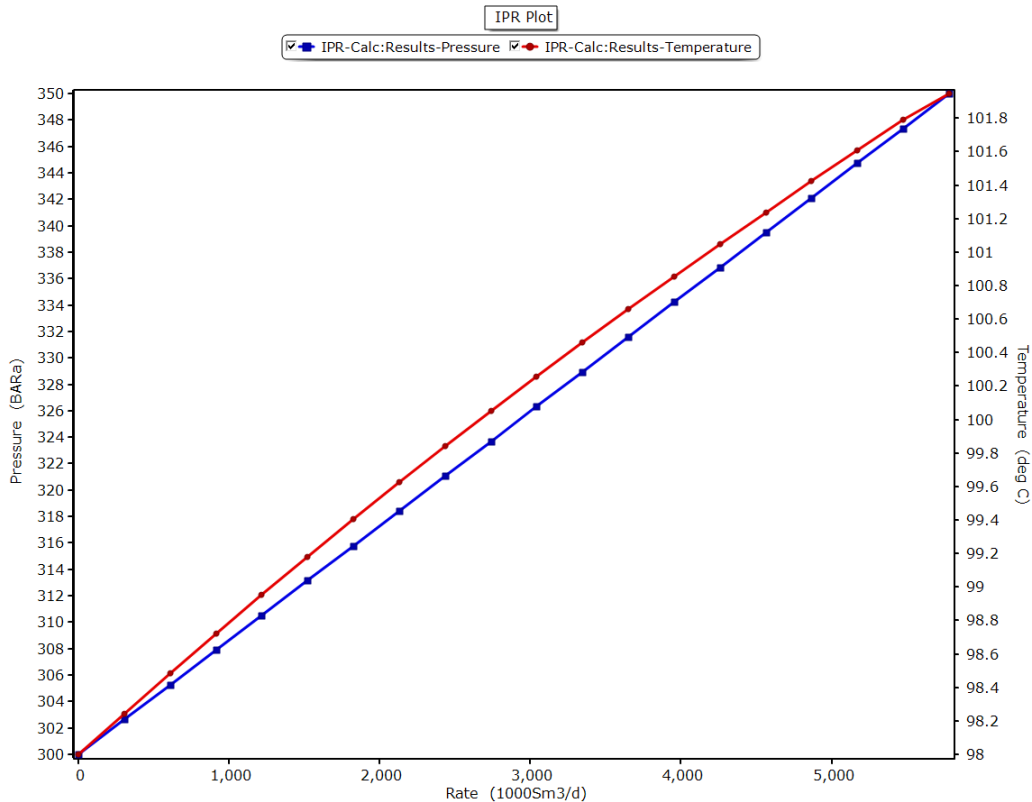


Figure 4.4: The IPR plot shows the bottom hole pressure variation as a function of rate, this is depicted in the plot by the blue line. The temperature plot, represented by the red line, also displays the change in bottom hole temperature as a function of rate.

4.3 System IPR + VLP

Figure 4.6 illustrates how the model predicts the well rate if the wellhead pressure is 100 bar and the WGR and CGR are zero, then the model predicts that the well will flow at approximately 2739.315 1000Sm³/day and that the corresponding solution node pressure (which is equivalent to the Flowing Bottom-hole Pressure FBHP) is 323.69 bar. On the straight line IPR curve, it can be seen that at higher rates the relationship of increasing pressure being required to inject a higher rate is established. As an intersection occurs, the model predicts that at these conditions the reservoir rock may fracture. To analyze

this in more detail, calculate the propagation of the fracture through the reservoir, and judge the impact that this fracture will have on the injection rate over time, there is a need to consult a reservoir simulator that, can deal with both the thermal and fracture mechanics aspects, however, this thesis did not cover this scope. Figure 4.5, 4.7 also show the system IPR + VLP recalculated for other cases

4.4 Case Study

- Case 1 - Based Case - Homogeneous Formation
- Case 2 - Heterogeneous Formation
- Case 3 - Increasing Reservoir Pressure

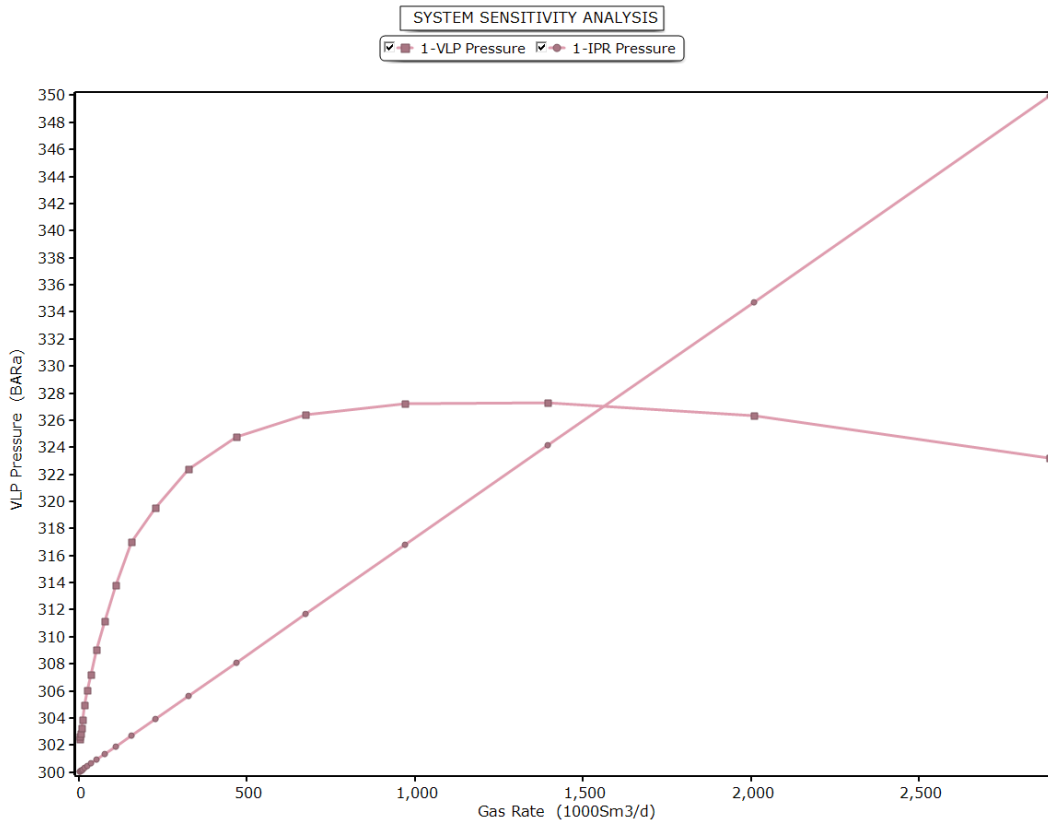


Figure 4.5: Shows how the model predicts the well rate if the wellhead pressure is 100 bar and the WGR and CGR are zero, then the model predicts that the well will flow at approximately 1600 1000Sm3/day and that the corresponding solution node pressure is 326 bar

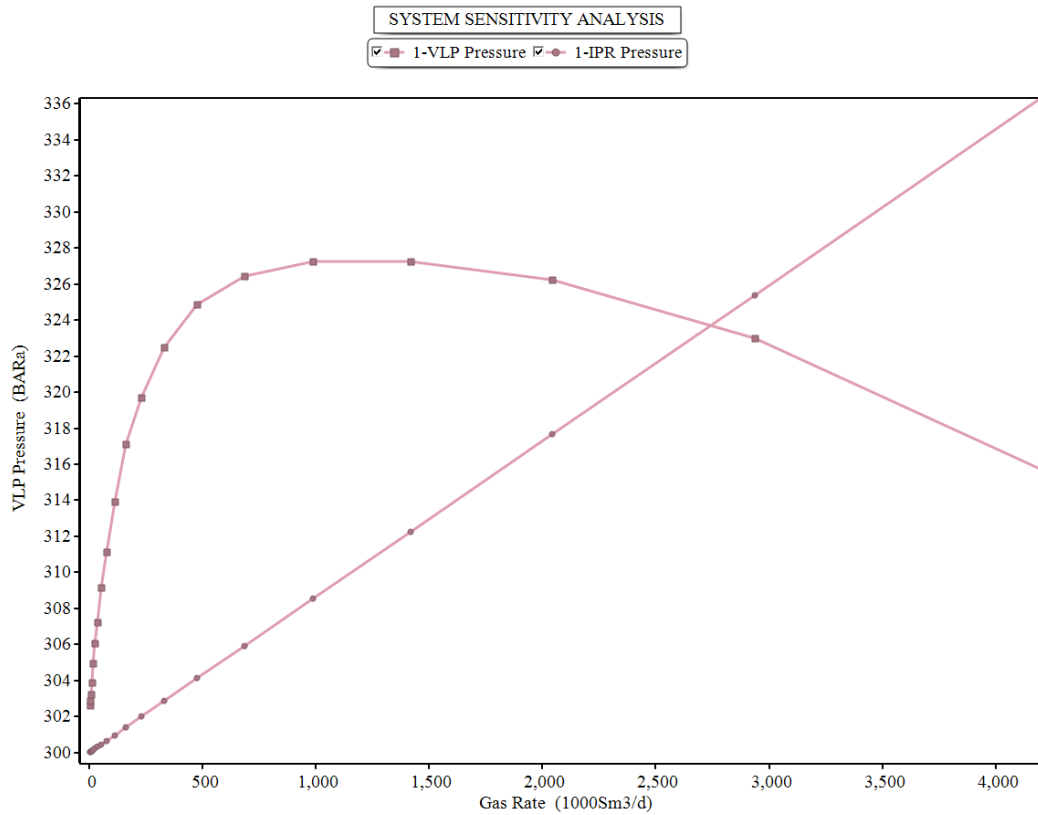


Figure 4.6: Illustrate how the model predicts the well rate if the wellhead pressure is 100 bar and the WGR and CGR are zero, then the model predicts that the well will flow at approximately 2739.315 1000Sm³/day and that the corresponding solution node pressure is 323.69 bar

4.5 Case 1 - Based Case - Homogeneous Formation

Snøhvit field, which features a single injection well, served as the basis for the model used in this case in GAP. To enable sensitivity study, the model was scaled up to six wells, with three wells per cluster (see Figure 4.8). Because of its homogeneous formation, all six wells share the same injectivity index, reservoir pressure, temperature, and other characteristics. The base case system plot is also shown in Figure 4.6. In this base case, Tubåen Formation's original injectivity index of 133,440sm³/day/bar (10 t/h/bar) was scaled down to 115,619.31 Sm³/d/bar (9 t/h/bar). According to Ji-Quan Shia et al [55], Tubåen's average total injectivity index between January and April 2009 was roughly 133,440 sm³/day/bar (10 t/h/bar). The reservoir pressure and temperature were set to 300 bar and 98^oC respectively during the simulation period. Table 4.1 displays the parameters for the pipeline system. The simulation in GAP took 4.469 seconds to complete, after five iterations, the solver reached a solution with a final error of 0.000116723. To prevent hydrate formation, the inlet fluid temperature was set to 23^oC, for the hydrate

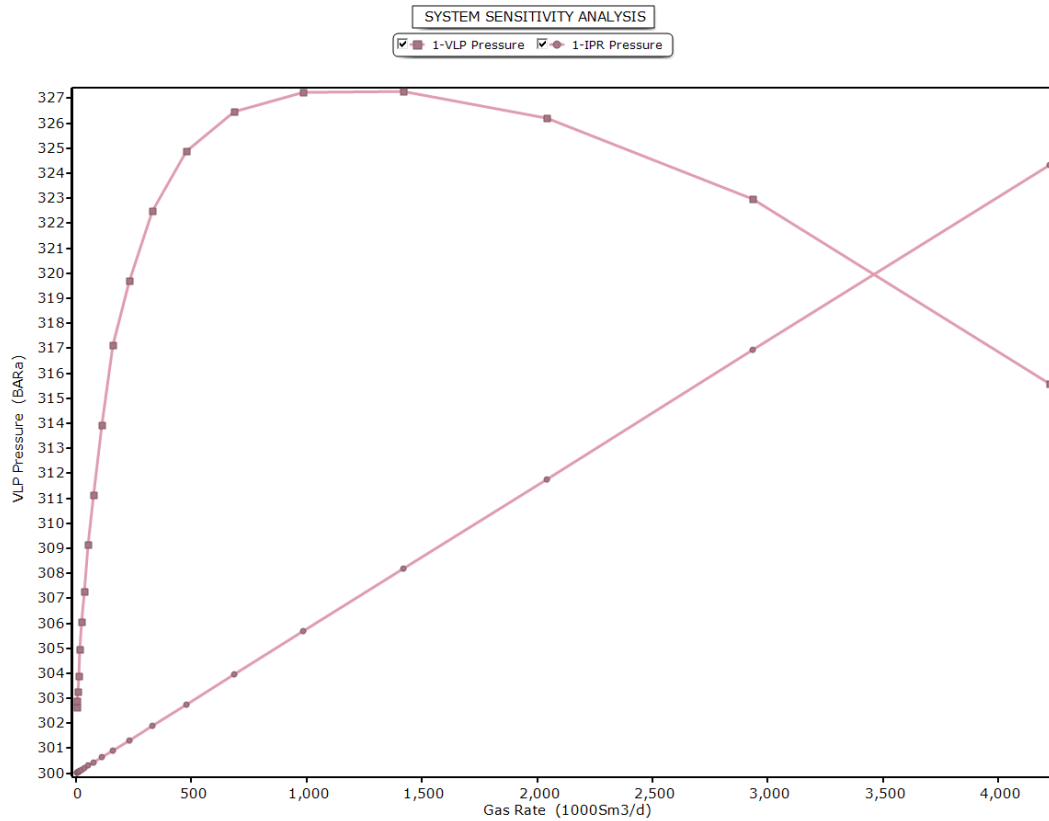


Figure 4.7: Illustrate how the model predicts the well rate if the wellhead pressure is 100 bar and the WGR and CGR are zero, the model predicts that the well will flow at approximately 3400 1000Sm3/day and the corresponding solution node pressure is 320 bar

line, see Figure 4.2. The following sections present the analysis of the results from the simulation.

4.6 Base Case’s Analytical Results

4.6.1 Variations in Pipeline Pressure (80bar Injection Pressure)

Following the completion of the simulation, pressure data were extracted from GAP and plotted as a function of pipeline length, the graph is presented in Figure 4.9. The plot clearly illustrates how the pressure profile follows the pipeline’s trajectory; as the pipeline’s elevation changes due to the sea floor’s topography, pressure increases with increasing elevation, leading to pressure loss, and decreases with decreasing elevation. Most of the pressure loss occurred at the two main elevations. After 148km, there will be about 89.47 bar pressure available. The pressure drop along the 5km flowline is small and insignificant approximately 0.5 bar and as such was not considered in this analysis,

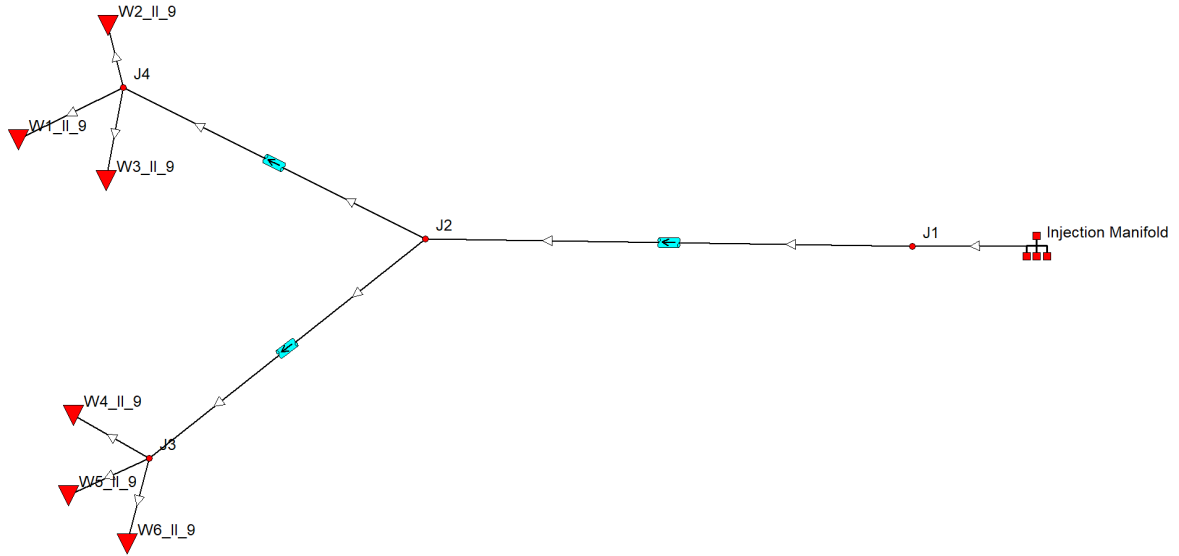


Figure 4.8: Shows a comprehensive representation of the pipeline network, extending from the injection manifold through the flowline, reaching the templates, and subsequently channeling into the six injection wells

Description	Length	Diameter	Roughing
Pipeline	148 km	0.315m	1.54E-05
Well	2798m	0.1778m	1.54E-05
Flowline	5km	0.315m	1.54E-05

Table 4.1: Pipeline Description Table

just the 148 km pipeline simulation result was taken into consideration. The available pressure at the wellhead following the CO₂ traveling through the 153 km (148km + 5km) pipeline and flowline is 88.97 bar. The wellhead pressure is between 83 to 110 bar, according to many literature reports [32]. The possible causes of the wellhead pressure difference between the model and reality could be as follows: first, the pipeline model was simplified; second, the injected fluid temperature was 23 degrees Celsius in the model, but around 5 degrees Celsius in some literature; and third, the Snøhvit pipeline is approximately 148 km long, but the model's length including the flowline is 153 km. In addition, the Snøhvit field has a single well, but this model includes six wells. The Snøhvit field's initial reservoir pressure is reported to be about 290 bar see Figure A.4, whereas the model has an initial reservoir pressure of 300 bar. Based on these differences, it may be concluded that the model closely predicted the field wellhead when compared with the literature values, based on this factor it can be concluded that the model predicts the wellhead pressure very closely.

According to Dongjie et al [56] elevation has a significant impact on the pressure drop performance of the CO₂ pipeline, so detailed topography of the objective district

must be considered when designing a CO₂ pipeline: if the elevation increases significantly within a certain distance, such as when climbing up a mountain, CO₂ pressure will drop dramatically, so boosting pump stations could be necessary at certain points, to make up the pressure loss; if the elevation decreases significantly within a certain distance, such as when climbing down a mountain, CO₂ pressure will increase dramatically, so thicker pipe might be needed for this section

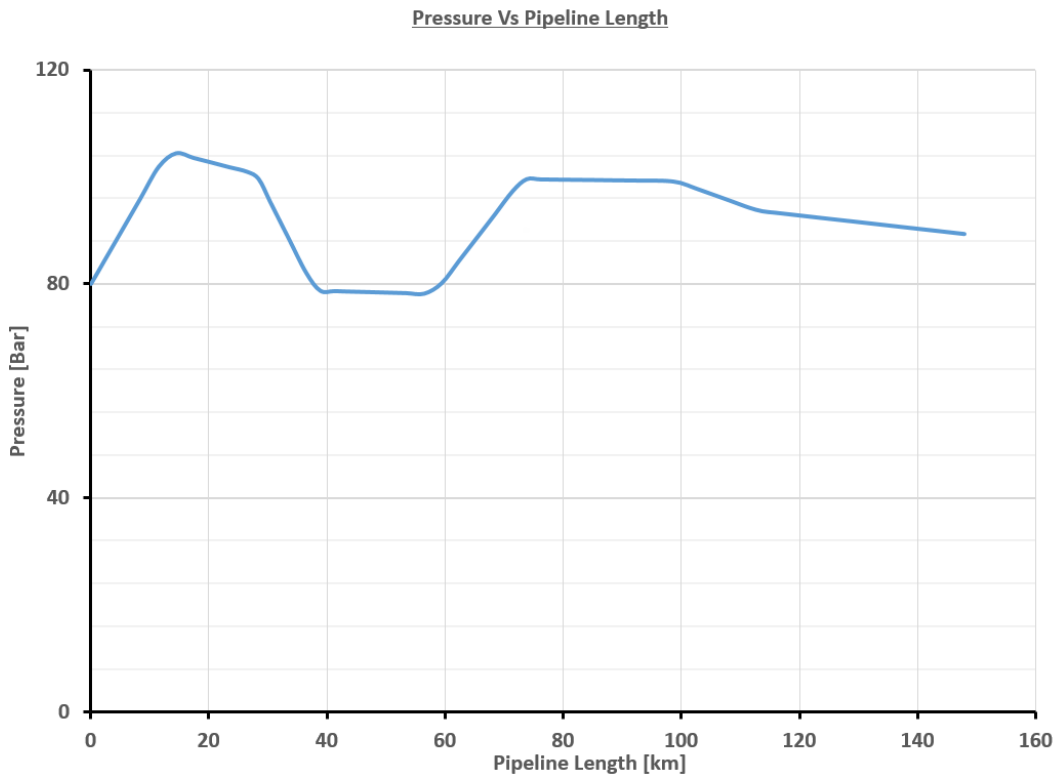


Figure 4.9: The plot shows pressure change along the pipeline, as a function of elevation. Higher elevations cause increased pressure, resulting in pressure loss, and decreases with decreasing elevation. Most pressure loss happens at two main elevation points.

4.6.2 Pipeline's pressure variance with different pipe correlations (80 & 100bar Injection Pressure)

The analysis was extended to check the result of different pipeline corrections available in GAP, seven distinct correlations were chosen, and the pipeline spanning 148 km was simulated at two distinct pressures 100 bar and 80 bar using the various correlations. According to the graph, every correlation has the same general pattern for both 100 and 80bar injection pressure showing consistency with one another. All correlations gave similar results since their main difference is when there is multiphase flow, it's worth noting that multiphase flow was not encountered during the simulation see Figure 4.10. This demonstrates that, even with irregular topography and a temperat-

ure of 23°C during the simulation, all correlations are effective for forecasting pressure drop in the pipeline. Section 2.5.7 covered the specifics of many relationships. Beggs and Brill's correlation is the best correlation for inclined flow, with many gathering lines and long-distance pipelines passing through areas of hilly terrain at any angle of inclination. Details about pressure behavior in uneven topography can be found in the Zhang et al [56]. literature; a quick overview of the subject is provided in appendix A.1.

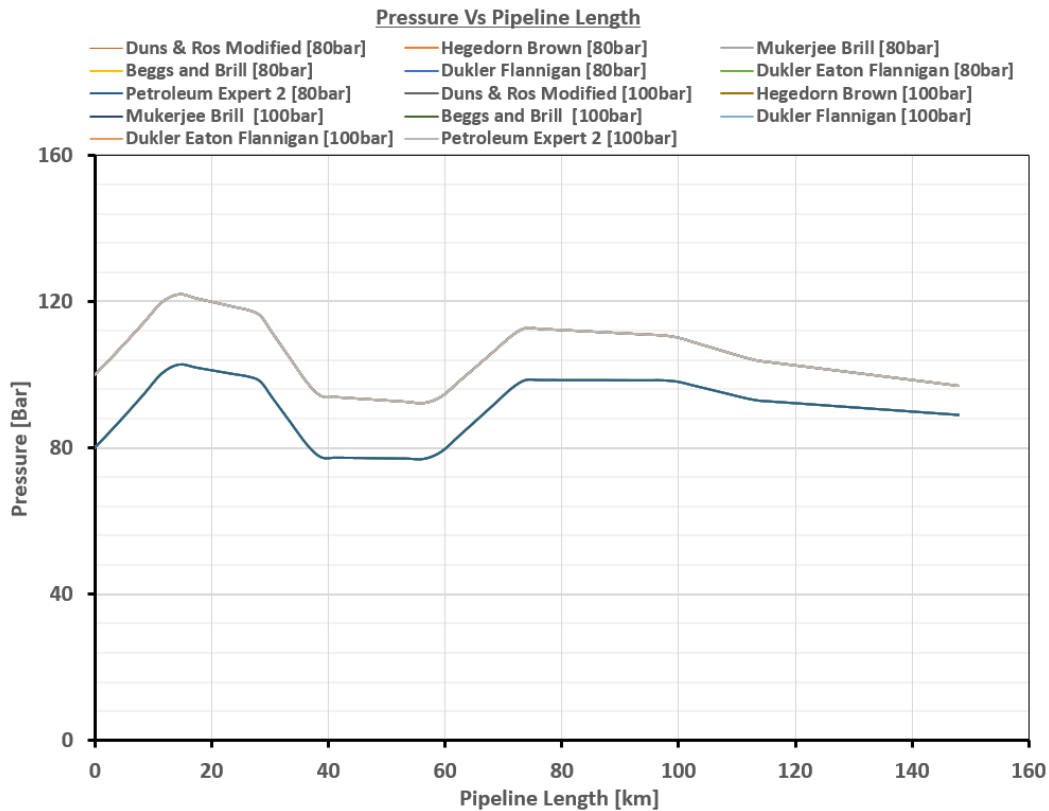


Figure 4.10: The simulation studied seven different pipeline correlations available in GAP for a 148 km pipeline at two injection pressures (100 bar and 80 bar). The graph shows a consistent pattern among all correlations, indicating their effectiveness in predicting pressure drop despite varied conditions like irregular topography.

4.6.3 Friction-induced pressure drop in the 148km pipeline (80 & 100bar Injection Pressure)

Friction loss is a measure of the amount of energy the piping system loses because fluids are meeting resistance. As fluid flows through pipes, it carries energy with it. Unfortunately, whenever there's resistance to the flow rate, it diverts fluid and energy escapes. These opposing forces cause friction loss in pipes. Figure 4.11 shows the plot of friction loss along the 148km pipeline at an injection pressure of 100 and 80bar. From the plot, friction losses increase as the fluid travels through the pipeline, which shows that longer

pipes will naturally have a higher potential for friction loss than shorter pipes. Moreso, friction loss increases with an increase in injection pressure. The 100bar injection pressure shows higher friction loss when compared with the 80bar injection pressure. When friction loss occurs, it means energy is escaping the system, because the piping system has to work harder to push fluids past resistance, it burns more energy [57].

From the Technical Achievement 2010 Snøhvit CO₂ Storage: Snøhvit CO₂ Tubåen Formation. storage capacity and injection strategy study Page 40 of 132 it is reported that "Pipeline pressure measured on the F-template is usually about 10 bar higher than on Melkøya. This pressure difference is influenced by the height change and friction loss in the pipe." [4]

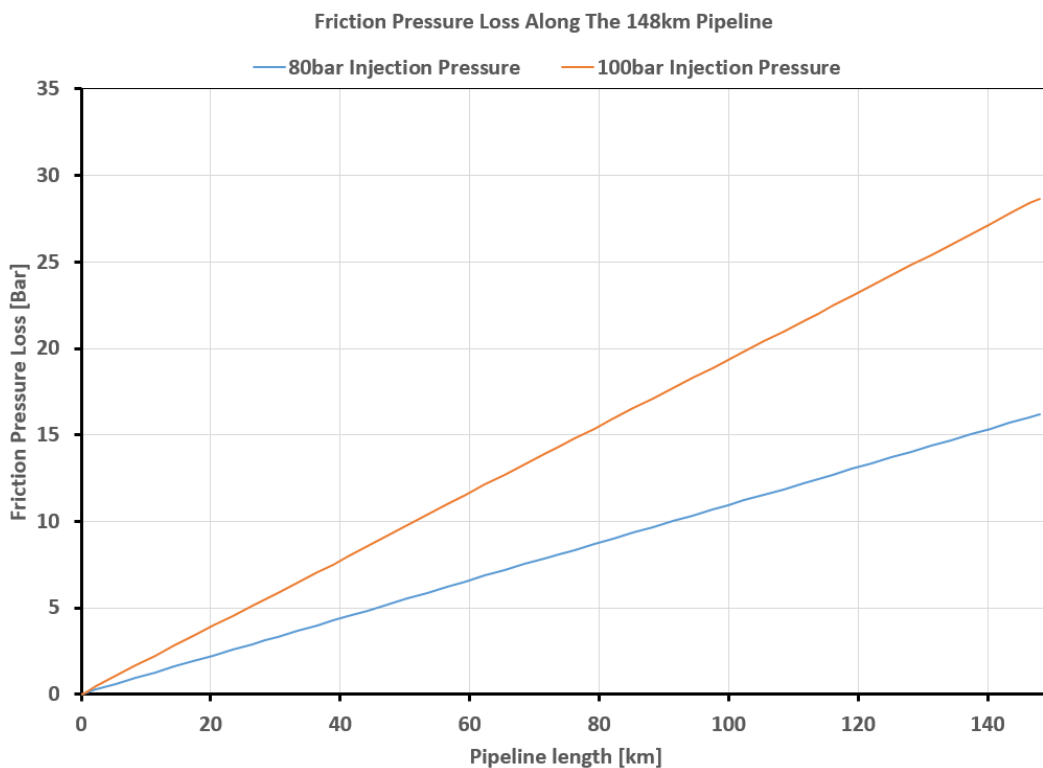


Figure 4.11: The plot depicts friction loss along the 148km pipeline at 100bar and 80bar injection pressure, higher injection pressure leads to increased friction loss, with 100bar showing higher losses than 80bar. Moreso Longer pipes usually exhibit more friction loss compared to shorter ones

Some of the reason for friction losses includes

- Changes in pipe slope

If pipes change in elevation, it can force liquids to work against gravity and result in energy loss along the way. That's why uneven or sagging pipe runs can draw energy out

of the system.

- Pipe length

The further fluids have to travel, the harder they have to work. Longer pipe runs will naturally have a higher potential for friction loss than shorter runs.

- Valves and fittings

Internal pipe walls are not the only things that contribute to friction loss. Valves and fittings can also inhibit flow and cause more friction.

How to Reduce Friction Loss in Pipes

- Increase Pipe Diameter

By widening pipe diameters, liquids do not have to work as hard to squeeze through pipes. In turn, reduces flow resistance and friction loss in pipes.

- Reduce Turns

By straightening out pipe runs and clearing the pipe's path, friction loss can be avoided. Accomplish this by removing tees, fittings, and other sharp turns whenever it is possible.

4.6.4 Variations in Temperature Along the Pipeline (80 & 100bar Injection Pressure at 23 °C & 15 °C)

In order to investigate how the fluid temperature changes with changing injection pressure and temperature, Figure 4.12 shows a plot at various injection temperatures and pressures. Both the injection temperature and pressure were changed from 23 to 15⁰C and 100 to 80 bar, respectively, as the graph illustrates. When the injection temperature and pressure were set at 23⁰C and 100 bar, the temperature decreased from 23⁰C to 10⁰C from the injection point to approximately 50 km of the pipeline length and stayed at that level until the end of the pipeline. In contrast, When the injection temperature and pressure were set at 23⁰C and 80 bar respectively, the temperature stabilized to 10⁰C at approximately 30km of pipeline length.

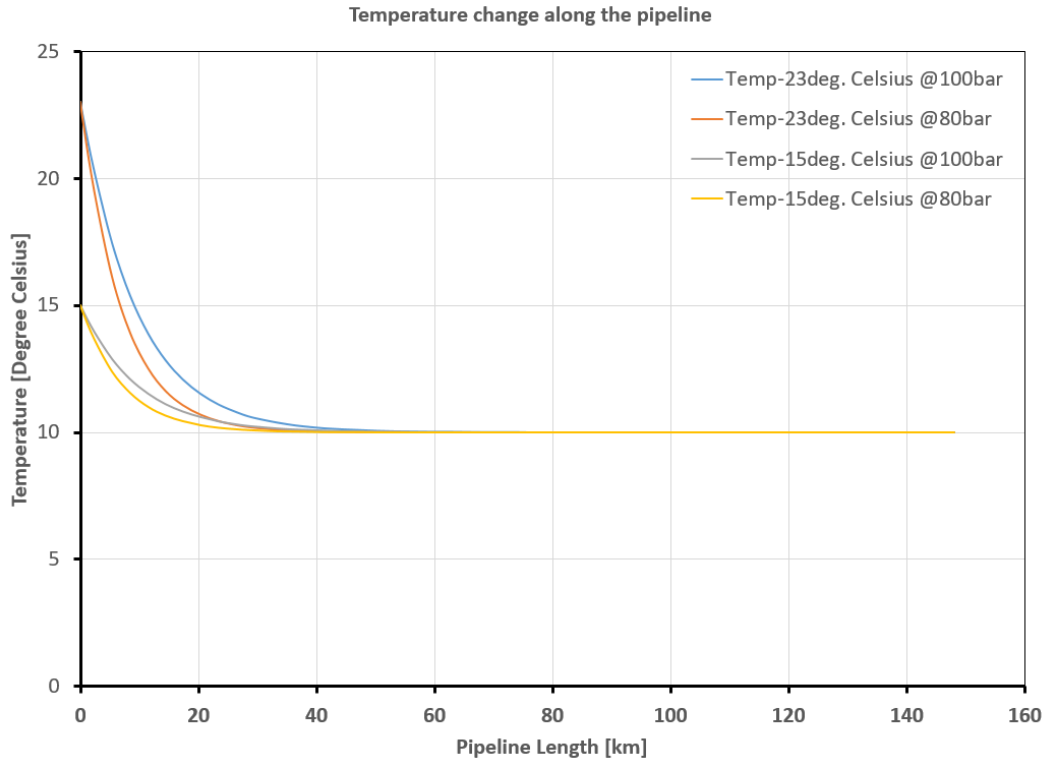


Figure 4.12: shows how temperature changes with different injection temperatures and pressures along a pipeline. At 23°C and 100 bar, the temperature drops to 10°C over 50 km, remaining steady to the end. At 23°C and 80 bar, it stabilizes at 10°C by 30 km. In the second scenario, For 15°C injecting at 80 bar and adjusting to 100 bar, the temperature quickly drops to 10°C. The 80 bar injection pressure causes a faster temperature decrease than 100 bar, regardless of the injection temperature (23°C or 15°C).

On the other hand, the second scenario had the injection pressure set at 80 bar initially, then adjusted to 100 bar, and the injection temperature set at 15°C for both injection pressures. After a few kilometers, the temperature drops to a stable temperature of 10°C for both injection pressures. The only significant variation is that the temperature drops more quickly at 80 bar injection pressure. However, the temperature drop for 80bar is faster when compared to 100bar for both 23 and 15°C temperature. This result suggests that high injection temperature may not be very important because eventually, all temperatures become equal regardless of the original injection pressure and temperature. Given this outcome, transporting CO₂ at a lower temperature is preferred. It is important to consider the temperature of hydrate formation prior to selecting the injection temperature.

The result mimics the result presented in the simulation of Zhang et al. [56] on page 131. Zhang et al proposed that transporting liquid CO₂ at a relatively low temperature is preferred from the viewpoint of reducing pressure drop along the pipeline. Gas phase transport is disadvantaged by the low density (and consequently large pipe dia-

meter) and high-pressure drops. Generally, CO₂ transportation in the subcooled liquid state has some advantages over supercritical state transport, most importantly because of the lower compressibility and higher density of the liquid within the pressure range considered here, which permits smaller pipe sizes or lower pressure losses. Pumps rather than compressors can be used to boost pressure along the line or for injection at the well end.[58]

4.6.5 Fluid Phase Transition Along The Pipeline (Injection Pressure 80bar)

For CO₂ pipelines, it is important to understand how the temperature and pressure of the fluid vary along the pipeline, as the temperature and pressure determine the phase of the fluid and affect density, and pressure drop [56]. The objective is to study the

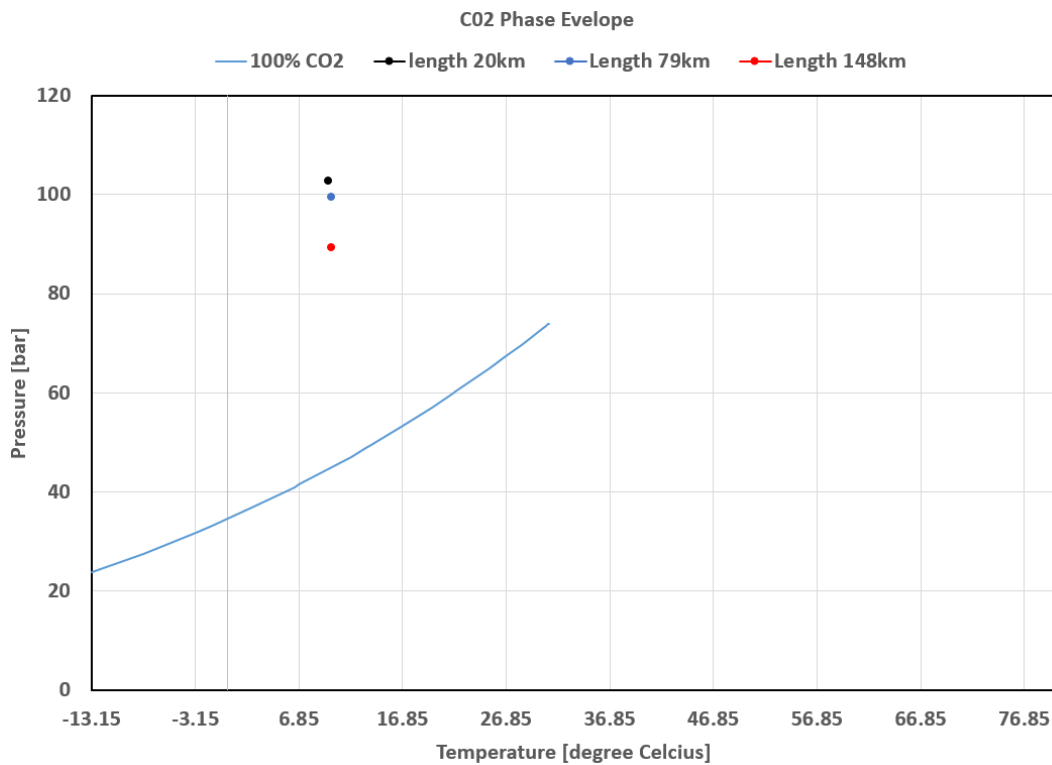


Figure 4.13: The pure CO₂ phase diagram is depicted by the blue line. The three dots on the graph correspond to various points along the pipeline. Based on the graph, it can be inferred that the CO₂ remains in the liquid phase along the whole 148 km pipeline,

phase change of CO₂ along the pipe. To plot the phase diagram of pure CO₂, pressure, and temperature data were extracted from Prosper's PVT section assuming a 100% CO₂. The resulting plot is shown in Figure 4.13, The pure CO₂ phase diagram is depicted by the blue line. Thus, based on the outcome of the GAP simulation run for the 148 km pipeline, temperature and pressure readings were obtained from strategic locations at 20km, 79km, and 148km along the pipeline and plotted on the CO₂ phase envelope.

The three dots on the graph correspond to these three results at various points along the pipeline. Based on the graph, it can be inferred that the CO₂ remains in the liquid phase along the whole 148 km pipeline, which is consistent with the findings published in the literature.[32]

4.6.6 Variations in Density Along the Pipeline (80 & 100bar Injection Pressure)

A plot of the CO₂ density behavior along the pipeline at injection pressures of 80 and 100 bar can be seen in Figure 4.14. After the simulation, the density data were extracted from GAP and plotted as a function of the pipe length. For an injection pressure of 80 bar, the density of the CO₂ increased slightly, from 774 kg/m³ at 404 km to roughly 884 kg/m³ at 20 km. Moreover, when injection pressure rises to 100bar, so does the CO₂ density. Because more pressure is needed to push the CO₂ up the elevation, it can be seen that the CO₂ density rises and falls with each elevation change along the pipeline.

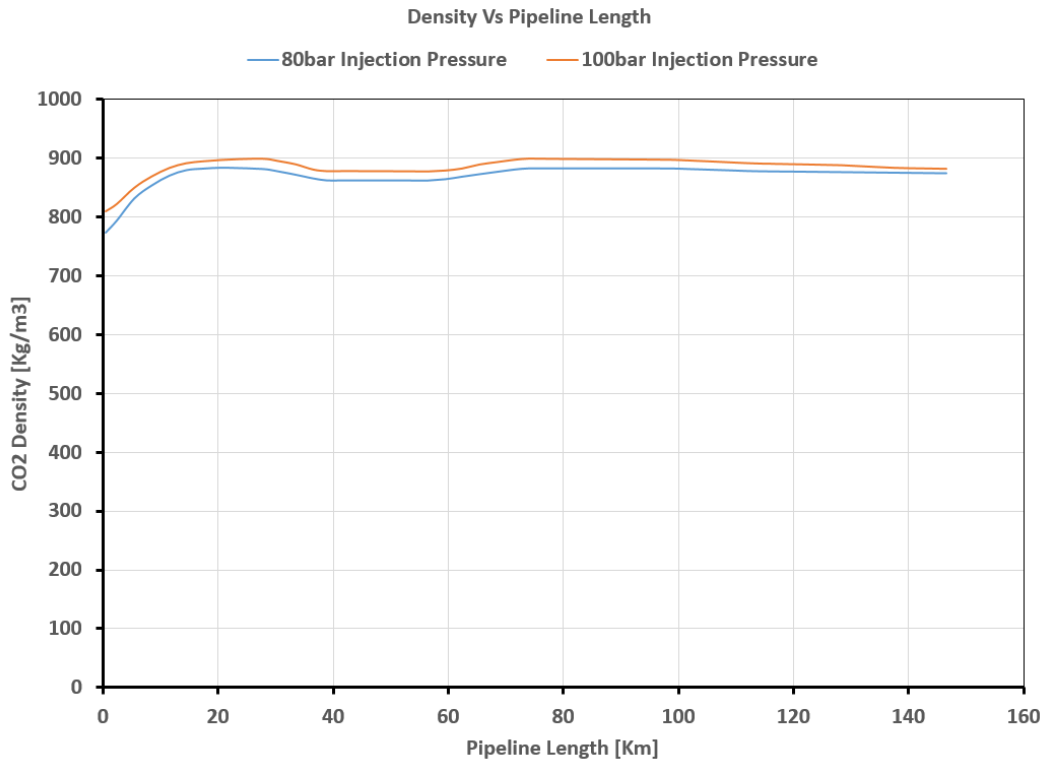


Figure 4.14: The CO₂ density increases with higher injection pressures. At 80 bar injection pressure, the density fluctuates along the pipeline due to elevation changes, varying between 774 kg/m³ and 884 kg/m³. A similar trend is observed at 100 bar injection pressure, where the density also rises and falls in relation to elevation alterations along the pipeline.

For the 80bar injection pressure, between approximately 38km and 60km, the dens-

ity of CO₂ decreased to 863kg/m³ and remained constant until a rise to 883kg/m³ was noted at 73km. A consistent pattern of stable density persisted until reaching 100km, followed by a slight decline in density to 875kg/m³ at the terminus of the 148km pipeline.

The injection pressure of 100 bar exhibits a comparable trajectory, albeit at an elevated density level, as depicted in the graphical representation. The fluctuations in CO₂ density predominantly stem from the increased pressure demands associated with higher elevations. In a theoretical scenario where the pipeline assumes complete horizontal orientation, it is anticipated that the density along its length would have exhibited a relatively stable pattern [56, 59].

From the Technical Achievement 2010 Snøhvit CO₂ Storage: Snøhvit CO₂ Tubåen Formation. Storage capacity and injection strategy study [4] Page 40-41 of 132 it is reported that "*with pressures above 80 bars CO₂ is in liquid phase and density will be around 940 – 1010 kg/m³*" from the simulation result average CO₂ density between 875-884kg/m³ is observed, which is quite close to the actual CO₂ density observed in the field. The disparity between the simulation result and actual density could potentially arise from the omission of certain components from the simulation, such as nitrogen, which is present in the Snøhvit field CO₂ composition, nitrogen was excluded from the simulation to streamline the fluid complexity for the model.

4.6.7 Velocity variation along the pipeline (80 & 100bar Injection Pressure at 23 °C & 15 °C)

Figure 4.15 illustrates the variation in velocity across the 148-kilometer pipeline, considering injection pressures of 100 bar and 80 bar at temperatures of 23°C and 15°C. The results portray a fluctuating pattern in CO₂ flow velocity. Specifically, at 100 bar and 23°C, the velocity initially decreases gradually from about 1.19 m/s to 1.08 m/s over the initial 20 kilometers, falling below the velocity observed at 15°C. It stabilizes briefly until 30 kilometers before resuming an upward trend. A decline occurs around the 64-kilometer mark, succeeded by a gradual increase until the pipeline's end, recording a final velocity of 1.098 m/s.

Secondly, the velocity trajectory for the 80 bar follows a comparable pattern for 23°C and 15°C. The starting velocities range between 0.873 m/s for 15°C and 0.916 m/s for 23°C, with a final velocity of 0.81 m/s for 23°C which remains lower than the 0.83 m/s observed at 15°C at the pipeline's end. For the 100 and 80bar injection pressures, the trend suggests that higher injection pressures correspond to higher fluid velocities, while lower pressures result in reduced velocities. Additionally, lower temperatures exhibit higher velocities compared to higher temperatures. While temperature itself may not directly determine the required velocity, it can influence the fluid's properties, such as viscosity. As a fluid's temperature changes, its viscosity may change, affecting the required pumping velocity.

From the Technical Achievement 2010 Snøhvit CO₂ Storage: Snøhvit CO₂ Tubåen Formation storage capacity and injection strategy study [4] in page 40 of 132 it is reported that "Flow velocity is about 2 – 2.5 km/hour (0.56 0.69m/s) when injecting at 60-80 tons/h". The difference between the actual and model velocity is 0.116m/s which shows that the model prediction was close when compared to 80bar at 23^oC. The result also closely reflects the result presented by Zhang et al. [56] in the paper economic evaluation of CO₂ pipeline transport in China.

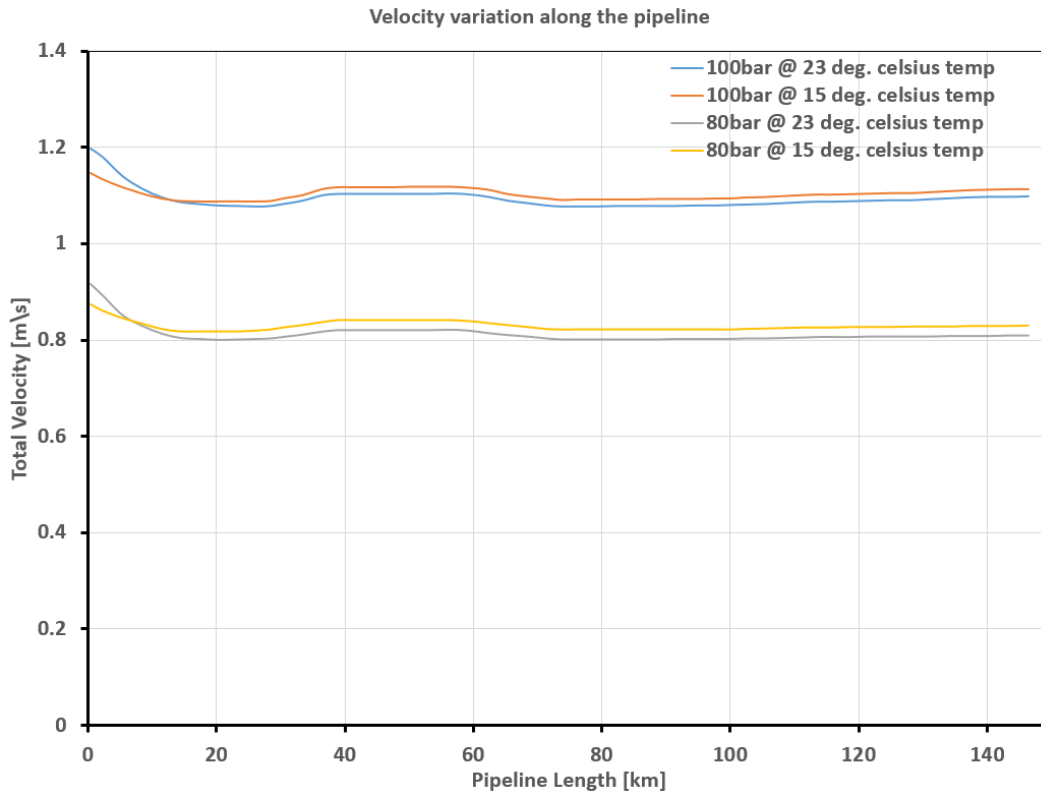


Figure 4.15: shows CO₂ velocity changes along a 148km pipeline at 100 bar and 80 bar injection pressures and temperatures of 23°C and 15°C. Initially, at 100 bar and 23°C, velocity drops from 1.19 m/s to 1.08 m/s over 20km, below the 15°C velocity. At 80 bar, velocities range from 0.873 m/s (15°C) to 0.916 m/s (23°C), ending at 0.81 m/s (23°C) and 0.83 m/s (15°C). lower temperatures exhibit higher velocities compared to higher temperatures

4.6.8 Well Simulation Result (80 & 100bar Injection Pressure at 23 °C & 15 °C)

The CO₂ injection well in snøhvit is slightly deviated, the well in this model is a vertical well, which might affect the injection rate by increasing the injection rate slightly higher than the actual injection rate at snøhvit field. Figure 4.16 shows the plot of injection rate versus injection pressure at two different temperatures 15^oC and 23^oC. From

the graph, it can be seen that at 80bar of 23^oC injection pressure, the injection rate is 2422MSm³/day, and for 80bar of 15^oC the injection rate is higher than the injection rate at 23^oC by 58.426 MSm³/day this clearly shown that injection at lower temperature yield a better injection rate, recall that this was the same conclusion in section 4.6.7. The injection pressure was increased to 100 bar also at different temperatures of 15^oC and 23^oC. From the graph, it can be seen that at 100 bar of 23^oC injection pressure, the injection rate is 3311 MSm³/day, and for 100 bar of 15^oC the injection rate is 3357MSm³/day which is higher than the injection at 23^oC by 46.311 MSm³/day this also clearly shows that injection at a lower temperature yields a better injection rate.

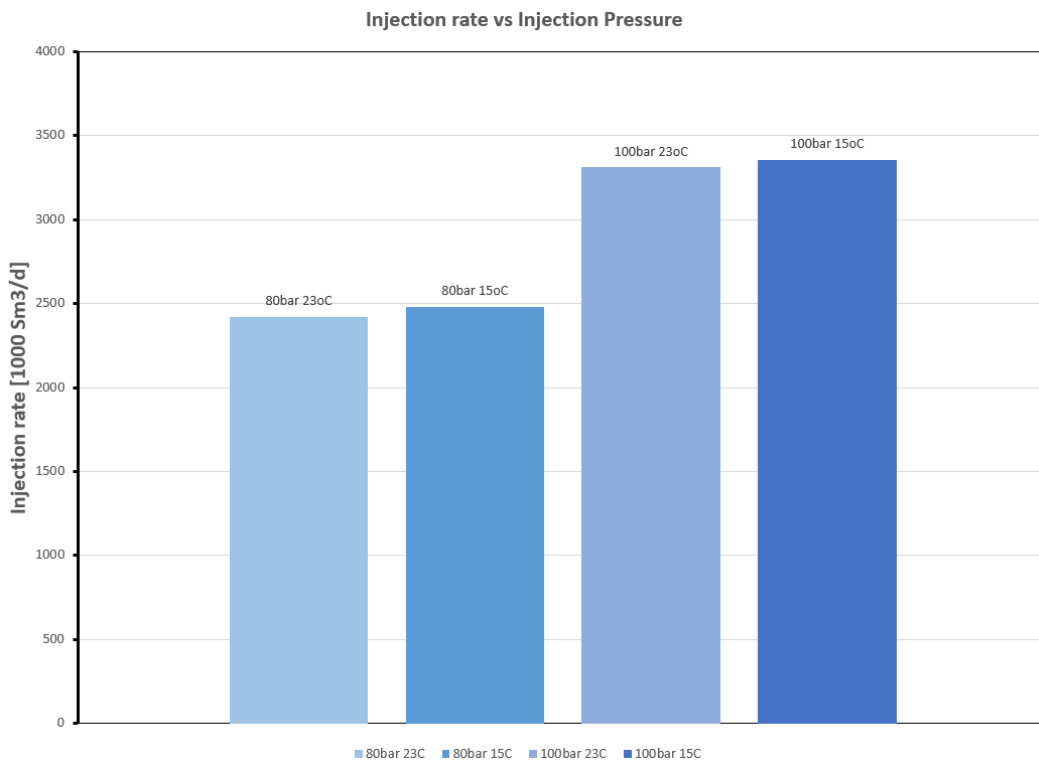


Figure 4.16: Compares injection pressures at 80 bar and 100 bar pressures, showcasing temperatures of 15^oC and 23^oC. At 80 bar and 23^oC, the rate is 2422 MSm³/day, while at 15^oC, it exceeds this by 58.426 MSm³/day, highlighting the temperature's impact. Similarly, at 100 bar and 23^oC, the rate is 3311 MSm³/day, but at 15^oC, it rises to 3357 MSm³/day, reinforcing the temperature's advantageous effect on injection rates

4.6.9 Bottom-Hole Pressure Varied by Pressure and Temperature (80 & 100bar Injection Pressure at 23 °C & 15 °C)

Figure 4.17 shows a plot of bottom hole pressure at the depth of the well of 2798m. The plot shows various manifold injection pressures for different fluid injection temperatures, the injection pressures are 100 and 80bar, and the temperature of 15^oC and 23^oC. The graphs show quite a difference in bottom hole flowing pressure for 80bar and

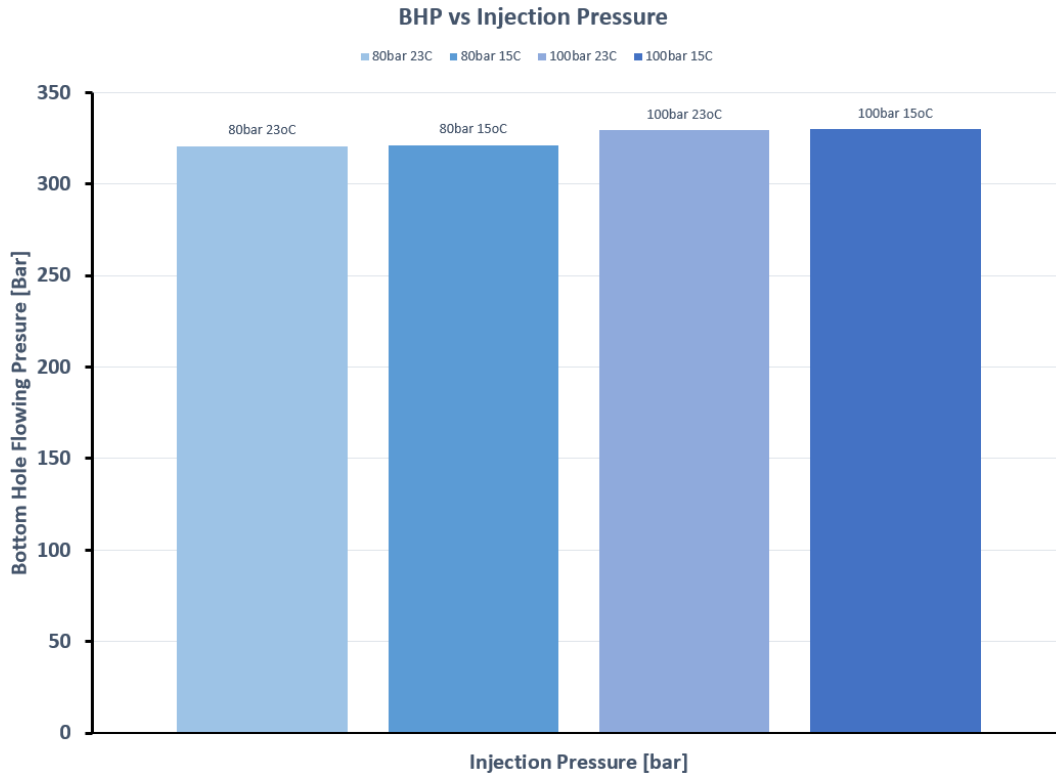


Figure 4.17: displays bottom hole pressures at 2798 meters for injection pressures of 100 bar and 80 bar at temperatures of 15^oC and 23^oC. Differences between 80bar and 100bar injection pressures are evident. However, temperature variations at the same pressure show minimal impact, with a slight difference of 0.56 bar between 15^oC and 23^oC at 80 bar, the former exhibiting slightly higher pressure.

100bar as expected. However, for different temperatures for the same injection pressure, its quite a small difference. For 80bar injection pressure for example the bottom flowing pressure at 23^oC is 320.71 bar and 15^oC is 321.27 bar the difference being 0.56bar, with 15^oC having the highest bottom hole pressure with 0.56bar higher than 23^oC. As earlier mentioned higher injection was achieved with lower injection temperature this also confirmed that conclusion.

4.7 Case Two - Heterogeneous Formation

For this case, the model was still based on the Snøhvit field, scaled up to two templates, three wells in each template, however, for this case the formation is heterogeneous. All wells in template 1 have 9t/h/bar injectivity, while the wells in template 2 have injectivity of 4.5t/h/bar which is 50% reduction in the base case injectivity. See Figure 4.5 for the case two system IPR vs VLP plots. The runtime of the tests was 2.31 seconds. The solver reached a solution after 5 interactions with the last error of 2.97×10^{-6} . The reservoir pressure for this case was set to 300 bar and reservoir temperature to 98^oC,

as well as the inlet fluid temperature to 23°C to avoid hydrate formation see Figure 4.2 for hydrate line. Parameters for the pipe system for this case are shown in Table 4.1.

4.7.1 Comparing Injectivity Index in Two Formation (Injectivity 9 & 4.5[t/h/bar] at 80bar & 100bar)

In this particular case, all wells within template 2 were modified to operate at 4.5[t/h/bar] approximately 28904[Sm³/d/bar], while wells in template 1 retained their initial injectivity of 9t/h/bar approximately 115619 [Sm³/d/bar] (referred to as the base case). This adjustment aimed to establish distinct geological formations within the two templates.

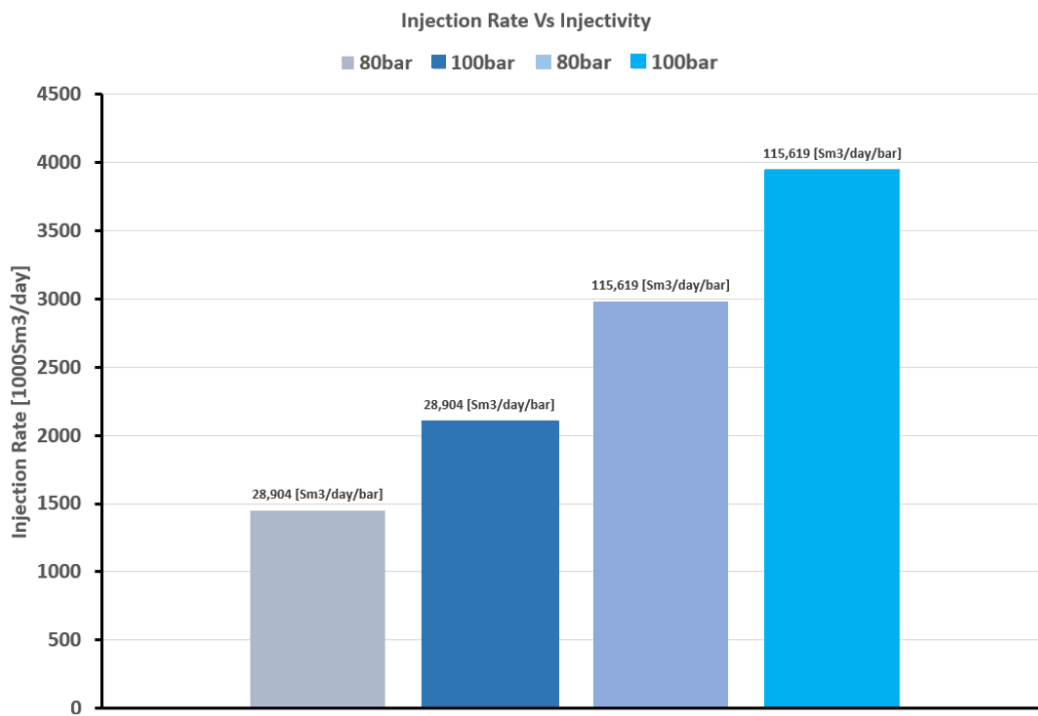


Figure 4.18: Comparison of injection rates between Templates 1 and 2 at 100 bar and 80 bar manifold pressures, highlighting varied injectivity impacts on injection rates within different formations.

Specifically, the Snohvit field features the Tubåen formation, comprising Tubåen 1(base), 2, and 3, each exhibiting varying injectivity properties. The simulation for this scenario was designed to mirror this inherent heterogeneity.

The findings, delineated in Figure 4.18, elucidate a comparison between the injection rates of wells in Templates 1 and 2. Notably, the injection manifold pressures were set at 100 bar and 80 bar.

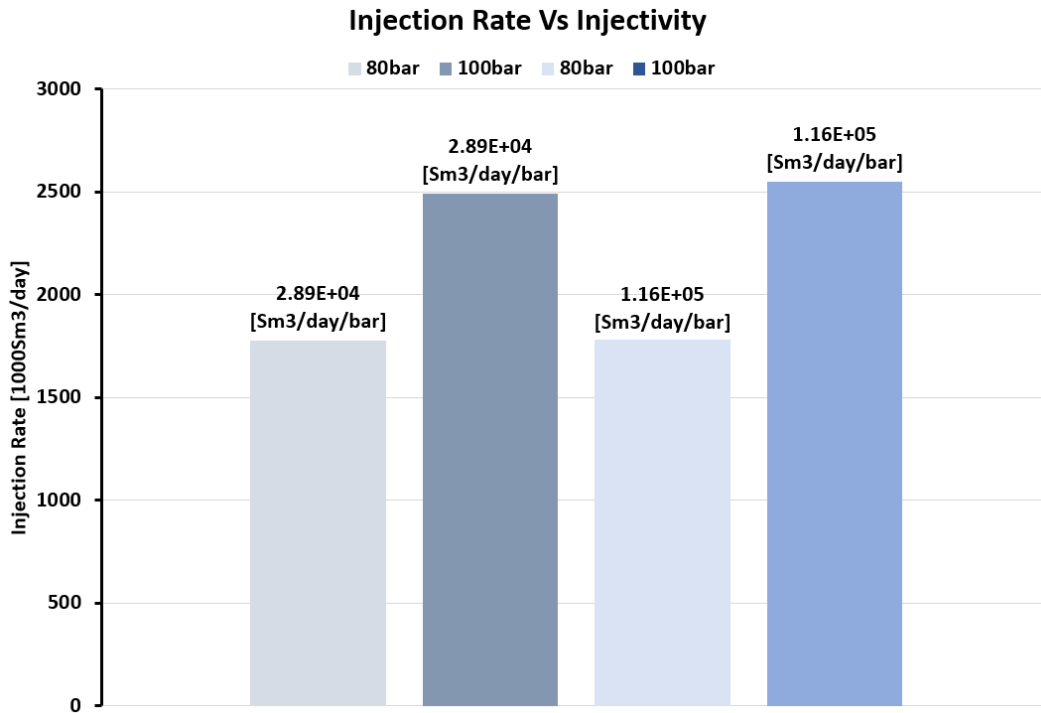


Figure 4.19: Implementation of 14 bar and 21 bar Differential Pressure (DP) Chokes on Template 1 wells for equitable injection rates at 80 bar and 100 bar manifold pressures, respectively

The results underscore an anticipated trend: formations characterized by lower injectivity manifest diminished injection rates under both 100 and 80bar injection pressures, while formations with higher injectivity exhibit proportionately higher injection rates.

To maintain an equal injection across both formations, a differential pressure (DP) choke of 14 bar was implemented on all wells in Template 1 possessing superior injectivity for 80 bar manifold pressure. Similarly, a 21bar differential pressure (DP) choke was applied for a 100bar manifold pressure. The outcome of this adjustment is depicted in Figure 4.19.

4.7.2 Comparing Injectivity Index in Three Formation

This case was modeled to represent Tubåen 1 (base), 2, and 3, ensuring a comprehensive representation of the three distinct formations. Figure 4.20 illustrates a plot of six wells characterized by varying injectivity index. The manifold pressure was consistently maintained at 80 bar, with all wells operating without choke. Specifically, Wells 1 and 4 injectivity index is 13.5 [t/h/bar], Wells 2 and 5, 9 [t/h/bar], and Wells 3 and 6, 4.5 [t/h/bar].

Both Template 1 and Template 2 comprise wells with distinct injectivity index. Analysis of the graph indicates that wells with the highest injectivity (e.g., Wells 3 and 6) showcase the highest injection rates, reaching 3477 MSm³/day, followed by Wells 2 and 5 with a rate of 2517.645 MSm³/day, and finally Wells 1 and 4 with a rate of 1076 MSm³/day.

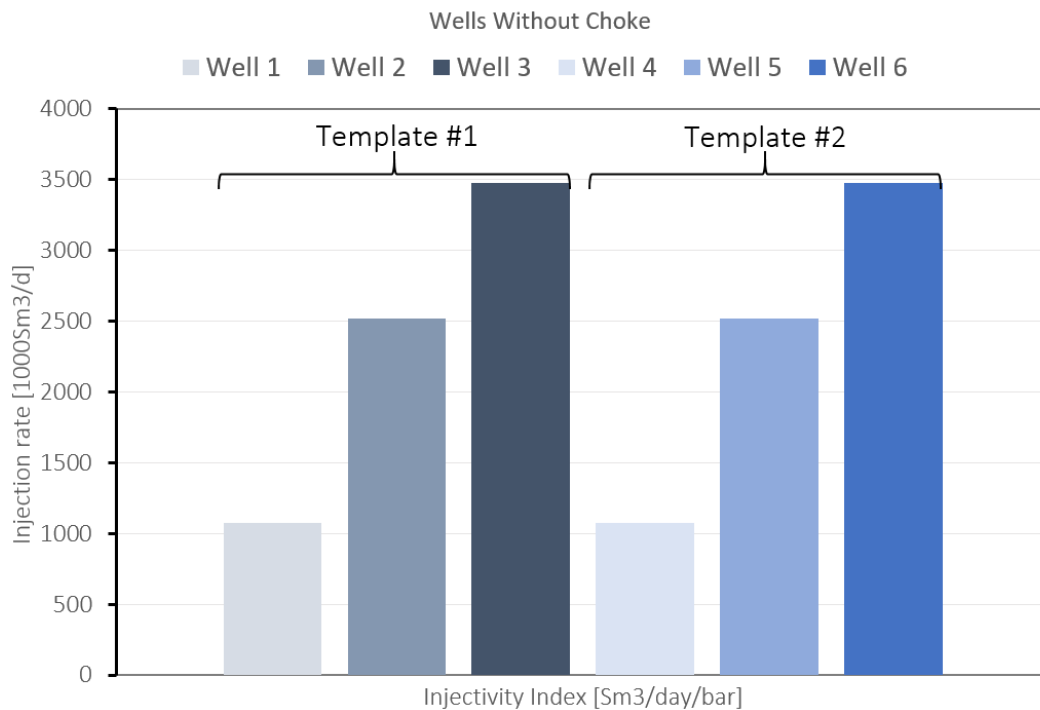


Figure 4.20: Relationship between injectivity index and injection rates of six wells at 80 bar manifold pressure. Higher injectivity wells (Wells 3 and 6) show the highest rates at 3477 MSm³/day, followed by Wells 2 and 5 at 2517.645 MSm³/day, and Wells 1 and 4 at 1076 MSm³/day."

In order to achieve uniform injection rates, wells with high injectivity were choked. Figure 4.21 demonstrates this adjustment, Well 3, 4, 5, and 6 were all choked. while Wells 1 and 2 remained unchoked. A maximum injection rate constraint of 1800 MSm³/day was imposed on Well 3, 4, 5, and 6, and the choke automatically calculated the pressure drop per well to achieve the specified rate and subsequently applied the calculated pressure drop to each well. This process requires a considerable amount of energy and simulation time. After choking these wells, more CO₂ flow into wells 1 and 2.

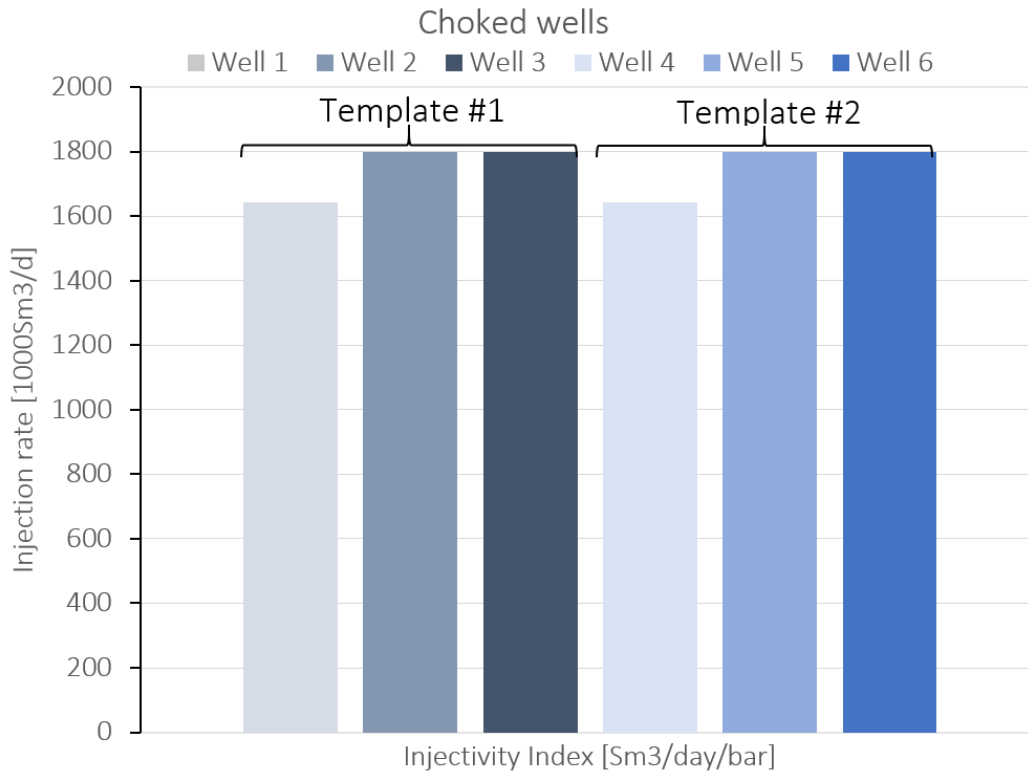


Figure 4.21: Illustration of choke implementation on Wells 3, 4, 5, and 6, while Wells 1 and 2 remain unchoked. A maximum injection rate limit of 1800 MSm³/day was set for Wells 3, 4, 5, and 6, with the choking mechanism automatically adjusting pressure drops to attain the Specified rates

4.7.3 Pressure Analysis Post Choking of Wells

After choking, it is expected that the pressure in the 148km pipeline will increase. Figure 4.22 presents the pressure change along the 148km pipeline pre-choke (indicated by the blue line) and post-choke (indicated by the red line). The findings distinctly illustrate a notable rise in pipeline pressure subsequent to the choking of high injectivity wells.

It can be seen from the plot that after around 15km into the pipeline the pressure after the choke started increasing and the increment continued until the end of the 148km long pipeline. The pressure at the end of the pipeline before the choke is 88.96 bar and after choking is 96.55 bar.

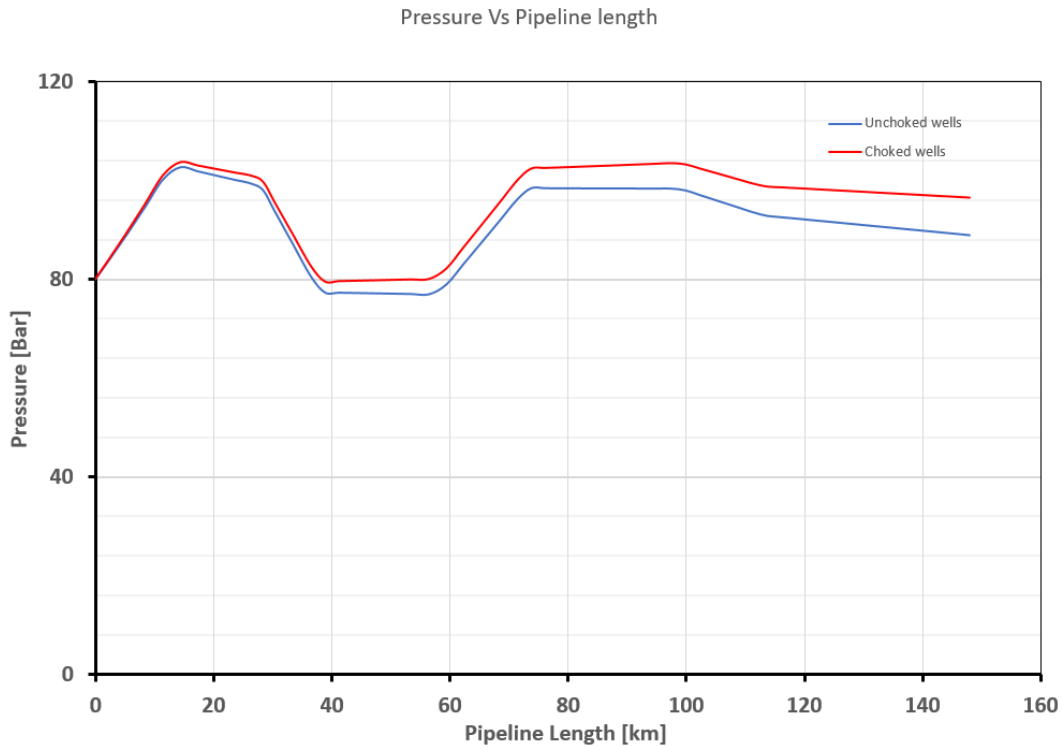


Figure 4.22: Shows increased pipeline pressure post-choke on high-injectivity wells along the 148km line (red line) compared to pre-choke (blue line)

4.8 Case three - Increase in reservoir pressure from 300 to 310bar

During the injection phase, an anticipated rise in reservoir pressure is expected due to the injection of CO₂ into the reservoir. Figure 4.23 shows the result of two reservoirs, one at 300bar reservoir pressure (base case) and the other at 310bar both subjected to varying manifold pressures.

At 50 bar, no injection occurred in both reservoirs. As can be seen from the graph the reservoir with higher reservoir pressure requires higher injection pressure. In the case of Snøhvit the initial reservoir pressure increased from 290bar to 315 between 14th August and 29th September 2008 [55] see Figure A.4 for details, this scenario is what was captured in this case. For this case, the injection pressure was increased from 300 to 310 bar.

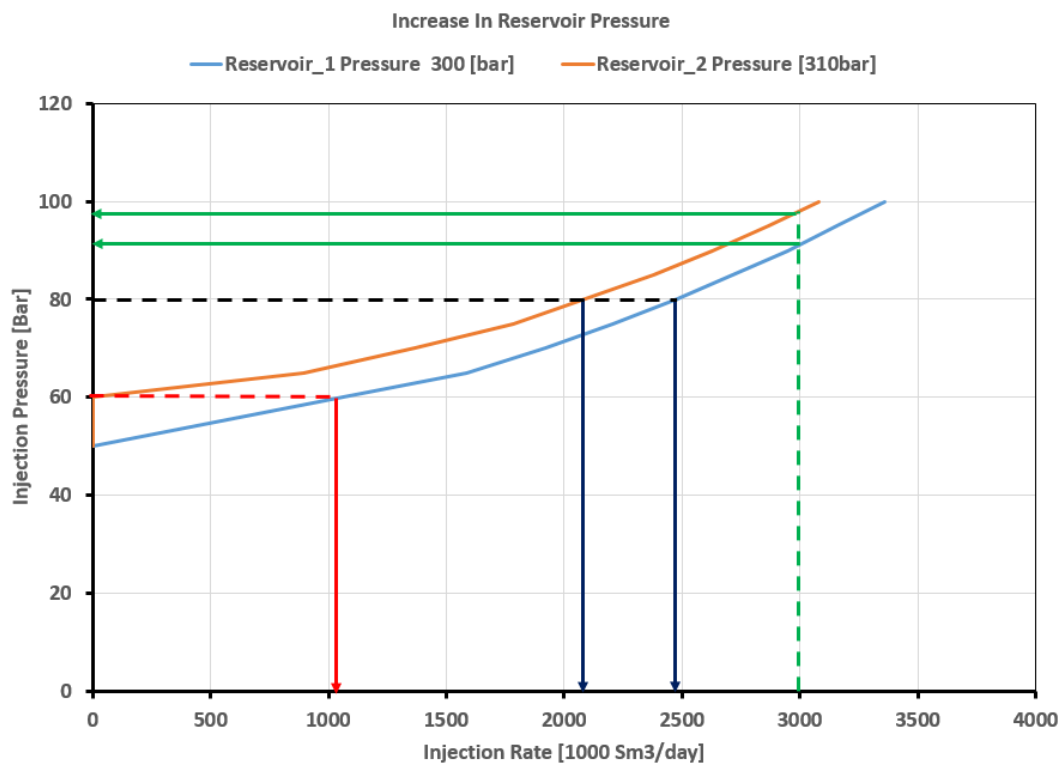


Figure 4.23: Comparison of two reservoirs at 300 bar and 310 bar reservoir pressures under varying manifold pressures. At 50 bar, no injection occurred. At 60 bar, Reservoir 1 injected at 1063 Msm³/day, while Reservoir 2 had no injection. At 80 bar, Reservoir 1 reached 2480 Msm³/day, and Reservoir 2 achieved 2090 Msm³/day injection rates.

Conclusion

In conclusion, the goal of this thesis was to model a synthetic case based on Snøhvit CO₂ storage, obtain and analyze results using GAP and Prosper which are software primarily developed for oil and gas applications. Run sensitivity analyses such as change in injection pressure, temperature, injectivity index, wellhead choke, etc., and predict CO₂ characteristics. The objective was successfully accomplished.

The results obtained from the Prosper well model and GAP simulation unveiled crucial insights into the behavior of the CO₂ injection system. Understanding the CO₂ phase envelope, hydrate formation, temperature variations, inflow performance relationship (IPR), system IPR + VLP, friction-induced pressure drop, fluid phase transitions, density variations, velocity profiles, and bottom-hole pressures allowed for comprehensive analyses.

The simulations showcased the significance of maintaining injection fluid temperatures above hydrate-forming temperatures, and the impact of elevation changes on pressure drops along the pipeline. Sensitivity analyses demonstrated how varying parameters such as injection pressure, temperature, and injectivity index affected system behavior, highlighting the need for tailored solutions in heterogeneous formations to achieve desired injection rates.

Moreover, comparisons between simulation results and real-world observations from Snøhvit field data revealed close alignment in key metrics such as pressure profiles, CO₂ density, and injection rates under specific conditions. These findings validate the model's ability to simulate real-world scenarios with close accuracy.

The study also highlighted the importance of choke implementation in regulating injection rates, showcasing the potential increase in pipeline pressure post-choke.

In summary, this thesis provided valuable insights into the dynamics of CO₂ transportation and injection systems, emphasizing the utility and reliability of modeling tools like Prosper and GAP in capturing the behavior of such systems. The findings contribute

to enhancing understanding of CO₂ transportation and injection strategies, paving the way for improved operational planning and decision-making in subsea environments.

Future Research Recommendations in Subsea CO₂ Transportation and Injection Systems

Based on the extensive analysis conducted in this thesis regarding modeling subsea CO₂ transportation and injection networks, the case of Snøhvit field, there are several potential avenues for future research and exploration within this domain:

Enhanced Simulation Techniques Integration of Reservoir Simulation: Incorporating a more detailed reservoir simulation model into the pipeline network analysis could provide a more comprehensive understanding of the interactions between the reservoir and the transport system. This integration could better capture the dynamic behavior and impacts of varying reservoir conditions on CO₂ injection and transportation.

Advanced Flow Assurance Studies: Hydrate Formation and Mitigation: Further investigation into hydrate formation risks and strategies for prevention or mitigation could be crucial. Studying the effectiveness of various inhibitors or innovative technologies to prevent hydrate formation in subsea CO₂ pipelines could be a significant focus.

Optimization and Robustness: Pipeline Design Optimization: Exploring ways to optimize pipeline design considering varying terrains and topographies could be valuable. Research could focus on identifying the most suitable pipeline configurations and materials to minimize pressure drop, energy consumption, and maintenance costs while ensuring robustness and reliability.

Environmental and Economic Perspectives: Environmental Impact Studies: Conducting comprehensive studies on the environmental impact of CO₂ transportation and injection networks could be vital, focusing on factors like greenhouse gas emissions, environmental safety, and potential ecological effects.

Economic Viability and Risk Assessment: Evaluating the economic feasibility and

risk assessment of subsea CO₂ transportation systems considering varying factors such as market conditions, technological advancements, and regulatory changes.

Technological Advancements: Innovative Technologies, exploring and implementing innovative technologies such as AI-driven predictive maintenance, advanced monitoring systems, or adaptive control mechanisms to improve the efficiency, safety, and reliability of CO₂ transportation networks.

Real-Time Monitoring and Control: Development of Monitoring Systems: Designing and implementing real-time monitoring systems to continuously track the condition of the pipeline and detect any potential issues or anomalies to enable prompt and efficient maintenance.

Policy and Regulation Impact: Policy and Regulatory Studies: Analyzing the impact of policy changes or regulatory frameworks related to CO₂ transportation, storage, and environmental policies on the design, operation, and economics of subsea CO₂ networks.

Collaborative Research Initiatives: Collaborative Research: Encouraging collaborative research efforts involving multidisciplinary teams comprising engineers, environmental scientists, economists, policymakers, and industry experts to address the multifaceted challenges associated with subsea CO₂ transportation and injection networks.

Engaging in these areas of research could significantly contribute to the advancement of knowledge, innovation, and sustainability within the domain of subsea CO₂ transportation and injection networks, ultimately facilitating the transition towards more efficient and environmentally conscious carbon capture and storage solutions.

Bibliography

- [1] M. Al Lawati, 'Gas lift nodal analysis model–economical optimization approach,' in *SPE Artificial Lift Conference & Exhibition-North America*, OnePetro, 2014.
- [2] M. Vitali, C. Zuliani, F. Corvaro, B. Marchetti, A. Terenzi and F. Tallone, 'Risks and safety of co2 transport via pipeline: A review of risk analysis and modeling approaches for accidental releases,' *Energies*, vol. 14, no. 15, p. 4601, 2021.
- [3] E. V. Filippov, G. N. Chumakov, I. N. Ponomareva and D. A. Martyushev, 'Application of integrated modeling in the oil and gas industry,' *Perm Journal of Petroleum and Mining Engineering*, vol. 20, no. 4, pp. 386–400, 2020.
- [4] E. Ola, H. Olav R., N. Bamshad, H. Hilde, P. Britta, B. Hege M. Norgard, O. Svend and R. Philip, 'Snøhvit CO₂ tubåen fm. storage capacity and injection strategy study,' in *Statoil Technical Achievement 2010 Snøhvit CO₂ Storage*, June, 2010, pp. 1–132.
- [5] T. Ramachandra, B. H. Aithal and K. Sreejith, 'Ghg footprint of major cities in india,' *Renewable and Sustainable energy reviews*, vol. 44, pp. 473–495, 2015.
- [6] I. P. on Climate Change, *Global warming of 1.5° C: An IPCC special report on the impacts of global warming of 1.5° C above pre-industrial levels and related global greenhouse gas emission pathways, in the context of strengthening the global response to the threat of climate change, sustainable development, and efforts to eradicate poverty*. Intergovernmental Panel on Climate Change, 2018.
- [7] C. J. Rhodes, 'Only 12 years left to readjust for the 1.5-degree climate change option–says international panel on climate change report: Current commentary,' *Science progress*, vol. 102, no. 1, pp. 73–87, 2019.
- [8] C. J. Rhodes, 'The 2015 paris climate change conference: Cop21,' *Science progress*, vol. 99, no. 1, pp. 97–104, 2016.
- [9] O. R. Sahar Rashidbeigi and E. Speelman, 'The future is now: How oil and gas companies can decarbonize,' <https://www.mckinsey.com/industries/oil-and-gas/our-insights/the-future-is-now-how-oil-and-gas-companies-can-decarbonize>, 2020.
- [10] P. Ringrose, 'How to store co2 underground: Insights from early-mover ccs projects,' 2020.

- [11] T. Gill, 'Ten years of handling co₂ for sacroc unit,' in *SPE Annual Technical Conference and Exhibition*, OnePetro, 1982.
- [12] J. Ma, L. Li, H. Wang, Y. Du, J. Ma, X. Zhang and Z. Wang, 'Carbon capture and storage: History and the road ahead,' *Engineering*, 2022.
- [13] C. Marchetti, 'On geoengineering and the co₂ problem,' *Climatic change*, vol. 1, no. 1, pp. 59–68, 1977.
- [14] P. G. Brewer, 'A changing ocean seen with clarity,' *Proceedings of the National Academy of Sciences*, vol. 106, no. 30, pp. 12 213–12 214, 2009.
- [15] M. Wilson, M. Monea, S. Whittaker, D. White, D. Law and R. Chalaturnyk, 'Iea ghg weyburn co {sub 2} monitoring and storage project: Summary report 2000-2004,' 2004.
- [16] Z. Kapetaki, J. Simjanović and J. Hetland, 'European carbon capture and storage project network: Overview of the status and developments,' *Energy Procedia*, vol. 86, pp. 12–21, 2016.
- [17] H. Kongsjorden, O. Kårstad and T. A. Torp, 'Saline aquifer storage of carbon dioxide in the sleipner project,' *Waste management*, vol. 17, no. 5-6, pp. 303–308, 1998.
- [18] A. Chadwick, G. Williams, N. Delepine, V. Clochard, K. Labat, S. Sturton, M.-L. Buddensiek, M. Dillen, M. Nickel, A. L. Lima *et al.*, 'Quantitative analysis of time-lapse seismic monitoring data at the sleipner co₂ storage operation,' *The Leading Edge*, vol. 29, no. 2, pp. 170–177, 2010.
- [19] B. Hitchon, *Best practices for validating CO₂ geological storage: Observations and guidance from the IEAGHG Weyburn-Midale CO₂ monitoring and Storage Project*. Geoscience Publishing, 2012.
- [20] K. Brown, S. Whittaker, M. Wilson, W. Srisang, H. Smithson and P. Tontiwachwuthikul, 'The history and development of the iea ghg weyburn-midale co₂ monitoring and storage project in saskatchewan, canada (the world largest co₂ for eor and ccs program),' *Petroleum*, vol. 3, no. 1, pp. 3–9, 2017.
- [21] G. C. Institute, 'Global status of ccs 2020. report. melbourne:' *Global CCS Institute*, 2020.
- [22] R. Svensson, M. Odenberger, F. Johnsson and L. Strömberg, 'Transportation systems for co₂—application to carbon capture and storage,' *Energy conversion and management*, vol. 45, no. 15-16, pp. 2343–2353, 2004.
- [23] O. Skovholt, 'Co₂ transportation system,' *Energy Conversion and Management*, vol. 34, no. 9-11, pp. 1095–1103, 1993.
- [24] D. Golomb, 'Transport systems for ocean disposal of co₂ and their environmental effects,' *Energy Conversion and Management*, vol. 38, S279–S286, 1997.
- [25] R. Doctor, J. Molburg and J. Brockmeier, 'Transporting carbon dioxide recovered from fossil-energy cycles,' Argonne National Lab., IL (US), Tech. Rep., 2000.

- [26] H. Sarv and J. John, 'Technical and economical aspects of large-scale co₂ storage in deep oceans,' McDermott Technology, Inc., Alliance, OH (US), Tech. Rep., 2000.
- [27] J. Gale, 'Transmission of co₂: Safety and economic considerations. sixth int,' in *Conference. on Greenhouse Gas Control Technologies, Kyoto, September, 2002*, pp. 1–4.
- [28] S. Bachu, J. Adams, K. Michael and B. Buschkuehle, 'Acid gas injection in the alberta basin: A commercial-scale analogue for co₂ geological sequestration in sedimentary basins,' in *Proceedings of the Second Annual Conference on Carbon Dioxide Sequestration*, Citeseer, 2003, pp. 5–8.
- [29] R. Wright, F. Mourits, L. B. Rodriguez and M. D. Serrano, 'The first north american carbon storage atlas,' *Energy Procedia*, vol. 37, pp. 5280–5289, 2013.
- [30] M. Ciotta, D. Peyerl, L. Barrozo, L. S. Anna, E. M. dos Santos, C. Bermann, C. Grohmann, E. M. Moretto and C. Tassinari, 'An overview of carbon capture and storage atlases around the world,' *Environmental Geosciences*, vol. 27, no. 1, pp. 1–8, 2020.
- [31] P. S. Ringrose, 'The ccs hub in norway: Some insights from 22 years of saline aquifer storage,' *Energy Procedia*, vol. 146, pp. 166–172, 2018.
- [32] T. Maldal and I. Tappel, 'Co₂ underground storage for snøhvit gas field development,' *Energy*, vol. 29, no. 9-10, pp. 1403–1411, 2004.
- [33] O. Hansen, D. Gilding, B. Nazarian, B. Osdal, P. Ringrose, J.-B. Kristoffersen, O. Eiken and H. Hansen, 'Snøhvit: The history of injecting and storing 1 mt co₂ in the fluvial tubåen fm,' *Energy Procedia*, vol. 37, pp. 3565–3573, 2013.
- [34] O. Eiken, P. Ringrose, C. Hermanrud, B. Nazarian, T. A. Torp and L. Høier, 'Lessons learned from 14 years of ccs operations: Sleipner, in salah and snøhvit,' *Energy procedia*, vol. 4, pp. 5541–5548, 2011.
- [35] B. Nazarian, R. Held, L. Høier and P. Ringrose, 'Reservoir management of co₂ injection: Pressure control and capacity enhancement,' *Energy Procedia*, vol. 37, pp. 4533–4543, 2013.
- [36] P. N. Seevam, J. M. Race, M. J. Downie and P. Hopkins, 'Transporting the next generation of co₂ for carbon, capture and storage: The impact of impurities on supercritical co₂ pipelines,' in *International Pipeline Conference*, vol. 48579, 2008, pp. 39–51.
- [37] J. S. Lopez-Echeverry, S. Reif-Acherman and E. Araujo-Lopez, 'Peng-robinson equation of state: 40 years through cubics,' *Fluid Phase Equilibria*, vol. 447, pp. 39–71, 2017.
- [38] G. A. Melhem, R. Saini and B. M. Goodwin, 'A modified peng-robinson equation of state,' *Fluid Phase Equilibria*, vol. 47, no. 2-3, pp. 189–237, 1989.

- [39] R. Span and W. Wagner, 'A new equation of state for carbon dioxide covering the fluid region from the triple-point temperature to 1100 k at pressures up to 800 mpa,' *Journal of physical and chemical reference data*, vol. 25, no. 6, pp. 1509–1596, 1996.
- [40] W. Gilbert, 'Flowing and gas-lift well performance,' in *Drilling and production practice*, OnePetro, 1954.
- [41] A. Odeh, 'Pseudosteady-state flow equation and productivity index for a well with noncircular drainage area,' *Journal of Petroleum Technology*, vol. 30, no. 11, pp. 1630–1632, 1978.
- [42] H. D. Beggs, *Production Optimization Using Nodal (TM) Analysis*. OGCI, 2003.
- [43] H. Dmour, 'Optimization of well production system by nodal analysis technique,' *Petroleum science and technology*, vol. 31, no. 11, pp. 1109–1122, 2013.
- [44] M. O. Faruque, T. Hasan and M. A. Hussain, 'Optimization of gas-well production practices with special reference to kailashtilla gas field, north-east, bangladesh,' *J Sci Eng Res*, vol. 9, no. 7, pp. 1385–1396, 2018.
- [45] A. Jahanbani and S. Shadizadeh, 'Determination of inflow performance relationship (ipr) by well testing,' in *PETSOC Canadian International Petroleum Conference*, PETSOC, 2009, PETSOC–2009.
- [46] L.-b. Ouyang and K. Aziz, 'Steady-state gas flow in pipes,' *Journal of Petroleum Science and Engineering*, vol. 14, no. 3-4, pp. 137–158, 1996.
- [47] K. E. Brown, 'Technology of artificial lift methods. volume 1. inflow performance, multiphase flow in pipes, the flowing well,' 1977.
- [48] A. Ansari, N. Sylvester, C. Sarica, O. Shoham and J. Brill, 'A comprehensive mechanistic model for upward two-phase flow in wellbores,' *SPE Production & Facilities*, vol. 9, no. 02, pp. 143–151, 1994.
- [49] M. Shippen and W. J. Bailey, 'Steady-state multiphase flow*****
past, present, and future, with a perspective on flow assurance,' *Energy & Fuels*, vol. 26, no. 7, pp. 4145–4157, 2012.
- [50] M. A. Abd El Moniem and A. H. El-Banbi, 'Proper selection of multiphase flow correlations,' in *SPE North Africa Technical Conference and Exhibition*, SPE, 2015, D011S004R003.
- [51] D. H. Beggs and J. P. Brill, 'A study of two-phase flow in inclined pipes,' *Journal of Petroleum technology*, vol. 25, no. 05, pp. 607–617, 1973.
- [52] D. Surbey, B. Kelkar and J. Brill, 'Study of subcritical flow through multiple-orifice valves,' *SPE Production Engineering*, vol. 3, no. 01, pp. 103–108, 1988.
- [53] P. E. IPM13, 'Integrated production modelling user manuals,' October 2020.
- [54] F. E. Uilhoorn, 'Evaluating the risk of hydrate formation in co2 pipelines under transient operation,' *International Journal of Greenhouse Gas Control*, vol. 14, pp. 177–182, 2013.

- [55] J.-Q. Shi, C. Imrie, C. Sinayuc, S. Durucan, A. Korre and O. Eiken, 'Snøhvit co2 storage project: Assessment of co2 injection performance through history matching of the injection well pressure over a 32-months period,' *Energy Procedia*, vol. 37, pp. 3267–3274, 2013.
- [56] Z. Dongjie, W. Zhe, S. Jining, Z. Lili and L. Zheng, 'Economic evaluation of co2 pipeline transport in china,' *Energy Conversion and Management*, vol. 55, pp. 127–135, 2012.
- [57] F. Ntengwe, M. Chikwa and L. Witika, 'Evaluation of friction losses in pipes and fittings of process engineering plants,' *International Journal of Scientific and Technology Research*, vol. 4, no. 10, pp. 330–336, 2015.
- [58] Z. Zhang, G. Wang, P. Massarotto and V. Rudolph, 'Optimization of pipeline transport for co2 sequestration,' *Energy Conversion and Management*, vol. 47, no. 6, pp. 702–715, 2006.
- [59] B. Wetenhall, J. Race, H. Aghajani and J. Barnett, 'The main factors affecting heat transfer along dense phase co2 pipelines,' *International Journal of Greenhouse Gas Control*, vol. 63, pp. 86–94, 2017.

Additional Material

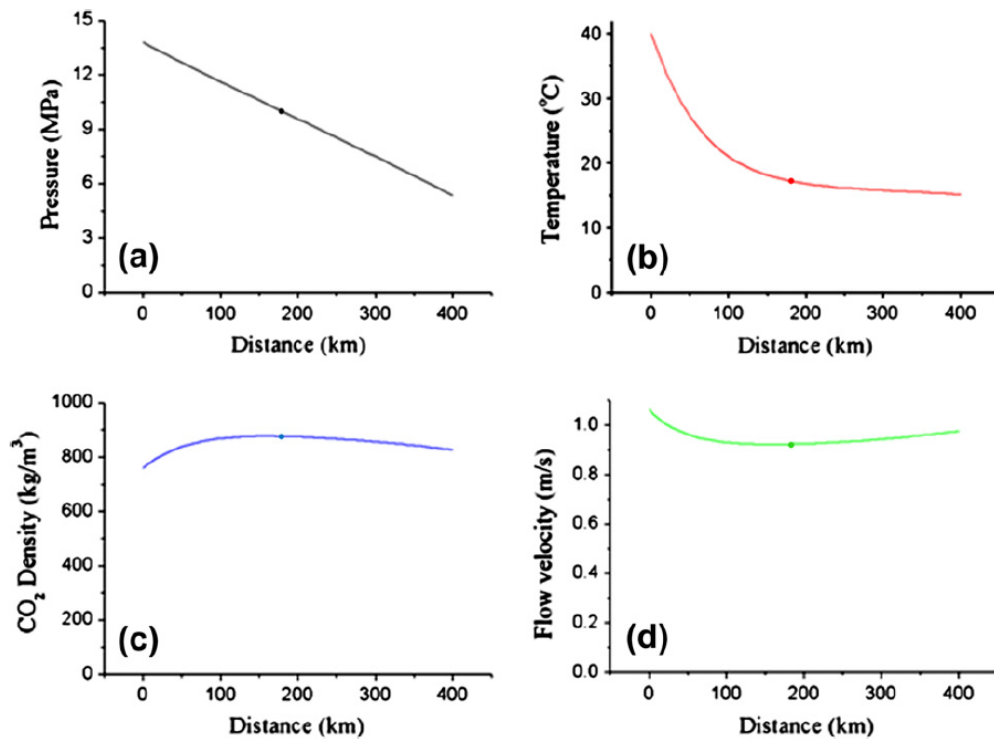


Figure A.1: Hydrodynamic performances of the CO₂ pipeline in the Base Case (a) pressure change (b) temperature change (c) density change and (d) flow velocity change, along with transport [56]

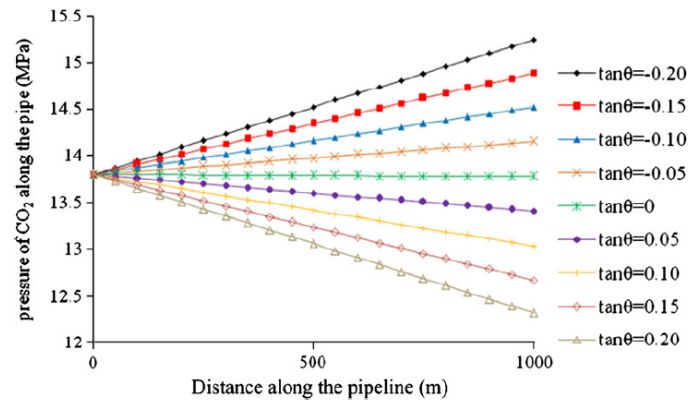


Figure A.2: Pressure drop of the pipeline with a sloping angle [56]

A.1

Pressure drop of the pipeline with a sloping angle of θ Figure A.2 shows the pressure drop behavior of the CO₂ pipeline when there is a sloping angle of θ with the pipe, which is significantly different with the case when no slope exists. When the pipeline is horizontal, the dominant factor for CO₂ pressure change is the friction force from the pipe wall, with an average pressure dropping rate of 2.16 MPa/100 km. In Fig. ??, only 1 km of transport distance is presented, so that the pressure drop can hardly be seen. When there is a sloping angle h ($\theta \neq 0$) with the pipe, the impact of the friction force of the pipe wall is totally outweighed by gravity. If the pipeline slopes upwards, when $\tan\theta = 0.05$, pressure drop within 1 km (the elevation increases by 50 m) along the pipeline can be as big as 0.464 MPa, while when $\tan\theta = 0.20$, pressure drop within 1 km (the elevation of CO₂ increases by 200 m) along the pipeline can be as big as 1.738 MPa, far exceeding the pressure drop caused by frictional force. This indicates that elevation has a significant impact on the pressure drop performance of the CO₂ pipeline, so that detailed topography of the objective district must be considered when designing a CO₂ pipeline: if the elevation increases significantly within a certain distance, such as when climbing up a mountain, CO₂ pressure will drop dramatically, so boosting pump stations could be necessary at certain points, to make up the pressure loss; if the elevation decreases significantly within a certain distance, such as when climbing down a mountain, CO₂ pressure will increase dramatically, so thicker pipe might be needed for this section.[56]

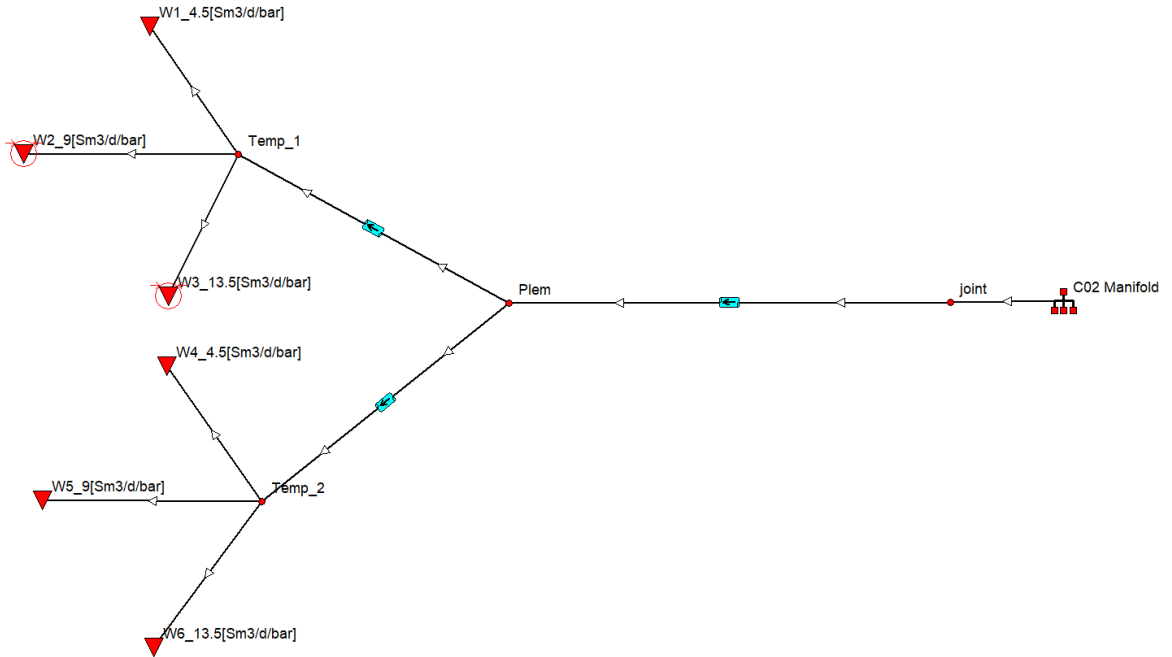


Figure A.3: shows a comprehensive representation of the pipeline network, extending from the injection manifold through the flowline, reaching the templates, and subsequently channeling into the six injection wells, in this case all wells have different injectivity, and some wells are choked.

Name	Mole Per- cent (percent)	Critical Temp. (deg.C)	Critical Pressure (BARa)	Critical Volume m3/kg.mole	Acentric Factor	Molec. Weight	Sp.Gravity
CO2	98	30.94	73.9777	0.0939	0.239	44.01	1.101
C1	2	-82.51	46.407	0.099201	0.011	16.04	0.415
C2	1E-6	32.11	48.8388	0.1483	0.099	30.1	0.546
C3	1E-6	96.67	42.5668	0.203	0.153	44.1	0.585

Table A.1: Composition Table I

Boiling Point	Vol. Shift	OmegaA	OmegaB	Parachor	Costald Volume	Costald AF	Melting Point	Enthalpy of Fusion
deg C					m3/kg.mol			
-78.45	—	0.45724	0.07779	78	0.09383	0.23725	-183.23	4001.21
-161.55	-0.154	0.45724	0.07779	70	0.09939	0.0074	-159.6	473.904
-88.55	-0.1002	0.45724	0.07779	115	0.14575	0.0983	-138.33	1756.61
-42.05	-0.0850	0.45724	0.07779	155	0.20008	0.1532	-159.89	1773.84

Table A.2: Composition Table II

Company	Simulator	Extension
Schlumberger	ECLIPSE	.ECL
Schlumberger	INTERSECT	.IFX
WellDrill	SIMCO 3	.SIM
ExxonMobil	PEGASUS	.MOB
SSI	COMP4	.CP4
FranLab	FRAGOR	.FRA
Beicip FranLab IFP	PUMAFLOW	.PUM
SSI	COMP3	.CP3
LandMark	VIP	.VIP
Roxar	MORE	.MOR
Petroleum Experts	GAP/MBAL	.TPD
Shell	MORES	.MRS
FranLab	Athos	.ATH
BP	GCOMP	.GCM
Chevron Texaco	CHEARS	.CHE
Exxon Mobil	EMPOWER	.EMP
Conoco Phillips	PSIM	.WBH
CMG (old format)	IMEX/GEM	.IMX
CMG (release 2009.10)	IMEX/GEM	.CMG
Saudi Aramco	POWERS	.FG2

Table A.4: Shows Prosper supported Export formats

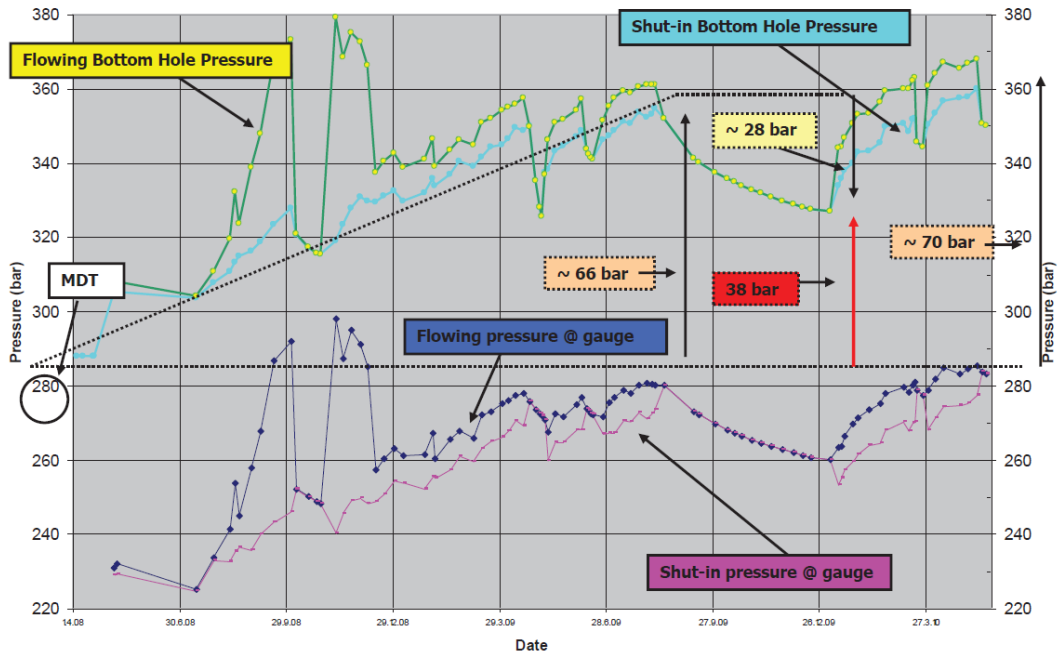


Figure A.4: Flowing bottom hole pressure and reservoir pressure history throughout the snøhvit injection well [55]

IPR Method	Oil and water	Dry and Wet Gas	Retrograde Condensate
Back Pressure		X	X
C and n		X	X
Composite	X		
CBM Producer (available when well type is set to CBM Producer)			
Darcy	X		
Dual Porosity	X	X	X
External Entry	X	X	X
Fetkovich	X		
Forchheimer		X	X
Forchheimer with Pseudo - Pressure		X	X
Multirate Forchheimer with Pseudo - Pressure		X	X
Horizontal well - No Flow Boundaries	X	X	X
Horizontal well - Constant Pressure upper boundary	X		
Horizontal well - dP friction	X	X	X
Horizontal well - transverse vertical fractures	X	X	X
Hydraulically fractured	X	X	X
Jones	X	X	X
Multi-lateral	X	X	X
Multi-layer	X	X	X
Multi-layer - dP Loss	X	X	X
Multi-rate C and n		X	X
Multi-rate Fetkovich	X		
Multi-rate Jones	X	X	X
Modified Isochronal IPR		X	X
Petroleum Experts		X	X
PI. Entry	X		
SkinAide	X	X	X
Thermally Induced Fracture (injection only)	X		
Transient	X		
Vogel	X		
SPOT	X	X	X

Table A.3: Inflow Performance Relationship (IPR) methods available in Prosper